

University of Windsor

## Scholarship at UWindor

---

Electronic Theses and Dissertations

Theses, Dissertations, and Major Papers

---

1-1-2019

# Numerical Investigation of Conformal Cooling Channels in Injection Molds

Shu Chen

*University of Windsor*

Follow this and additional works at: <https://scholar.uwindsor.ca/etd>

---

### Recommended Citation

Chen, Shu, "Numerical Investigation of Conformal Cooling Channels in Injection Molds" (2019). *Electronic Theses and Dissertations*. 8162.

<https://scholar.uwindsor.ca/etd/8162>

This online database contains the full-text of PhD dissertations and Masters' theses of University of Windsor students from 1954 forward. These documents are made available for personal study and research purposes only, in accordance with the Canadian Copyright Act and the Creative Commons license—CC BY-NC-ND (Attribution, Non-Commercial, No Derivative Works). Under this license, works must always be attributed to the copyright holder (original author), cannot be used for any commercial purposes, and may not be altered. Any other use would require the permission of the copyright holder. Students may inquire about withdrawing their dissertation and/or thesis from this database. For additional inquiries, please contact the repository administrator via email ([scholarship@uwindsor.ca](mailto:scholarship@uwindsor.ca)) or by telephone at 519-253-3000ext. 3208.

# Numerical Investigation of Conformal Cooling Channels in Injection Molds

by

Shu Chen

A Thesis  
Submitted to the Faculty of Graduate Studies  
through the Department of Mechanical, Automotive & Materials Engineering  
in Partial Fulfillment of the Requirements for  
the Degree of Master of Applied Science  
at the University of Windsor

Windsor, Ontario, Canada

2019

© 2019 Shu Chen

# Numerical Investigation of Conformal Cooling Channels in Injection Molds

by

Shu Chen

APPROVED BY:

---

H. Hu

Department of Mechanical, Automotive & Materials Engineering

---

A. Fartaj

Department of Mechanical, Automotive & Materials Engineering

---

R. M. Barron, Co-Advisor

Department of Mechanical, Automotive & Materials Engineering

---

R. Balachandar, Co-Advisor

Department of Mechanical, Automotive & Materials Engineering

December 16, 2019

# Declaration of Co-Authorship

## / Previous Publication

### I. Co-Authorship

I hereby declare that this thesis incorporates material that is the result of research undertaken under the supervision of Dr. R. Barron and Dr. R. Balachandar and in collaboration with Dr. K. Fukuda. The collaboration is covered in Chapter 3 of the thesis. In all cases, the key ideas, primary contributions, numerical simulation designs, data analysis and interpretation were performed by the author, and the contribution of co-authors in the associated publication for the conference was primarily through the discussion of the numerical results and editing of the manuscript.

I am aware of the University of Windsor Senate Policy on Authorship and I certify that I have properly acknowledged the contribution of other researchers to my thesis and have obtained written permission from each of the co-authors to include the above material in my thesis.

I certify that, with the above qualification, this thesis, and the research to which it refers, is the product of my own work.

## II. Previous Publication

This thesis includes one original paper that has been previously accepted for publication in peer reviewed conference proceedings:

Thesis Chapter	Publication title/full citation	Publication status
Chapter 3	S. Chen, K. Fukuda, R. M. Barron, R. Balachandar. Numerical Investigation of Conjugate Heat Transfer in a Straight Cooling Channel. 14 <sup>th</sup> International Symposium on Numerical Analysis of Fluid Flows, Heat and Mass Transfer – Numerical Fluids 2019, ICNAAM 2019, Rhodes, Greece, Sept. 2019.	Published

I certify that I have obtained written permission from the copyright owner to include the above material in my thesis. I certify that the above material describes work completed during my registration as a graduate student at the University of Windsor.

I declare that, to the best of my knowledge, my thesis does not infringe upon anyone's copyright nor violate any proprietary rights and that any ideas, techniques, quotations, or any other material from the work of other people included in my thesis, published or otherwise, are fully acknowledged in accordance with the standard referencing practices. Furthermore, to the extent that I have included copyrighted material that surpasses the bounds of fair dealing within the meaning of the Canada Copyright Act, I certify that I have obtained a written permission from the copyright owners to include such materials in my thesis.

I declare that this is a true copy of my thesis, including any final revisions, as approved by my thesis committee and the Graduate Studies office, and that this thesis has not been submitted for a higher degree to any other University or Institution.

# Abstract

To accommodate the increasing demand for consumer plastic products with higher quality and the industry's desire for injection molding processes with higher production rate, metal 3D printing technologies have been introduced into the injection molding industry to fabricate cooling channels which can be placed more conformal to the working surface of the injection mold. These channels are referred to as conformal cooling channels. Since the manufacturing cost of mold-inserts with conformal cooling channels are higher than those with conventional cooling channels, it is necessary to confirm the advantage of using conformal cooling channels rather than conventional cooling channels. In this thesis, CFD simulations are used to compare the performances of a conventional cooling system and a conformal cooling system. The conformal cooling system is shown to have better cooling performance while not consuming more pumping power. Since the injection mold cooling system design is highly dependent on the geometry of the molded plastic part, it is difficult to construct general design guidelines for all conformal cooling channels. Therefore, commonly used conformal cooling systems that consist of U-shape bends are studied in this thesis. The influences of three geometrical design parameters, namely configuration of the U-shape bends, cooling channel depth from the heating surface and number of cooling channels, on the cooling performance are examined in a parametric study.

# Dedication

To my parents,  
Shouyu Chen and Li Yang

# Acknowledgements

This research was co-funded by the Ontario Centre of Excellence and the Proper Group International. This work was also made possible by the facilities of the Shared Hierarchical Academic Research Computing Network (SHARCNET: [www.sharcnet.ca](http://www.sharcnet.ca)) and Compute/Calcul Canada.

The research presented in this thesis is rendered possible by the combined effort and support of the people I am fortunate enough to cross paths with. Most importantly, I am grateful for the guidance and support of my advisors, Dr. Barron and Dr. Balachandar. I owe a great deal of the knowledge and skills that I have today to them, as they have patiently guided me over the last two years. Without their encouragement and advice, I would not have been able to successfully complete the research. Special thanks is given to our industrial partners Mr. Tabbert and Mr. Cameron at Proper Group International for their support in this research. I would also like to thank my committee members Dr. Hu and Dr. Fartaj for their time in reviewing my thesis and insightful suggestions on improvements.

To the members of the Computational Fluid Dynamics Laboratory and Fluid Dynamics Research Institute, I would like to thank you for the advice and support you provided me that aided me in completing this thesis. Specifically, I would like to acknowledge Dr. Fukuda, he patiently guided me through the research in this thesis.

I would also like to extend my thanks to all faculty and staff members of the Department of Mechanical, Automotive & Materials Engineering and Faculty of Graduate Studies for their help and support.

Finally, I would like to thank my parents, Shouyu Chen and Li Yang. Without their endless support and unwavering belief, I would not be where I am today. I own them a great deal.



# Contents

Declaration of Co-Authorship / Previous Publication.....	iii
Abstract .....	v
Dedication.....	vi
Acknowledgements .....	vii
List of Figures .....	xi
List of Tables .....	xiv
Nomenclature.....	xv
Chapter 1 Introduction .....	1
Chapter 2 Literature Review.....	8
2.1 Previous Studies .....	8
2.2 Turbulence Modelling.....	12
2.2.1 Reynolds-Averaged Navier-Stokes (RANS) Modelling .....	13
2.2.1.1 Standard $k$ - $\varepsilon$ Model .....	14
2.2.1.2 Realizable $k$ - $\varepsilon$ Model .....	15
2.2.1.3 Standard $k$ - $\omega$ Model .....	16
2.2.1.4 Shear Stress Transport (SST) $k$ - $\omega$ Model .....	17
Chapter 3 Validation.....	18
3.1 Numerical Model Setup.....	20
3.1.1 Computational Domain and Governing Equations.....	20
3.1.2 Boundary Conditions.....	21
3.1.3 Physical Properties.....	23
3.1.4 Mesh.....	24
3.2 Validation Results and Analyses .....	25

Chapter 4 Comparison between a Conventional and a Conformal Cooling System .....	35
4.1 Numerical Model Setup .....	37
4.1.1 Geometric Setup .....	37
4.1.2 Computational Domain .....	38
4.1.3 Boundary Conditions.....	39
4.1.4 Physical Properties .....	42
4.1.5 Mesh .....	43
4.1.5.1 Meshing Methods .....	43
4.1.5.2 Mesh Independence Study .....	44
4.2 Results and Analyses.....	46
4.3 Summary.....	53
Chapter 5 Parametric Study .....	54
5.1 Design of the Parametric Study .....	55
5.1.1 Test Mold-insert Design .....	55
5.1.2 Cooling System Design.....	56
5.2 Numerical Model Setup .....	63
5.2.1 Computational Domain .....	63
5.2.2 Boundary Conditions.....	63
5.2.3 Physical Properties .....	65
5.2.4 Mesh .....	65
5.3 Results and Analyses.....	65
5.3.1 Coolant Flow Analyses .....	66
5.3.1.1 Dean Vortex.....	66
5.3.1.2 Main Flow Development .....	69
5.3.1.3 Temperature Distribution in the Channel .....	73
5.3.1.4 Heat Transfer Coefficient .....	77
5.3.2 Cooling Performance Analyses .....	78
5.3.2.1 Maximum Temperature on the Heating Surface.....	78
5.3.2.2 Temperature Uniformity on the Heating Surface .....	81

5.3.2.3 Pressure Drop in the Cooling System.....	83
5.4 Summary .....	85
Chapter 6 Conclusions and Future Work .....	87
6.1 Summary and Conclusions.....	87
6.2 Potential Future Work .....	90
References .....	91
Appendix A.....	95
Vita Auctoris .....	99

# List of Figures

Figure 1.1:	Typical molding cycle and cycle time in injection molding [1] .....	3
Figure 1.2:	Simple schematics of a conventional and a conformal cooling system ( <i>reprinted from Sachs et al., 2016 [5]</i> ) .....	3
Figure 1.3:	Plastic fog lamp cover .....	5
Figure 3.1:	Geometry of the straight pipe heat exchanger and positions of the nine measuring points [21,23].....	19
Figure 3.2:	Meshes with different base cell sizes: (a) 0.75 mm, (b) 1 mm, (c) 1.25 mm .....	25
Figure 3.3:	Effect of prism layer stretching factors: (a) 1.3, (b) 1.5, (c) 1.7 ..	25
Figure 3.4:	Temperature distribution at nine measuring points with different mass flow rates: (a) 0.124 kg/s, (b) 0.225 kg/s (Exp refers to [21]) .....	27
Figure 3.5:	Temperature distribution on central plane using SST $k-\omega$ model .....	28
Figure 3.6:	Cross-sectional velocity profiles at three measuring positions ( $V_i$ is the streamwise velocity in the pipe and $V_{in}$ is the inlet velocity) .....	30
Figure 3.7:	Cross-sectional temperature profiles at three measuring positions.....	32
Figure 3.8:	Heat transfer coefficient along the channel wall in the heating section.....	33
Figure 4.1:	CAD model of the core-insert with all the features.....	36
Figure 4.2:	The conventional cooling system and the working surface of the core-insert.....	37
Figure 4.3:	The conformal cooling system and the working surface of the core-insert.....	38

Figure 4.4:	Computational domain and boundary conditions of the core-insert with conventional cooling system .....	39
Figure 4.5:	Illustration of the polyhedral mesh on the middle cross-sectional plane which is perpendicular to the inlet flow direction.....	44
Figure 4.6:	Temperature distribution on heating surfaces of core-inserts with conventional and conformal cooling channels with mass flow rates of 0.031 kg/s, 0.078 kg/s, 0.124 kg/s and 0.171 kg/s ..	47
Figure 4.7:	Maximum temperature on the heating surface vs total inlet mass flow rates.....	48
Figure 4.8:	Temperature uniformity on the working surface for both conventional and conformal cooling systems .....	49
Figure 4.9:	Temperature distribution in the middle cross-section of (a) conventional cooling system; (b) conformal cooling system .....	50
Figure 4.10:	Pressure drop vs mass flow rates .....	51
Figure 4.11:	Coolant temperature increase vs mass flow rates.....	52
Figure 4.12:	Heat transfer coefficient vs mass flow rates.....	53
Figure 5.1:	Schematic of the mold-insert for the parametric study.....	55
Figure 5.2:	Schematics of test inserts with one cooling channel, .....	59
Figure 5.3:	Schematic of test inserts with two cooling channels, (a) Case 2-1: $H = 2D, \delta_1 = 1$ and $\delta_2 = 1$ ; (b) Case 2-10: $H = 5D, \delta_1 = 1$ and $\delta_2 = 1$ .....	61
Figure 5.4:	Schematic of testing models with three cooling channels, (a) Case 3-1: $H = 2D, \delta_1 = 1, \delta_2 = 1$ and $\delta_3 = 1$ ; (b) Case 3-5: $H = 5D, \delta_1 = 1, \delta_2 = 1$ and $\delta_3 = 1$ .....	62
Figure 5.5:	CAD model of test mold-insert and some boundary conditions .	64
Figure 5.6:	Dean vortex ( <i>reprinted from Dean and Hurst 1927 [34]</i> ).....	66
Figure 5.7:	Secondary flow velocity at $0^\circ$ , $45^\circ$ and $90^\circ$ of the $90^\circ$ bend. Viewed from the streamwise direction (For all cross-sections, left-hand side is the inside of the bend. White dots in the figures represent the centre of the Dean vortices).....	68

Figure 5.8: Velocity magnitude and streamlines in the symmetry planes and streamwise velocities in selected cross-sections for case 1-1, 1-2 and 1-5.....	70
Figure 5.9: Turbulent kinetic energy in the symmetry planes for case 1-1, 1-2 and 1-5.....	71
Figure 5.10: Velocity magnitude and streamlines in the symmetry planes of test case (a) 1-1, (b) 2-1 and (c) 3-1.....	72
Figure 5.11: Pressure drop vs curvature ratio in the channel of test cases with one cooling channel, (a) $H = 2D$ , (b) $H = 5D$ .....	73
Figure 5.12: Channel cross-sections used for the study of temperature distribution in the coolant flow and channel sections used for the study of heat transfer coefficient at the cooling channel wall ...	73
Figure 5.13: Temperature distribution in five channel cross-sections for cases with channel depth of $2D$ .....	75
Figure 5.14: Temperature distribution in five channel cross-sections for cases with channel depth of $5D$ .....	76
Figure 5.15: Heat transfer coefficient at channel wall of four consecutive channel-sections (defined in Fig 5.11) from test cases with one cooling channel.....	78
Figure 5.16: Temperature distribution on the heating surface for cooling systems with different cooling channel depths and bend configurations (red circle represents location of the hot spot) ...	80
Figure 5.17: Maximum temperature and pressure drop vs. curvature ratio of the channel bend for the single channel cases, (a) $H = 2D$ , (b) $H = 5D$ .....	81
Figure 5.18: Temperature uniformity vs. curvature ratio of second $90^\circ$ bend after the inlet of the cooling channel, (a) $H = 2D$ , (b) $H = 5D$ ....	82
Figure 5.19: Pressure drop of cooling systems with one, two and three channels.....	85

# List of Tables

Table 4.1:	Relationship between mass flow rates and Reynolds number for the conventional and the conformal cooling systems .....	42
Table 4.2:	Thermal properties of standard P20 mold steel .....	42
Table 4.3:	Important meshing parameters .....	44
Table 4.4:	Results of the testing with base cell size .....	45
Table 4.5:	Results of the testing of four sub meshing parameters.....	46
Table 5.1:	Design parameters for test cases with one cooling channel.....	58
Table 5.2:	Design parameters for test cases with two cooling channels .....	61
Table 5.3:	Design parameters for test cases with three cooling channels ..	62
Table 5.4:	Details of the analytical calculation of the pressure drop in the cooling system .....	84

# Nomenclature

## Symbols

$C_p$	Specific Heat Capacity
$D$	Diameter
$De$	Dean Number
$E$	Energy
$h$	Heat Transfer Coefficient
$H$	Channel Depth from the Heating Surface
$I$	Turbulence Intensity
$k$	Turbulent Kinetic Energy
$L_e$	Entrance Length
$\dot{m}$	Mass Flow Rate
$Nu$	Nusselt Number
$p$	Pressure
PC	Polycarbonate
$\dot{q}$	Heat flux
$R_c$	Radius of 90° Bends
$Re$	Reynolds Number
$t$	Time
$T$	Temperature
$u$	Velocity
$\dot{V}$	Volumetric Flow Rate
$x,y,z$	Cartesian axis directions
$\alpha$	Thermal Diffusivity
$\delta$	Curvature Ratio of 90° Channel Bends
$\varepsilon$	Dissipation Rate
$\mu$	Dynamic Viscosity
$\nu$	Kinematic Viscosity



$\rho$	Density
$\sigma$	Surface Tension
$\tau$	Shear Stress
$\omega$	Specific Dissipation Rate
$\Omega$	Wave Growth Rate

### Abbreviations

1D	One Dimensional
3D	Three Dimensional
CAD	Computer Aided Design
CFD	Computational Fluid Dynamics
DNS	Direct Numerical Simulation
DOE	Design of Experiment
DTUL	Deflection Temperature Under Load
FoM	Figure of Merit
LES	Large Eddy Simulation
RANS	Reynolds-Averaged Navier-Stokes
SST	Shear Stress Transport

# Chapter 1

## Introduction

Thermal plastic injection molding is one of the most efficient and popular manufacturing methods for consumer plastic products due to its capability of producing plastic parts with complex geometries and tight tolerances. Importantly, injection molding also provides a high degree of consistency among parts through long production runs. The injection molding process requires a hot molten polymer to be injected into a cavity inside a mold, in which the molten polymer is cooled and solidified. Once the temperature of the plastic has fallen to a certain threshold level the part is ejected from the mold. The molder, i.e., the company who uses the injection mold to manufacture the plastic products, needs to collaborate with a mold maker to design, manufacture and test run the corresponding injection mold before any parts can be manufactured. As a result, the initial investment in plastic injection molding is huge. Therefore, to reduce manufacturing costs of an injection mold and meet the requirements of the production rate and product quality, it is crucial to predict the performance of the injection mold in advance.

Injection molding is a cyclic manufacturing process. A complete molding cycle consists of six major phases: mold closing, filling, packing, cooling, mold opening and part ejection. A typical molding cycle [1] is illustrated in Fig. 1.1, which indicates that the cooling phase accounts for

nearly half of a complete molding cycle. In fact, depending on the geometry of the molded part and the design of the cooling system, the cooling phase can take up to 80% of a complete molding cycle [2]. Obviously, reduction of the cooling time can significantly reduce the cycle time, thereby increasing the production rate. The cooling system also has an impact on the temperature distribution of the part when it is ejected from the mold. A poorly designed cooling system will lead to common cooling related defects of the molded parts, such as sink marks and thermal residual stress. Also, since approximately 5% of part shrinkage takes place after the part is ejected [3], parts that are ejected before being sufficiently cooled may exhibit warpage. Thus, it is clear that improving the design of the cooling system can enhance the overall performance of injection molds. Yet, the cooling system remains one of the most under-engineered systems in injection molds [4]. The probable reason for this lack of attention is that the configuration of the conventional cooling systems is severely restricted by the traditional method of creating cooling channels – gun-drilling, and the subsequent conflict between the arrangement of the cooling system and other components in the mold, such as ejector pins and support pillars. However, with the increasing demand for higher quality and increased complexity of injection molded plastic products and higher production rate for the molding process, improvement and optimization of the cooling system of injection molds has become a focus of researchers and mold designers. Hence, the investigations carried out in this study focus on a non-conventional cooling system, known as conformal cooling, and its potential for improving the performance of injection molds. Simple schematics of a conventional and a conformal cooling system are shown in Fig. 1.2.

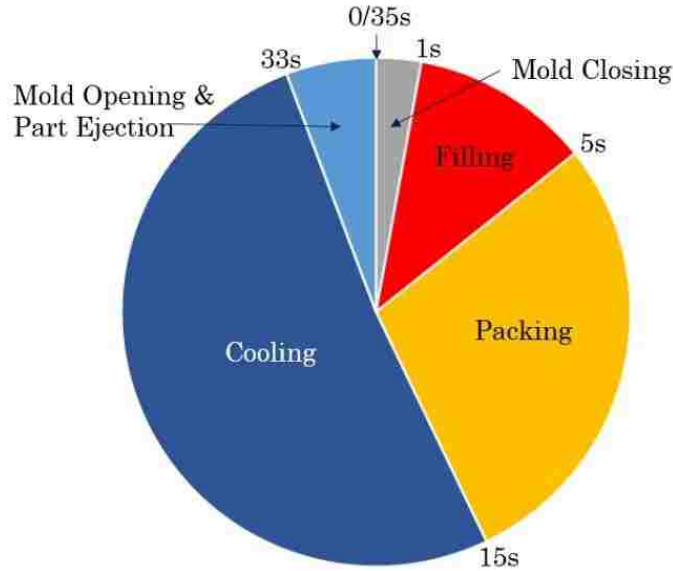


Figure 1.1: Typical molding cycle and cycle time in injection molding [1]

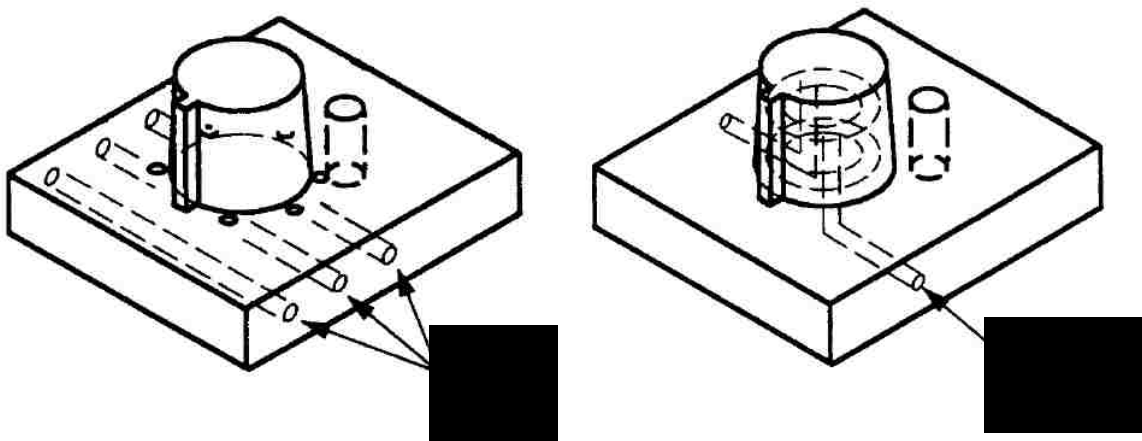


Figure 1.2: Simple schematics of a conventional and a conformal cooling system (reprinted from Sachs et al., 2016 [5])

The cooling of injection molds is carried out by internal cooling channels within the molds. In terms of manufacturing methods, there are two types of cooling channels. One is the conventional (or traditional) cooling channel which is manufactured by gun-drilling and routed by baffles, bubblers, cooling plugs, etc. The design of such conventional cooling channels is still largely based on the known design principles and designers' personal experience and is also influenced by the available machining methods. On the other hand, there is the relatively new concept of conformal cooling channels

which are fabricated by 3D printing technologies such as stereolithography [6], fused deposition modeling [7] and selective laser sintering [8]. With the introduction of metal 3D printing technologies, cooling channels can be designed and manufactured to be more conformal to the working surface from which the heat needs to be removed. This technology offers mold designers a significant degree of freedom in designing new cooling systems. The industry is looking for optimal cooling channel designs that can fully unleash the advantage of conformal cooling channels and lead to a shorter processing time and more uniform cooling [5].

Computational Fluid Dynamics (CFD) can be used to analyze a number of different designs and conduct parametric studies to test the significance of different design parameters. Therefore, a series of simulations have been conducted in order to acquire a more complete understanding of the key parameters that affect the cooling performance. Furthermore, to ensure that the design meets expected performance, the accurate prediction of heat transfer characteristics at the solid-fluid interface is of great importance.

In view of the above remarks, the motivations of the current research are: 1) to identify and determine the influence of important parameters on simulating internal cooling applications, 2) to analyze the potential of conformal cooling channels over conventional cooling channels and 3) to develop general suggestions for the design of conformal cooling channels with U-shape bends.

In the first stage of this numerical investigation, the simulation in a simple geometry is conducted to validate the numerical models and simulation setup, and to identify the parameters that have a significant effect on the modelling of heat transfer in complicated conformal cooling channels.



Figure 1.3: Plastic fog lamp cover

In an injection mold, two mold inserts, referred to as the core-side and cavity-side, form a cavity to produce the plastic part. Conformal cooling channels have the potential to be placed more aligned to the working surface of the mold (cavity wall) and remove the heat faster and more uniformly. This is especially true in the core-side of the mold, because the cooling of the core-side is hard to render with conventional manufacturing methods. Therefore, in the second stage of this study, one specific core-side mold-insert, which is used to produce the plastic fog lamp cover showed in Fig. 1.3 is used to compare the cooling performance of conventional cooling channels and conformal cooling channels. CAD models of the conventional cooling channel and the conformal cooling channel were provided by Proper Group International.

The design of the cooling system of an injection mold requires a number of considerations, such as coolant quality, pressure drop, available pumping power, displacement of the sprue-runner-gate system and ejection system. Aside from these factors, we focus attention on the three-dimensional configurations of the cooling channels in this study.

Since the design of an injection mold cooling system is highly dependent on the geometry of the molded part, a general design scheme is subsequently hard to pursue. This also explains why conformal cooling channels are highly effective in some applications and are usually easier to manufacture but are not universally the best option. For example, for plate-shaped plastic parts, a conventional cooling channel is quite efficient and is cheaper to manufacture and maintain. Therefore, in the third part of this research, instead of going after a general design method for all injection molds, a simplified core-side mold-insert which represents injection molds that are used to produce plastic products which have a deep concave geometry is constructed using CATIA v5 package. Traditionally, baffles or bubblebers are employed in conventionally drilled straight cooling channels for this type of plastic part. The newly introduced conformal cooling channels have the potential to be uniformly placed in these regions. Specifically, the cooling performance of conformal cooling channels with U-shaped bends and its influencing factors are studied in this part of the research.

Computational Fluid Dynamics (CFD) is utilized in this study to simulate the turbulent coolant flow in the cooling channel and the conjugate heat transfer within the mold. The commercial CFD code Star-CCM+ v11.06 is used to set up the meshes in the computational domain and to define the physics at the boundaries and in different regions. Since the overall cooling performance is of interest in this study, steady state simulations are employed. For these simulations, it is assumed that the working surface is constantly being heated and the cooling system reaches an equilibrium state.

This thesis consists of six chapters. In chapter 2, the literature about conformal cooling channel design and analysis is reviewed along with a discussion of turbulence modelling methodologies. The validation of the numerical model utilized in this study is discussed in the third chapter. In chapter 4, the cooling performances of a conventional cooling system and a conformal cooling system for one specific mold insert, which is used to

produce the plastic fog lamp shown in Fig 1.3, are compared in light of numerical results. To obtain general suggestions for future designs of conformal cooling channels, a parametric study utilizing a simplified CAD model is discussed in chapter 5. Finally, conclusions are drawn in the sixth chapter.



# Chapter 2

## Literature Review

With the increasing consumer demand for higher quality plastic products and the injection molding industries demand for higher production rates, many researchers and mold designers have been investigating the performance of the cooling system in injection molds. As demonstrated in Fig. 1.1, a well-designed cooling system has great potential to improve the overall performance of injection molds and the molding process. Researchers are especially focused on conformal cooling channels which are rendered feasible by the growth of metal 3D printing technologies. In this chapter, previous studies of conformal cooling channels are reviewed and summarized. Also, due to the importance of conjugate heat transfer in internal cooling applications, methodologies for modelling the turbulent flow and heat transfer are reviewed as well, and four commonly used turbulence models are summarized at the end of the chapter.

### 2.1 Previous Studies

The potential benefit of conformal cooling channels on improving the performance of injection molds was first reported by Sachs et al. [5]. A comparison was made between a 3D printed conformal cooling channel and a straight drilled conventional cooling channel for an injection mold which is used to produce a split-ring-shape plastic part. The temperature in three

locations in the mold and the dimensions of the molded parts were measured. Both experimental and numerical methods were used, and good agreement was found between the experimental and numerical results. The research concluded that conformal cooling channels can provide superior temperature control within the molding cavity, less elevation of mold temperature as the molding runs start, lower magnitude of transient temperature changes within an individual molding cycle and better molded part quality compared to molding inserts with straight-drilled cooling channels. A criterion for a cooling system to be considered as conformal was also derived based on the transient cooling behaviour at the beginning of the molding runs. Xu et al. [9] further provided a modular design methodology of conformal cooling channels by decomposing the complex mold working surface into manageable cooling zones. This modular design approach was then coupled with the geometrical design window confined by six design rules to generate conformal cooling channels for cavity with complex geometries. The six design rules used by Xu et al. [9] are the requirement of conformal cooling (i.e., the mold temperature reaches steady state within the first molding cycle), the requirement of pressure drop, coolant temperature uniformity, sufficient part cooling, uniform cooling and the requirement of mold strength and deflection. Xu and Sachs [10] also reported a study on the performance of a conformal cooling channel in thermal control for mold heating purposes, thereby extending the advantage of conformal cooling channels to rapid thermal cycling.

A number of other researchers have also reported comparison studies between conventional cooling channels and conformal cooling channels, or between different conformal cooling channel designs, using different numerical methodologies and different commercial packages. Marquez et al. [11] reported a numerical study on two different conformal cooling channel configurations, namely parallel and series routing, for the mold insert which is used to produce a plastic tray holder for eggs. The commercial code Moldflow was used. Hsu et al. [12] provided comparison studies between

conventional and conformal cooling channels for a mold insert which is used to produce a plastic cover of a hand tool, using Moldex3D. The same research group also conducted a similar study [13] on a mold insert which is used to produce a plastic camera cover. Moldex3D was also used in this study and turbulence of the coolant flow and the effect of surface roughness of the cooling channel walls were also considered. All of these comparison studies concluded that the conformal cooling channel has the potential to provide superior cooling performance against conventionally straight drilled cooling channels.

Agazzi et al. [14] suggested a new design approach for conformal cooling channels based on morphological surfaces. The shape of the channel cross-section is no longer limited to circular in this type of design approach. However, this approach may generate other problems, in particular the structural integrity of the large cooling cavity could be compromised by such a design.

The research group at Indiana University - Purdue University has conducted a series of numerical studies on optimizing a spiral cooling channel for the mold inserts which are used to produce a bottle cap shaped plastic part by utilizing ANSYS workbench [15–18]. Design parameters provided by Kazmer [4], namely channel diameter, depth of channel and pitch distance between channels, which were initially derived for the design of conventional cooling channels, were used to construct a parametric study to find the optimal combination of these parameters for spiral conformal cooling channels. Fauzun et al. [19] has also developed a formula to determine the size and position of spiral conformal cooling channels for a cylindrical shaped plastic part.

Kurnia et al. [20] reported a study on comparing the cooling performance of different cooling channel designs for electronic chips using numerical simulations. Also, they developed Figure of Merit (FoM) parameter

which is essentially the heat withdrawn per unit pumping power. It is a good measurement of the overall performance of the cooling system.

There are also studies on using conformal cooling channels in other industrial applications. Hu et al. [21] reported a numerical study which compared five internal cooling channel designs for hot stamping tools. The commercial code Star-CCM+ was used to model the turbulent coolant flow and conjugate heat transfer within the hot stamping tool. Four Reynolds number covering the range 4000 to 400,000 were tested. Six assessment criteria were used to compare the cooling performance between different cooling channel designs: maximum temperature, average temperature, temperature uniformity, pressure drop, maximum velocity in the channel and FoM. It was concluded that parallel longitudinal configurations provide the best cooling performance at high Reynolds numbers considering the six aforementioned assessment criteria. He et al. [22] further improved and optimized the conformal cooling channels with longitudinal configurations for a specific hot stamping tool insert. Experiments with a single straight pipe heat exchanger have also been used by Hu et al. [21] to validate their numerical model and simulation set up for the numerical study of five conformal cooling channel designs. Ying et al. [23] used the results of the single straight pipe experiments to investigate the convection heat transfer coefficient of circular cross-sectional channels and the significances of its influencing factors, such as inlet flow mass flow rate, inlet flow temperature, inlet flow turbulent intensity, channel diameter, surface roughness and furnace temperature.

Park and Dang [2] reported a numerical study on optimizing conventional cooling channels with arrays of baffles to achieve an equivalent conformal cooling effect. They also created a reciprocal algorithm by conjugating transient 1D simulations with steady 3D simulations to approximate the cyclic temperature behaviour of the injection mold. Heat transfer in the polymer material is treated as transient and solved by a 1D

finite difference method, while heat transfer in the mold is treated as cycle-averaged steady state and solved by a 3D finite element method.

The current study focuses on cooling channels for a type of injection mold with a deep concave core, and straight channels with U-shaped bends are utilized in the cooling channel configurations. Cvetkovski et al [24] studied and compared the individual effect of Dean number and Reynolds number on the cooling and heating performance of channels consisting of straight and U-shape bends for geothermal applications. Two Reynolds numbers (2000 and 5000) and three Dean numbers (1500, 1750 and 2000) were tested by DOE (Design of Experiment) with full factorial design. From their study they concluded that Reynolds number has a significant effect on the averaged heat flux through the channel wall of the entire cooling system. On the other hand, Dean number has greater effect on the cooling performance in the curved sections of the cooling channel.

The previous studies on conformal cooling channels can be roughly classified into two types. One type of study is focused on comparing performances of different cooling system designs. Various analysis approaches from this type of research are adopted in this thesis to compare the performance of a conventional and a conformal cooling system. The other type of research aims to produce general design guidelines for new conformal cooling channels by using various methodologies. In the last part of this thesis, three geometrical design parameters for conformal cooling channels consisting of U-shape bends are chosen to conduct a parametric study to evaluate their significance on the cooling performance.

## **2.2 Turbulence Modelling**

The numerical model of fluid flow and heat transfer is developed from the conservation laws of physics: conservation of mass, conservation of momentum (Newton's second law) and conservation of energy (first law of thermodynamics) [25]. These fundamental laws are expressed as:

Conservation of mass:

$$\frac{\partial \rho}{\partial t} + \nabla \cdot (\rho \vec{u}) = 0 \quad (2.1)$$

Conservation of momentum:

$$\frac{\partial}{\partial t} (\rho \vec{u}) + \nabla \cdot (\rho \vec{u} \vec{u}) = -\nabla p + \nabla \cdot \vec{\tau} \quad (2.2)$$

Conservation of energy:

$$\frac{\partial}{\partial t} (\rho E) + \nabla \cdot (\rho E \vec{u}) = -\nabla \cdot (\rho \vec{u}) + \nabla \cdot (k \text{ grad } T) + \nabla \cdot (\vec{u} \cdot \vec{\tau}) \quad (2.3)$$

All variables in Eqns. (2.1) - (2.3) are defined in the Nomenclature.

### 2.2.1 Reynolds-Averaged Navier-Stokes (RANS) Modelling

To reduce the computational cost of turbulent flow simulations, the solutions of the exact Navier-Stokes equations are decomposed into time-averaged and fluctuating components as following [26]:

$$\vec{u} = \bar{\vec{u}} + \vec{u}' \quad (2.4)$$

$$\phi = \bar{\phi} + \phi' \quad (2.5)$$

where  $\bar{\vec{u}}$  represents velocity and  $\phi$  represents scalar quantities like pressure, energy, species, etc. The overbar notation represents the time-averaged component, and the prime symbol represents the fluctuating component.

Substituting Eqns. (2.4) and (2.5) into the original continuity and momentum equations (2.1) and (2.2), the time-averaged continuity equation and momentum equation are obtained as:

$$\frac{\partial \rho}{\partial t} + \nabla \cdot (\rho \bar{\vec{u}}) = 0 \quad (2.6)$$

$$\begin{aligned} & \frac{\partial}{\partial t} (\rho \bar{\vec{u}}) + \nabla \cdot (\rho \bar{\vec{u}} \bar{\vec{u}}) \\ & = -\nabla p + \mu \nabla (\text{grad } \bar{\vec{u}}) + \left[ -\frac{\partial}{\partial x} (\overline{\rho \vec{u}' u'}) - \frac{\partial}{\partial y} (\overline{\rho \vec{u}' v'}) - \frac{\partial}{\partial z} (\overline{\rho \vec{u}' w'}) \right] \end{aligned} \quad (2.7)$$

As mentioned previously, steady state simulations are utilized in the current study. Therefore, all the derivatives with respect to time become zero in the governing equations and following turbulence models.

Many turbulence models have been formulated and used to capture the characteristics of turbulence in the flow. The three most commonly used approaches to simulate turbulent flows are Reynolds-Averaged Navier-Stokes (RANS) equations, Large-Eddy Simulations (LES) and Direct Numerical Simulations (DNS) [26]. Though LES and DNS models have gain popularity in the academic research community, RANS models are still popular in industry for its economy, robustness and reasonable accuracy in simulating a wide range of turbulent flows [27]. Four different turbulence models which are commonly used in RANS modeling are briefly described below.

### 2.2.1.1 Standard $k$ - $\varepsilon$ Model

The standard  $k$ - $\varepsilon$  model is a semi-empirical two-equation RANS turbulence model which is represented by the transport equations for the turbulence kinetic energy ( $k$ ) and its dissipation rate ( $\varepsilon$ ) [28]:

$$\frac{\partial}{\partial t}(\rho k) + \nabla \cdot (\rho k \vec{u}) = \nabla \cdot \left[ \left( \mu + \frac{\mu_t}{\sigma_k} \right) \text{grad } k \right] + G_k - \rho \varepsilon \quad (2.8)$$

$$\frac{\partial}{\partial t}(\rho \varepsilon) + \nabla \cdot (\rho \varepsilon \vec{u}) = \nabla \cdot \left[ \left( \mu + \frac{\mu_t}{\sigma_\varepsilon} \right) \text{grad } \varepsilon \right] + C_{1\varepsilon} \frac{\varepsilon}{k} G_k - C_{2\varepsilon} \rho \frac{\varepsilon^2}{k} \quad (2.9)$$

in which the eddy viscosity ( $\mu_t$ ) and the production of turbulent kinetic energy ( $G_k$ ) are given by:

$$\mu_t = \rho C_\mu \frac{k^2}{\varepsilon} \quad (2.10)$$

$$G_k = -\rho \overline{u'_i u'_j} \frac{\partial u_j}{\partial u_i} \quad (2.11)$$

There are three dimensionless constants and two Prandtl numbers in the transport equations for the standard  $k$ - $\varepsilon$  turbulence model. Their values are determined as follows, by considering a wide range of turbulent flows:

$$C_\mu = 0.09, C_{1\varepsilon} = 1.44, C_{2\varepsilon} = 1.92, \sigma_k = 1.0 \text{ and } \sigma_\varepsilon = 1.3.$$

Fully developed flow was assumed in the derivation of the standard  $k$ - $\varepsilon$  model, and the effects of molecular viscosity are neglected. Also, curvature is not accounted for since the model is based on flow over a flat plate. Therefore, the standard  $k$ - $\varepsilon$  model is valid only for fully turbulent flows and is known to be sensitive in the near-wall region.

### 2.2.1.2 Realizable $k$ - $\varepsilon$ Model

The Realizable  $k$ - $\varepsilon$  model is development from the standard  $k$ - $\varepsilon$  model [29]. The standard  $k$ - $\varepsilon$  model and Realizable  $k$ - $\varepsilon$  model share the same transport equation for turbulent kinetic energy ( $k$ ), but the latter one has a new transport equation for the dissipation rate ( $\varepsilon$ ), which is derived from an exact equation for the transport of the mean-square vorticity fluctuation:

$$\frac{\partial}{\partial t}(\rho\varepsilon) + \nabla \cdot (\rho\varepsilon\vec{u}) = \nabla \cdot \left[ \left( \mu + \frac{\mu_t}{\sigma_\varepsilon} \right) \text{grad } \varepsilon \right] - C_2\rho \frac{\varepsilon^2}{k + \sqrt{v\varepsilon}} \quad (2.12)$$

The Realizable  $k$ - $\varepsilon$  model has the same formulation for the turbulent viscosity as Eqn. (2.10), but the coefficient  $C_\mu$  is not constant any more compared to the standard  $k$ - $\varepsilon$  model, and it is expressed as:

$$C_\mu = \frac{1}{A_0 + A_s \frac{kU^*}{\varepsilon}} \quad (2.13)$$

where

$$U^* = \sqrt{S_{ij}S_{ij} + \tilde{\Omega}_{ij}\tilde{\Omega}_{ij}} \quad (2.14)$$

and

$$\tilde{\Omega}_{ij} = \Omega_{ij} - 2\varepsilon_{ijk}\omega_k \quad (2.15)$$

$$\Omega_{ij} = \overline{\Omega_{ij}} - \varepsilon_{ijk}\omega_k \quad (2.16)$$

The coefficients which are different from the standard  $k$ - $\varepsilon$  model are

$$C_2 = 1.9, \sigma_\varepsilon = 1.2, A_0 = 4.04, A_s = \sqrt{6}\cos\phi$$



where

$$\phi = \frac{1}{3} \cos^{-1}(\sqrt{6}W), W = \frac{S_{ij}S_{jk}S_{ki}}{\tilde{S}^3}, \tilde{S} = \sqrt{S_{ij}S_{ij}}, S_{ij} = \frac{1}{2} \left( \frac{\partial u_j}{\partial x_i} + \frac{\partial u_i}{\partial x_j} \right)$$

The Realizable  $k$ - $\varepsilon$  is substantially better than the standard  $k$ - $\varepsilon$  model for many applications. Furthermore, the Realizable Two-Layer  $k$ - $\varepsilon$  model is a turbulence model offered by Star-CCM+ v10.06, it combines the Realizable  $k$ - $\varepsilon$  model with a two-layer approach. The coefficients in the model are identical with the Realizable  $k$ - $\varepsilon$  model, but the model gains the added flexibility of an all  $y^+$  wall treatment [29].

### 2.2.1.3 Standard $k$ - $\omega$ Model

The standard  $k$ - $\omega$  model, also known as Wilcox's  $k$ - $\omega$  model, is another empirical two-equation turbulence model based on model transport equations for the turbulent kinetic energy ( $k$ ) and the specific dissipation rate ( $\omega$ ). The transport equations are as follows:

$$\frac{\partial}{\partial t}(\rho k) + \nabla \cdot (\rho k \vec{u}) = \nabla \cdot \left[ \left( \mu + \frac{\mu_t}{\sigma_k} \right) \text{grad } k \right] + G_k - \beta^* \rho k \omega \quad (2.17)$$

$$\frac{\partial}{\partial t}(\rho \omega) + \nabla \cdot (\rho \omega \vec{u}) = \nabla \cdot \left[ \left( \mu + \frac{\mu_t}{\sigma_\omega} \right) \text{grad } \omega \right] + \alpha \frac{\omega}{k} G_k - \beta_1 \rho \omega^2 \quad (2.18)$$

where the eddy viscosity ( $\mu_t$ ) is given by:

$$\mu_t = \alpha^* \frac{\rho k}{\omega} \quad (2.19)$$

in which the coefficient  $\alpha^*$  damps the turbulent viscosity causing a low-Reynolds-number correction. The rate of production of turbulent kinetic energy ( $G_k$ ) is given by:

$$G_k = -\rho \overline{u_i' u_j'} \frac{\partial u_j}{\partial u_i} \quad (2.20)$$

The empirical constants in the standard  $k$ - $\omega$  model are:

$$\sigma_k = 2.0, \sigma_\omega = 2.0, \gamma_1 = 0.553, \beta^* = 0.09 \text{ and } \beta_1 = 0.075$$

The standard  $k$ - $\omega$  turbulence model is known to be sensitive to the inlet freestream turbulence properties.

#### 2.2.1.4 Shear Stress Transport (SST) $k$ - $\omega$ Model

The SST  $k$ - $\omega$  model, also known as Menter's  $k$ - $\omega$  model, has the same  $k$ -equation as in the standard  $k$ - $\omega$  model, but the  $\omega$ -equation is transformed from an  $\varepsilon$ -equation by substituting  $\varepsilon = k\omega$ . This yields [26]:

$$\begin{aligned} & \frac{\partial}{\partial t}(\rho\omega) + \nabla \cdot (\rho\omega\vec{u}) \\ & = \nabla \cdot \left[ \left( \mu + \frac{\mu_t}{\sigma_{\omega,1}} \right) \text{grad } \omega \right] \\ & + 2(1 - F_1)\rho\sigma_{\omega 2} \frac{1}{\omega} \text{grad}k(\text{grad}\omega) + \alpha \frac{\omega}{k} G_k - \beta\rho\omega^2 \end{aligned} \quad (2.21)$$

in which  $F_1$  is the blending function. The production term of turbulent kinetic energy ( $G_k$ ) is defined in the same manner as Eqn. (2.19) in the standard  $k$ - $\omega$  model.

The revised model constants are:

$$\sigma_k = 1.0, \sigma_{\omega,1} = 2.0, \beta^* = 0.09 \text{ and } \beta_1 = 0.083$$

This transformation effectively blends the freestream independence of the  $k$ - $\varepsilon$  model in the freestream with the robust and accurate formulation of the  $k$ - $\omega$  model near the wall. SST  $k$ - $\omega$  model is selected in this study due to its ability of resolving turbulence flow with negative pressure gradient and flow separations.

# Chapter 3

## Validation

Due to the existence of unavoidable uncertainties in CFD modelling [26], a basic requirement for any CFD study is to conduct a rigorous process of validation to determine the level of confidence in the numerical results. The validation process is carried out by comparing the results of numerical simulation with experimental data. If the difference between the computational and experimental results of the target quantity is sufficiently small, the CFD model is considered to be validated. Once the numerical model has been validated, it will be used for a comparative study of the cooling performance of a conventional cooling channel and a conformal cooling channel for a specific mold core-insert for the fog lamp shown in Fig. 1.3. Due to the high cost of the fabrication of inserts with conformal cooling channels, it is not feasible to manufacture the specific test insert used for this study. Therefore, the experimental data reported by Hu et al. [21] and Ying et al. [23] have been used for the validation of the numerical model utilized in this study. They examined the heat transfer mechanism along a single straight cooling pipe.

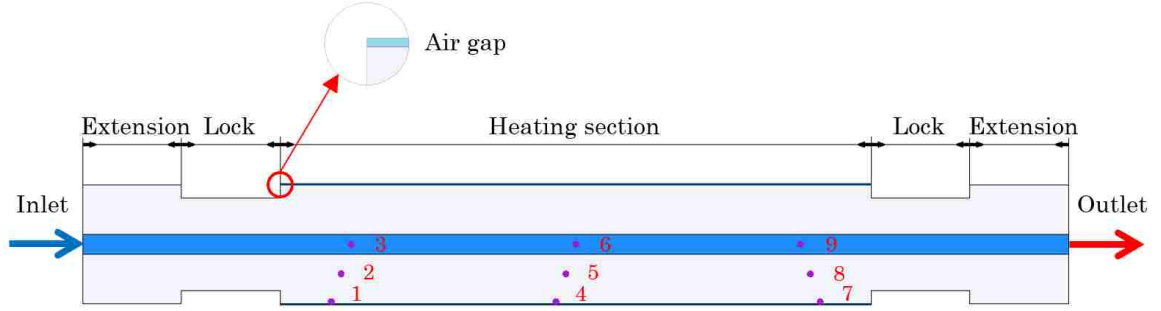


Figure 3.1: Geometry of the straight pipe heat exchanger and positions of the nine measuring points [21,23]

Figure 3.1 shows a sketch of the heat exchanger used in the experiments [21]. The heat exchanger consists of a H13 steel cylinder block with a circular cross-section straight cooling channel running through the centre of it. The cylinder block has the length of 500 mm and the diameter of 60 mm. The diameter of the cooling channel through the cylinder block is 10 mm. The surface of the middle section (Heating section in Fig. 3.1) of the steel block is constantly heated by an electric resistance furnace which maintains the temperature at 600 °C. Two steps (Lock sections in Fig. 3.1) are manufactured on the block to hold the steel block and fix its location in the electric furnace. Water, as the coolant, is supplied from one side of the channel at a temperature of 20 °C and at two different mass flow rates of 0.124 kg/s and 0.225 kg/s. Temperature data from nine measuring points were collected after the readings became steady [21]. The data acquired from the experiments were used by Ying et al. [23] to evaluate the convective heat transfer coefficient of the straight cooling channel in both the hydrodynamic and thermal entrance regions and assess the influence of several key parameters, including inlet mass flow rate, inlet temperature, inlet turbulence intensity, channel diameter, channel wall surface roughness and furnace temperature.

The  $k-\varepsilon$  turbulence model is widely adopted by industries to simulate turbulent flow because of its robustness and less computational cost. However, for the complex geometries associated with conformal cooling

channel applications, the heat transfer mechanism within the boundary layer needs to be well resolved due to its influence on the performance of the entire system. The  $k\text{-}\omega$  turbulence model with a low Reynolds number correction can predict flow in such regions more accurately than a  $k\text{-}\varepsilon$  model. In the current study, the Shear Stress Transport (SST)  $k\text{-}\omega$  turbulence model, a modified version of the standard  $k\text{-}\omega$  turbulence model, is used to simulate the coolant flow and the convective heat transfer in the cooling channel. This study aims to establish the validity of the SST  $k\text{-}\omega$  turbulence model for simulating turbulent flow in a circular cross-section channel with conjugate heat transfer.

To accurately predict the cooling performance of internal cooling channels, it is critical to properly model the heat transfer mechanism near the solid-liquid interfaces. The effect of two important influencing factors are also studied during the validation process. First, two commonly used turbulence models, Realizable  $k\text{-}\varepsilon$  and SST  $k\text{-}\omega$  models, are applied in the simulations and the numerical results are compared with experimental results to assess the performance of these models and confirm their validity on simulating internal cooling applications. Then two inlet flow conditions, namely uniform velocity inlet and fully developed velocity inlet, have been applied at the inlet boundary to compare their effect on the heat transfer. A mesh independence study also has been conducted to ensure the accuracy of the numerical results.

## **3.1 Numerical Model Setup**

### **3.1.1 Computational Domain and Governing Equations**

The computational domain of the validation simulations is defined with the same dimensions of the test heat exchanger used in the experiments of Hu et al. [21]. It consists of three regions, namely air, water (fluid) and solid regions. The air region is created to simulate the thermal radiation and conduction in the air gap between the working surface of furnace and the

heated surface of the test pipe (see Fig. 3.1), which provides a heat source to the heating section of the test pipe. The effect of convective heat transfer is assumed negligible due to the small distance between the working surface of the furnace and the heated surface of the test pipe compared to the axial dimension of the air gap. Therefore, the main heat transfer models applied for the air region is surface-to-surface radiation and conductive heat transfer. The essence of the applications within a solid block with a cooling channel running through it is conjugate heat transfer. Conductive heat transfer is the main heat transfer mechanism in the solid region, governed by Fourier's Law. For the fluid region, the Reynolds-Averaged Navier-Stokes (RANS) equations are solved to predict the turbulent flow inside the cooling channel, and convective heat transfer is considered as well through the energy equation. The SST  $k-\omega$  model is of interest since the conformal cooling channels have complex geometries and the flow is turbulent with adverse pressure gradients and separations. The SST  $k-\omega$  model will be compared with Realizable  $k-\epsilon$  predictions of the performance for internal cooling applications.

### 3.1.2 Boundary Conditions

#### Air region:

Due to the significant effect of thermal radiation in the air region, proper radiative properties are assigned based on the materials of the test pipe and furnace. The emissivity of the furnace working surface is taken as 0.8 and the emissivity of the pipe surface is taken as 0.9.

- **Working surface of the furnace:** The temperature of 600 °C is applied at the working surface of the furnace (the outer surface of the air gap) shown in Fig. 3.1 [21], i.e.,
  - $T_{Heating\ surface} = 600\ ^\circ\text{C}$
- **Side walls:** Side walls of the air region are assumed to be adiabatic due to their small size compared to the axial dimensions. According to Ying

et al. [23], the gap between the furnace heating surface and heated surface of the pipe is assumed to be 0.7 mm. Therefore,

- $\dot{q}_w = 0, T_w = \textit{computed}$

**Solid region:**

- **Extension sections:** Both extension sections shown in Fig. 3.1 are exposed to the surrounding areas in the experiments [21], so environmental boundary conditions, which simulate the radiation and natural convective heat transfer between the exposed pipe surface and surrounding areas, are applied, i.e.,

- $\dot{q}_w = h_\infty(T_\infty - T_w)$

In this expression  $T_\infty$  is ambient temperature, equal to 20 °C,  $h_\infty$  is the external heat transfer coefficient, specified as 20 W/m<sup>2</sup> · K and the emissivity of the exposed surface is 0.1, as determined by Ying et al. [23]. Wall temperature  $T_w$  and wall heat flux  $\dot{q}_w$  are computed during the simulation.

- **Lock sections:** Both lock sections are assumed to be adiabatic because they are in contact with the insulation material of the furnace and are not directly heated by the working surface of the furnace, therefore

- $\dot{q}_w = 0, T_w = \textit{computed}$

**Fluid region:**

- **Inlet:** Two mass flow rates, 0.124 kg/s and 0.225 kg/s, and two different inlet flow conditions, namely uniform velocity inlet (or mass flow inlet) and fully developed velocity inlet, are applied at the inlet boundary. Based on the channel diameter of 10 mm, the corresponding Reynolds number for the two mass flow rates of 0.124 kg/s and 0.225 kg/s are 17739 and 32188, respectively. The fully developed velocity inlet is obtained from separate simulations with a channel of same diameter as the cooling channel in the test pipe, and a periodic interface created between inlet and outlet. The velocity, turbulence intensity and

turbulence viscosity ratio data of the fully developed flow are mapped at the inlet boundary of the validation simulations. The temperature at the inlet is specified as 20 °C for all simulations.

- Uniform velocity inlet:  $V_{in} = constant$
- Fully developed velocity inlet:  $V_{in} = f(v, I, \mu_t/\mu, x, y, z)$   
Here,  $I$  represents turbulence intensity and  $\mu_t/\mu$  is turbulence viscosity ratio.
- $T_{in} = 20^\circ\text{C}$
- **Outlet:** With a split ratio of 1, flow split outlet is assigned to conserve the mass flow rate specified at the inlet, i.e.,
  - $\dot{m}_{out} = \dot{m}_{in}$

Mapped contact interfaces between the air and solid regions and between the solid and fluid regions are created to properly transmit the data through the interfaces in between, which is critical for simulating the conjugate heat transfer problem.

### 3.1.3 Physical Properties

In the application of injection molding, the temperature of the coolant adjacent to the cooling channel wall can be much higher than that in the centre of the channel, mainly due to the high temperature of melt polymer. Thus, temperature dependent properties of water are represented as a polynomial or a field function of temperature and programmed into the software. Equations for relevant flow parameters are:

The density of water [23] as a function of temperature is expressed as:

$$\rho_w = 3.7 \times 10^{-7}T^3 - 3 \times 10^{-3}T^2 + 1.4T + 838.46. \quad (3.1)$$

The dynamic viscosity of water [20] is related to temperature by

$$\mu_w = 2.591 \times 10^{-5} \times 10^{\left(\frac{238.3}{T-143.2}\right)}. \quad (3.2)$$

and the thermal conductivity of water [20] is given by



$$k_w = -8.354 \times 10^{-6}T^2 + 6.53 \times 10^{-3}T - 0.5981. \quad (3.3)$$

The specific heat capacity of water is considered as constant, taken as  $4180 \text{ J/kg} \cdot \text{K}$  at the temperature of  $25 \text{ }^\circ\text{C}$  [30], due to its relatively small change over the temperature range of coolant in internal cooling applications.

Thermal properties of H13 steel which were used in the experiments [21,23] were determined by Ying et al. [23]. The density of H13 steel is taken as  $\rho_s = 7900 \text{ kg/m}^3$  and the specific heat capacity has a constant value of  $C_{p,s} = 450 \text{ J/kg} \cdot \text{K}$ . The thermal conductivity of H13 steel is represented by a polynomial of temperature:

$$k_s = -3 \times 10^{-5}T^2 + 5.7 \times 10^{-3}T + 42.624. \quad (3.4)$$

### 3.1.4 Mesh

Polyhedral meshes can be constructed with contiguous meshing at interfaces with complex geometry, which provides more accurate data transmission through these interfaces than a non-contiguous mesh. Thereby, a polyhedral mesh is used to discretize all three regions in the validation simulations. The same base mesh size is applied for three regions for consistency, with the minimum and target size of the mesh adjusted to control the density of the mesh in different regions. A larger target mesh size is adopted for the solid region to reduce the number of cells in this region, thereby reduces the overall computing time. Because the heat transfer mechanism near the cooling channel wall is of great importance in this study, 12 layers of prism cells are used to resolve the boundary layer along the cooling channel wall.

A mesh independence study has been conducted to ensure that the numerical results are mesh independent. Three base sizes, 0.75 mm, 1 mm and 1.25 mm, as illustrated in Fig. 3.2, yielding cell counts of 1982456, 1013269 and 622190 respectively, were tested. For a reduction of base size from 1 mm to 0.75 mm, it is found that the largest change of temperature at

the nine measuring points shown in Fig. 3.1 is only 1.7 %, while this difference is 2.4% while reducing the base mesh size from 1.25 to 1. Additional near-wall refinement was also tested using prism layer stretching factors of 1.3, 1.5 and 1.7, as shown in Fig. 3.3, tested along with base size of 1 mm. A difference of only 1 % in the temperature was observed between stretching factors of 1.5 and 1.7. Therefore, the mesh with base size of 1 mm and stretching factor of 1.5, with a cell count of 1013269, was chosen to conduct the single straight pipe simulations for the purpose of validation of the numerical model used in this study.

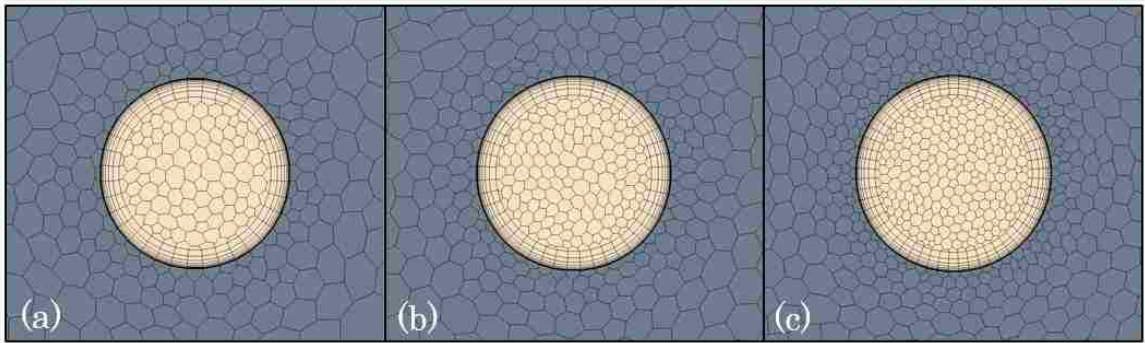


Figure 3.2: Meshes with different base cell sizes: (a) 0.75 mm, (b) 1 mm, (c) 1.25 mm

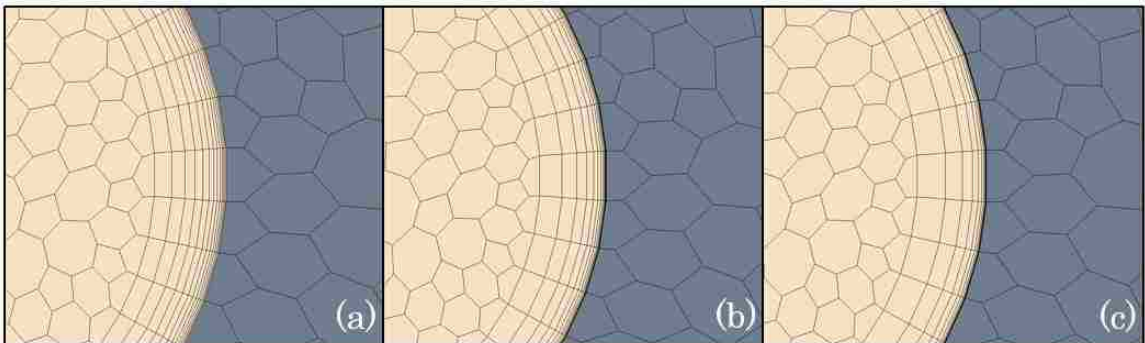


Figure 3.3: Effect of prism layer stretching factors: (a) 1.3, (b) 1.5, (c) 1.7

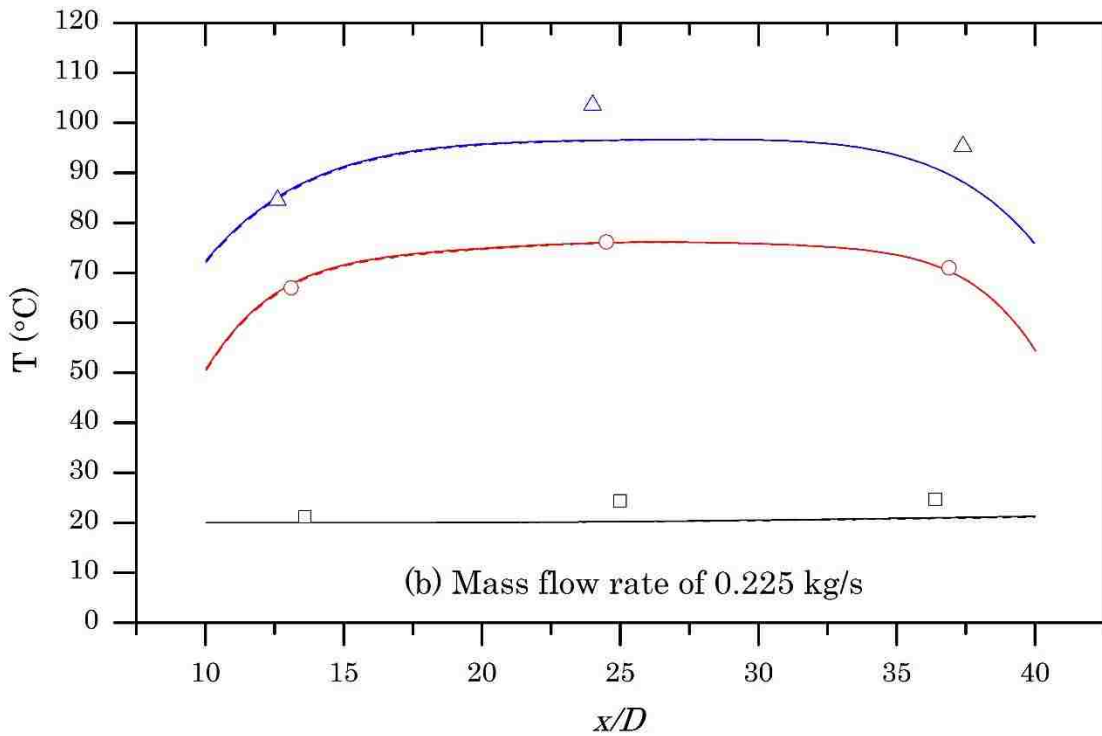
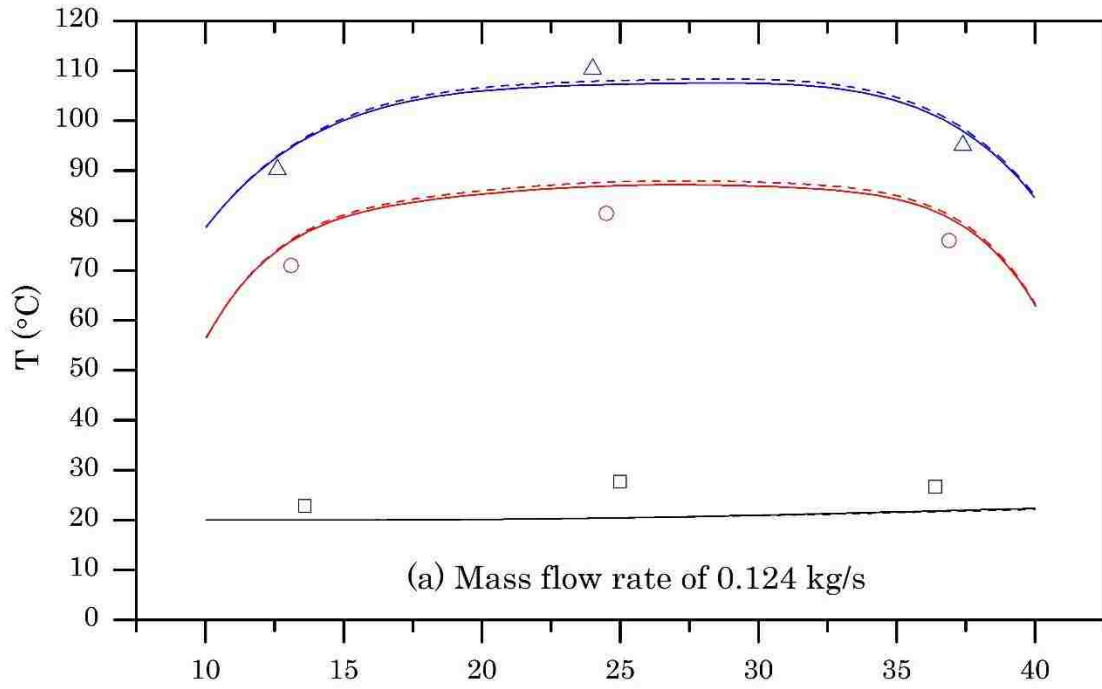
### 3.2 Validation Results and Analyses

First, the uniform velocity inlet is selected along with the two mass flow rates to compare the predictions from the two turbulence models, i.e., Realizable  $k-\varepsilon$  and SST  $k-\omega$  models, on simulating the conjugate heat transfer

problem in a straight cooling channel. Figure 3.4 shows a comparison between the experimental temperature data of Hu et al. [21] and the numerical data using SST  $k-\omega$  model and Realizable  $k-\varepsilon$  model. Results are shown at the centre of the channel, middle of the block (15 mm away from the centre of the channel) and at the surface of the block (30 mm away from the centre of the channel).

Both turbulence models predict the same trend of temperature distribution along both the axial and radial directions. The SST  $k-\omega$  model predicts a slightly lower temperature value than the Realizable  $k-\varepsilon$  model, but the difference become negligible at the higher inlet mass flow rate. At the mass flow rate of 0.124 kg/s, the SST  $k-\omega$  model shows an average error of 9.4% over the nine measuring points against the experimental results, while, at the mass flow rate of 0.225 kg/s, the average error reduces to 6%.

In terms of temperature prediction, Fig. 3.4 demonstrates that the SST  $k-\omega$  and Realizable  $k-\varepsilon$  models have similar performance. Both models have the capability to accurately simulate the conjugate heat transfer process in injection molding tool insets, accurately predicting the temperature distribution inside the tool material and the turbulent flow inside the cooling channel. However, for conformal cooling channel applications, the accuracy of the SST  $k-\omega$  model combined with its capability to resolve the boundary layer in flows with adverse pressure gradients and the recirculation due to flow separations at pipe elbows, suggests that it will have better performance than the Realizable  $k-\varepsilon$  turbulence model. Therefore, the SST  $k-\omega$  turbulence model was adopted for the following validation process and the numerical investigation of conformal cooling channels in Chapter 4 and Chapter 5.



—  $k-\omega$  centre of the channel    —  $k-\omega$  middle of the block    —  $k-\omega$  surface of the block  
 - - -  $k-\epsilon$  centre of the channel    - - -  $k-\epsilon$  middle of the block    - - -  $k-\epsilon$  surface of the block  
 □ Exp centre of the channel    ○ Exp middle of the block    △ Exp surface of the block

Figure 3.4: Temperature distribution at nine measuring points with different mass flow rates: (a) 0.124 kg/s, (b) 0.225 kg/s (Exp refers to [21])

As illustrated in Fig. 3.5, the temperature first increases in the axial direction due to the heat source at the heating section, then drops because of the absence of a heat source and the heat loss through the extension and lock areas at the end of the pipe. In the radial direction, the temperature on the block surface is higher than that in the solid material, which is higher than the temperature of the coolant. This is in good qualitative agreement with the experimental data plotted in Fig. 3.4. It can also be observed that there is heat dissipated to the extension and lock areas at both inlet and outlet ends of the pipe, especially at the outlet end. Even though the heat transfer mechanism in these areas would be complex, they do not have a significant impact on the cooling at the heating section. Therefore, the following analyses will only be focused on the heating section.

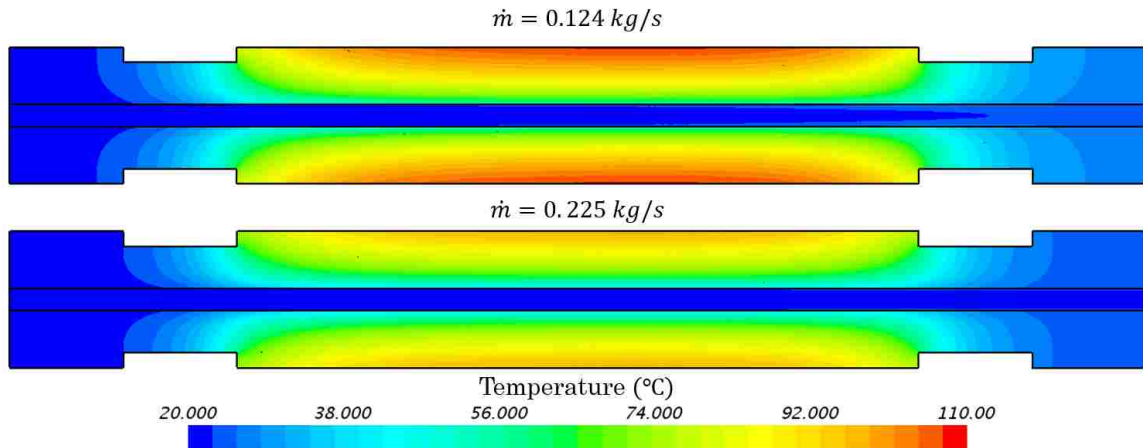


Figure 3.5: Temperature distribution on central plane using SST  $k$ - $\omega$  model

Next, the influence of the inlet flow condition is investigated. If the fully developed velocity inlet is applied, the flow will be in the hydrodynamic developed region at the beginning of the channel. If the uniform velocity inlet (or mass flow inlet) is used, then the flow will evolve to fully developed through a transitional region which is called the hydrodynamic entrance region. For turbulent flow, the length of this entrance region  $L_e$  can be estimated by the following empirical equation [31]:

$$L_e = 4.4(Re)^{\frac{1}{6}}D \quad (3.5)$$

where  $Re$  is the Reynolds number and  $D$  is the channel diameter.

Using Eqn. (3.5), the hydrodynamic entrance length is approximately  $22.5D$  for the mass flow rate of 0.124 kg/s, and  $25D$  for the mass flow rate of 0.225 kg/s. In Hu's experiments [21], the test pipe was connected to a pump which provides the turbulent flow through a tube, therefore, the flow condition at the inlet of the pipe is unknown. However, the combined length of the tube connected with the inlet and the length of extension and contact sections at the inlet is greater than  $25D$ . Therefore, the majority of the channel at the heating section should be within the hydrodynamic developed region for both mass flow rates.

Figure 3.6 shows the velocity profiles across the channel cross-sections at measuring points 3, 6 and 9. These velocity profiles from the simulations with the two different inlet flow conditions show only a very small difference. The largest velocity difference at the centre of the measuring points 3 cross-section is found to be 1.2% for the mass flow rate of 0.124 kg/s. At the cross-section at measuring point 9, where the flow should be fully developed for both inlet flow types, the velocity at the centre of the channel still has 0.6% difference, which is primarily due to the existence of the heat source and the temperature dependent density of water.

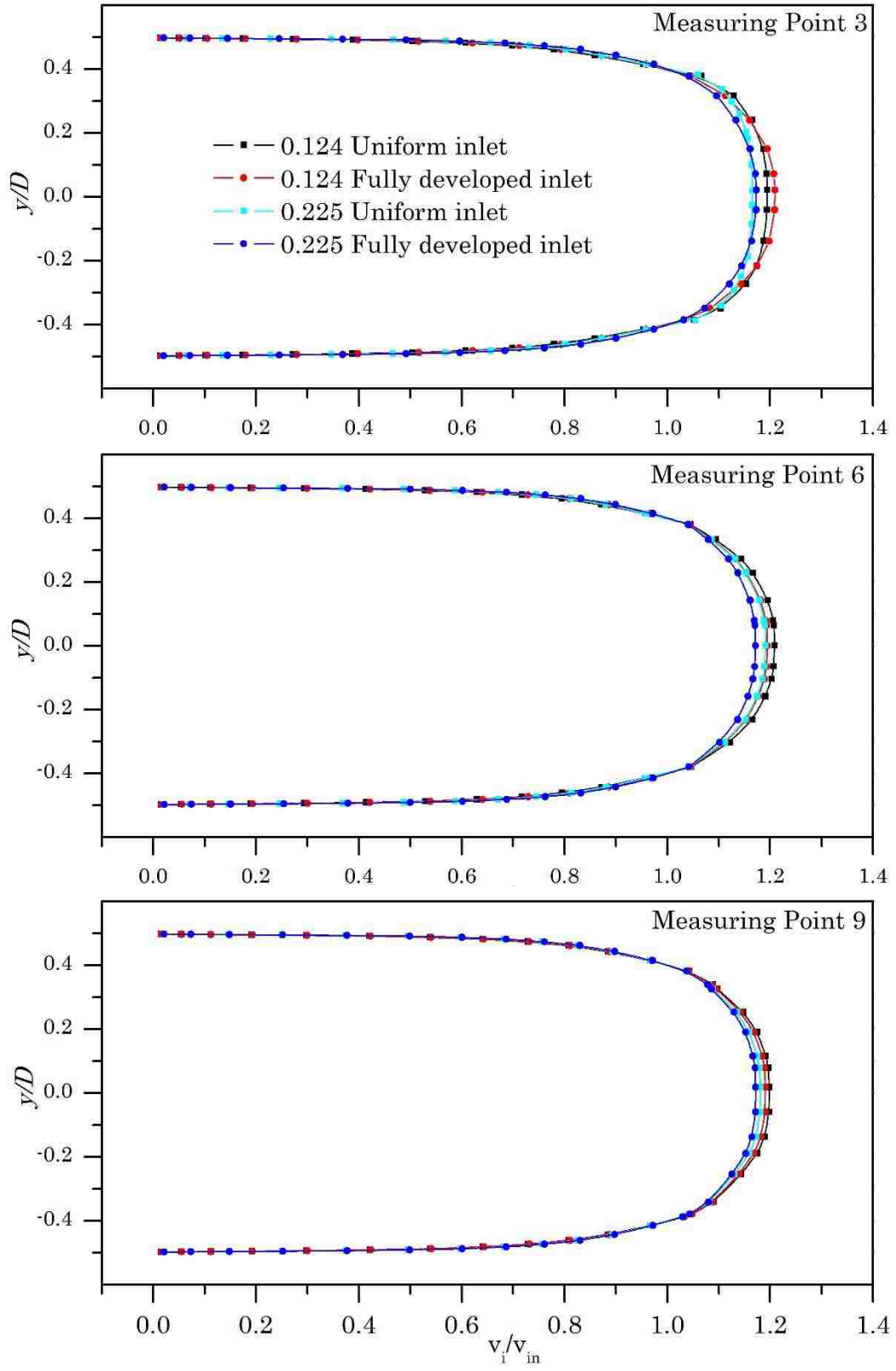


Figure 3.6: Cross-sectional velocity profiles at three measuring positions ( $V_i$  is the streamwise velocity in the pipe and  $V_{in}$  is the inlet velocity)

Figure 3.7 shows the temperature profiles across the pipe at the three measuring point cross-sections to further reveal the difference between the two inlet flow conditions and the mass flow rates on the heat transfer performance. As seen from Fig. 3.7, the cross-sectional temperature distributions at measuring points 3, 6 and 9 for the two inlet boundary conditions are nearly identical, with the largest difference being only 0.6%. The reason for the small difference in the temperature profiles of the two inlet flow conditions can be explained by considering Fig. 3.8, which shows the heat transfer coefficient along the channel wall within the heating section. The same trend appears for both mass flow rates and both inlet flow conditions. The heat transfer coefficient increases rapidly over the first  $5D$  of the heating section as the coolant enters the heat source region, then grows slowly until the last  $5D$ , after which it decreases due to the heat loss to the contact and extension areas near the end of the pipe.



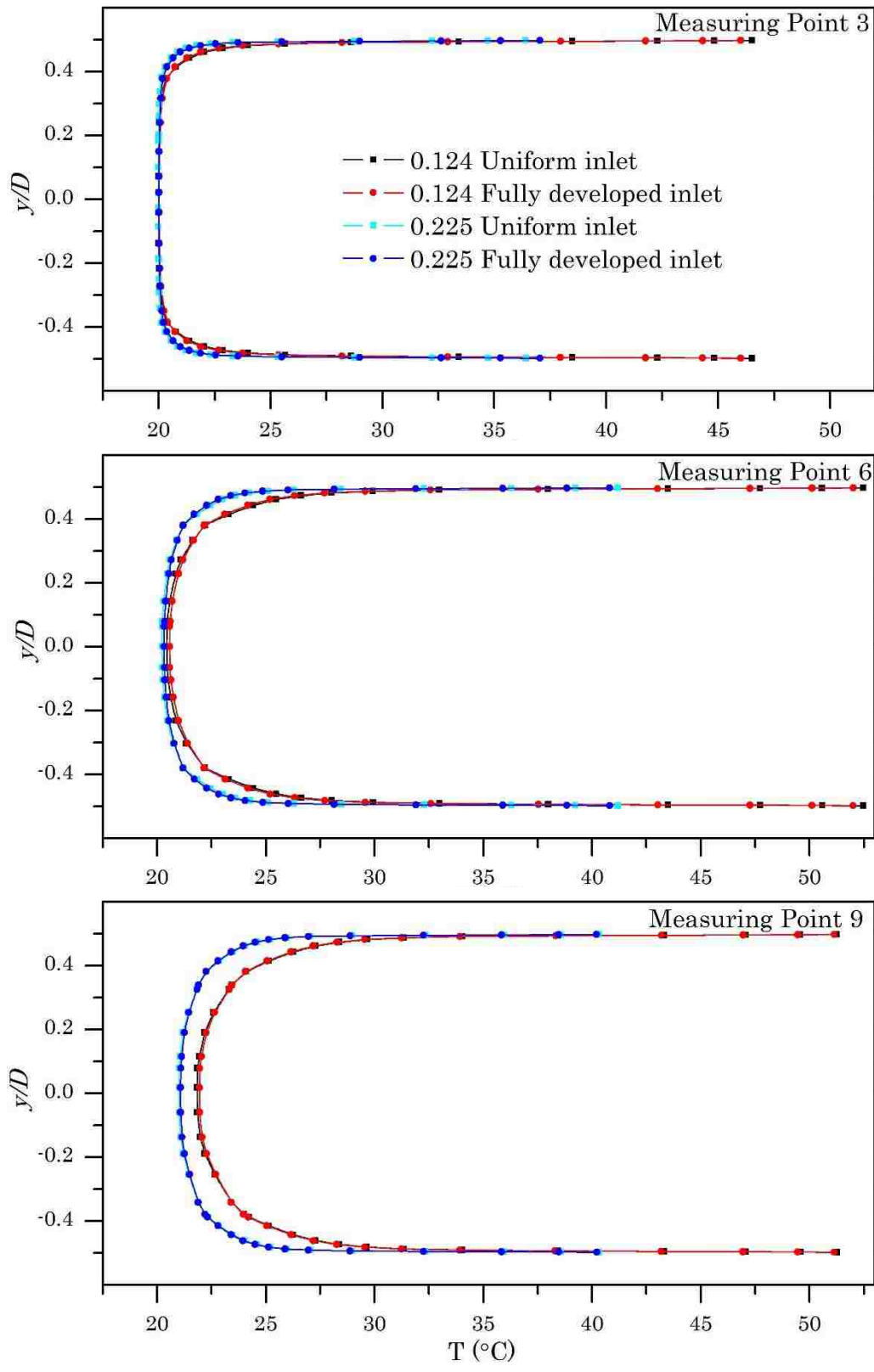


Figure 3.7: Cross-sectional temperature profiles at three measuring positions

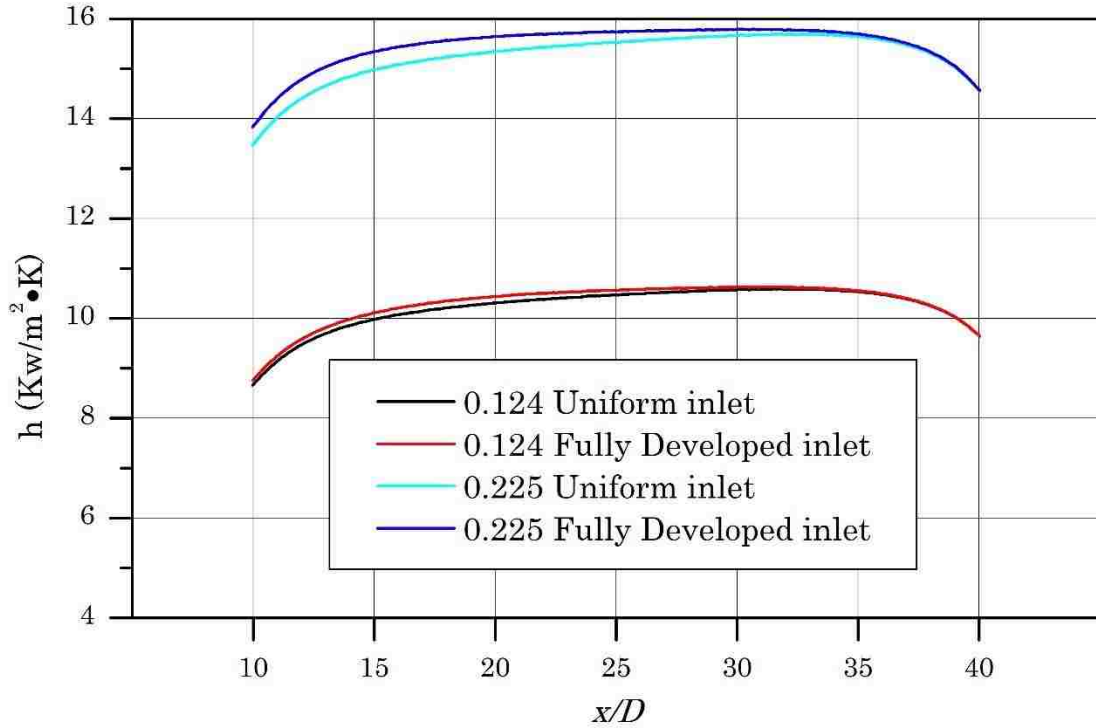


Figure 3.8: Heat transfer coefficient along the channel wall in the heating section

The largest difference in heat transfer coefficient due to the two different inlet flow conditions is observed at the beginning of the heating section, especially for the high mass flow rate case, but the difference becomes negligibly small towards the end of the heating section. However, the largest difference in heat transfer coefficient is just 2.7% for the mass flow rate of 0.225 kg/s. Therefore, whether the flow entering the system is hydrodynamically developed or not, both inlet flow conditions show similar results. Thus, either of the inlet flow condition can be adopted, the selection should be base on the interest of the specific study.

Based on the aforementioned analysis, it can be concluded that the type of inlet flow conditions has minimum influence on prediction of the heat transfer performance of internal cooling applications. The validity of the SST  $k-\omega$  turbulence model on simulating internal cooling applications has been confirmed by comparing numerical results and experimental data reported by

Hu et al. [21] and Ying et al. [23]. Combined with its capability to resolve turbulent flow with adverse pressure gradients and flow separations, as expected for the turbulent flow in complex conformal cooling channels, the SST  $k-\omega$  model can be used for simulating conformal cooling channels applications in plastic injection mold and will be used in the following studies.

## Chapter 4

# Comparison between a Conventional and a Conformal Cooling System

Under actual production circumstances, the determination of the cooling time of a single injection molding cycle is mainly based on the dimensional specifications of the plastic part being molded and is usually measured by try-and-error methods. Because the cooling time is a complex function of product material properties, mold material properties, cooling system design, the dimensional specifications of the molded part and operational conditions that varies between molders [4], the cooling time of one specific injection molding process is difficult to be precisely predicted before it is used in the production. However, the relative cooling performance of different cooling system designs can be compared with the benefit offered by numerical simulations.

A typical injection mold consists of at least two mold inserts, namely the core-insert and the cavity-insert (also known as the male-insert and the female-insert, respectively). These two mold-inserts form a cavity which has the shape identical to the desired molded plastic part. In this study, the core-insert and its cooling system are of interest to demonstrate the potential of conformal cooling channels on improving the cooling performance because the

core-insert is where most of the challenges are encountered by mold designers when designing the cooling system of injection molds. This chapter presents a comparison between the cooling performance of the conventional cooling system and the conformal cooling system which are designed specifically for the same core-insert that was used to produce the plastic fog lamp shown in Fig. 1.3. These two cooling system designs were provided by the industrial collaborator of this project - Proper Group International. The conventional cooling system is the design which is used traditionally in plastic injection mold production, whereas the conformal cooling system is a conceptual model. The CAD model of the core-insert with all the features is shown in Fig. 4.1. For simplicity, some detailed features such as ribs on the working surface and the fixing mount of the fog lamp are removed because the performance of the cooling system will not be reflected on these features. Additionally, the mesh cell count is reduced significantly by removing these small features, thereby reducing the computational cost. The other systems in the core-insert, other than the cooling system, such as the ejection system and the sprue-runner-gate system, have been removed as well to reduce the computational complexity and cost. The potential improvements to cooling performance by utilizing conformal cooling channels and the potential issues are demonstrated in this chapter.



Figure 4.1: CAD model of the core-insert with all the features

## 4.1 Numerical Model Setup

### 4.1.1 Geometric Setup

Figure 4.2 shows the working surface and the conventional cooling system of the core-insert. The conventional cooling system is manufactured by gun-drilling and routed by cooling baffles and plugs. The cooling baffles are cooling channel components which consist of a drilled hole perpendicular to a main cooling line and a thin plate separating the drilled hole into two semicircular channels. The plate directs the coolant to flow up in one side and into the core region, and down in the other side and out of the core region. There are other benefits of using baffles in the cooling system. By changing the direction of the coolant flow in cooling channels, the baffle creates turbulence around the U-shape bend at its top and thereby increases the heat transfer coefficient. However, it also increases the pressure loss around these bends within the cooling system, which increases the pumping power requirement [32].

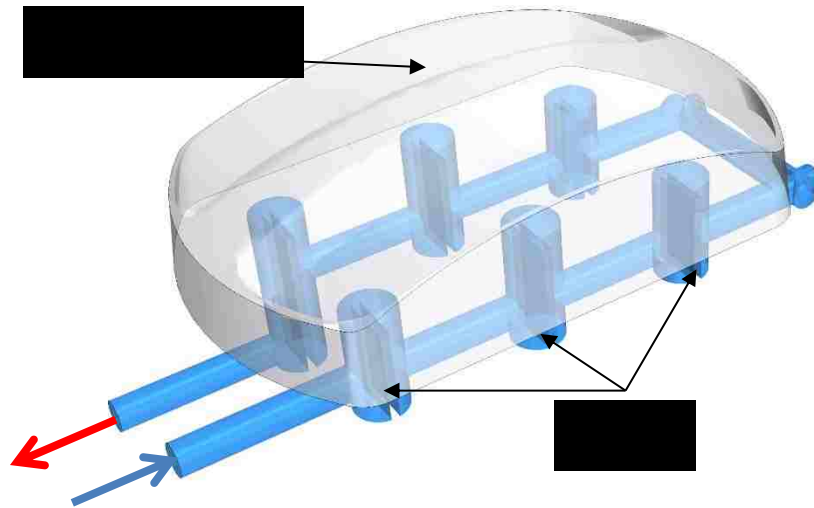


Figure 4.2: The conventional cooling system and the working surface of the core-insert

The conformal cooling system design tested in this study and the working surface of the core-insert is depicted in Fig. 4.3. This insert was

manufactured by metal 3D printing. Three cooling channels are placed in parallel configuration and the total inlet mass flow rate is equally divided into three by a manifold (not shown in the figure). The flow in the manifold is not considered in this study.

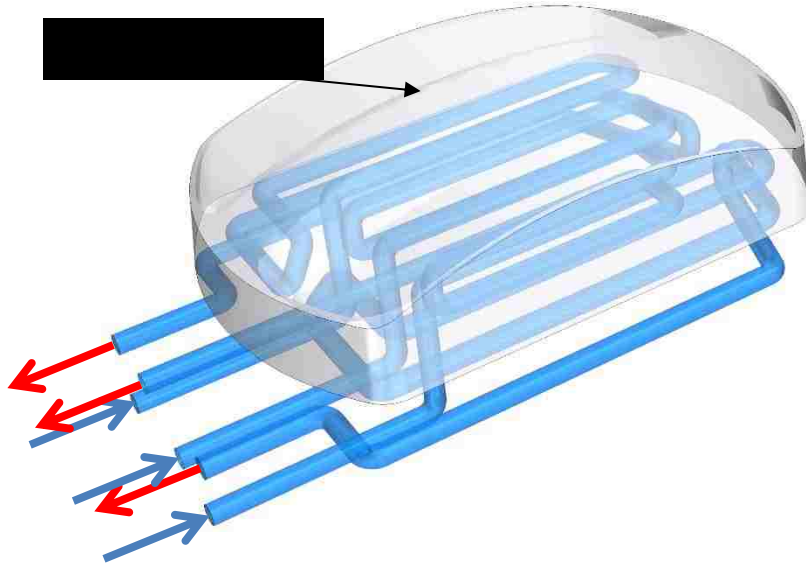


Figure 4.3: The conformal cooling system and the working surface of the core-insert

#### 4.1.2 Computational Domain

Taking the core-insert with conventional cooling system as an example, the computational domain of the simulation is depicted in Fig. 4.4. The computational domain for the simulations with the conformal cooling system is similar, only the channel geometry is changed. Both consist of a solid region and a fluid region. The solid region is used to apply the heat source, which resulted from the contact with the injected melt polymer on the working surface and to model the conductive heat transfer in the solid mold body. The fluid region takes the turbulent coolant flow and convective heat transfer into account and the SST  $k-\omega$  turbulence model is used to simulate the flow. An interface is created at any contact surface between the solid and fluid regions to render the data transmission between these two regions.

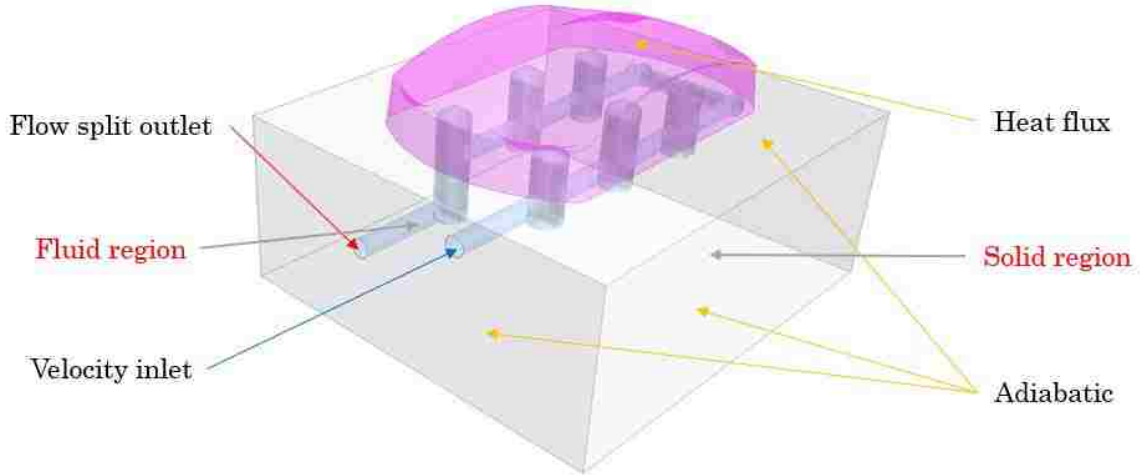


Figure 4.4: Computational domain and boundary conditions of the core-insert with conventional cooling system

#### 4.1.3 Boundary Conditions

##### Solid Region:

For boundary conditions of the solid region, we first consider the heating surface. The heating surface refers to the working surface of the injection mold, which has the form of the molded plastic part and is in direct contact with the injected melt polymer and absorbs the heat from it until the melt polymer is solidified and ejected. The cyclic molding process results in a cyclic behaviour in the mold temperature. However, since this study focuses on the overall cooling performance of the cooling system over production runs, the cycle averaged heat flux is used as the boundary condition of the heating surface, specified as:

$$\dot{q}_{heating\ surface} = Constant \quad (4.1)$$

The cycle averaged heat flux  $\dot{q}_{heating\ surface}$  is calculated based on the following process. First, the cooling time is estimated by using the following analytical equation [4]:

$$t_c = \frac{s^2}{\pi^2 \cdot \alpha} \ln \left( \frac{4 T_{injection} - T_{mold}}{\pi T_{ejection} - T_{mold}} \right) \quad (4.2)$$



where  $T_{mold}$  can be changed based on the design of the cooling system and the operational condition of the mold and the nominal wall thickness ( $s$ ) is taken as 3 mm based on the geometry of the molded plastic fog lamp. Equation (4.2) is commonly used in the injection mold industry at the early stage of the design. The thermal diffusivity ( $\alpha$ ) is taken as  $1.664 \times 10^{-7}$ . According to the production parameters provided by Proper Group International Inc., injection temperature ( $T_{injection}$ ) is 282 °C, ejection temperature ( $T_{ejection}$ ) is 129 °C, suggested average mold temperature ( $T_{mold}$ ) is 104 °C. The estimated cooling time, calculated from Eqn. (4.2), is  $t_c = 12.1$  s.

To maintain a higher production performance, most of the heat should be removed by the cooling system, and only a small portion of the heat is conducted across the mold body and dissipated through the natural convection on the external surfaces of the mold. For simplicity, it is assumed that all the heat is removed by the cooling system in this study. Therefore, the total energy that needs to be removed is calculated by the following equation:

$$\begin{aligned} Q_{plastic} &= m_{plastic} \cdot C_{p,plastic} \cdot (T_{injection} - T_{ejection}) \\ &= (A \cdot s \cdot \rho_{plastic}) \cdot C_{p,plastic} \cdot (T_{injection} - T_{ejection}) \end{aligned} \quad (4.3)$$

Given the total amount of heat that needs to be removed by the cooling system and the estimated cooling time,  $\dot{q}_{heating\ surface}$  can be calculated by using Eqn. (4.4) to Eqn. (4.6). Equation (4.5) is based on the assumption that the cooling system for both core and cavity inserts are well designed and balanced, which means they evenly removes the same amount of heat at the same rate.

$$\dot{Q}_{cooling} = \frac{Q_{plastic}}{t_c} \quad (4.4)$$

$$\dot{Q}_{cooling,core\ insert} = \frac{\dot{Q}_{cooling}}{2} \quad (4.5)$$

$$\dot{q}_{\text{heating surface}} = \frac{\dot{Q}_{\text{cooling,core insert}}}{A} \quad (4.6)$$

The rest of the external surface of the solid region are taken to be adiabatic, assuming that there is no energy transfer across these boundaries [29], i.e.,

$$\dot{q}_w = 0, \quad T_w = \text{computed} \quad (4.7)$$

**Fluid Region:**

Velocity inlet is used as the inlet boundary condition for the fluid region. Based on the analyses in Chapter 3, it is known that the inlet flow condition has minimum influence over the cooling performance of the entire cooling system. Considering both cooling system designs tested in this study, the effective cooling channel length is much longer than the hydrodynamic length of the inlet flow. Therefore, uniform velocity inlet is used for simplicity, specified as:

$$V_{in} = \text{constant} \quad (4.8)$$

Ten mass flow rates are tested for both the conventional cooling system and the conformal cooling system. For the conformal cooling system, a parallel configuration is adopted in which three cooling channels are used. The corresponding Reynolds numbers of these ten mass flow rates, when applied on the conventional and conformal cooling systems, are shown in Table 4.1. Turbulence is desired for cooling purposes since it facilitates the mixing process and increases the heat transfer coefficient. The coolant flow rates tested in this study are selected based on the Reynolds number ranging from 4000 to 22000. To ensure that the conventional and the conformal cooling systems are compared under the same condition, and since the conformal cooling system has three channels, the inlet mass flow rate for conformal system is equally divided into three for each cooling channel. Therefore, the Reynolds number for the conformal cooling system is lower.

Table 4.1: Relationship between mass flow rates and Reynolds number for the conventional and the conformal cooling systems

Mass flow rate (kg/s)		0.031	0.047	0.062	0.078	0.093	0.109	0.124	0.140	0.155	0.171
Re	Conventional	4000	6000	8000	10000	12000	14000	16000	18000	20000	22000
	Conformal (1 channel)	2114	3171	4229	5286	6343	7400	8457	9514	10571	11629

Flow split outlet is selected as the outlet boundary condition of the coolant flow, where the split ratio is set to 1, which is specified as:

$$\dot{m}_{out} = \dot{m}_{in} \quad (4.9)$$

The no slip condition is assigned at the channel wall, i.e.,

$$u_w = 0 \quad (4.10)$$

#### 4.1.4 Physical Properties

Due to the different manufacturing methods used to fabricate the mold inserts, different materials are used for the conventional and conformal cooling system; therefore, the thermal properties are different. However, because this study focuses on the influence of cooling channel designs on the cooling performance, the same material is used in all simulations. The thermal properties of the maraging steel (standard P20 mold steel equivalent) which is used to fabricate the mold for the conformal cooling channels are used, as listed in Table 4.2 [4].

Table 4.2: Thermal properties of standard P20 mold steel

Material parameter	Symbol	Value	Unit
Density	$\rho_{P20}$	7820	$kg/m^3$
Thermal conductivity	$k_{P20}$	32	$W/(m \cdot K)$
Specific heat	$C_{p,P20}$	500	$J/(kg \cdot K)$

## 4.1.5 Mesh

### 4.1.5.1 Meshing Methods

A polyhedral mesh is used to discretize both the solid and fluid regions. Data transmission through the solid-fluid interface is of importance for simulating conjugate heat transfer, and a polyhedral mesh can be constructed with a contiguous mesh at the interface with complex geometries, which provides more accurate data transfer through these interfaces than a non-contiguous mesh. Prism layers are also constructed on the cooling channel walls inside the fluid region to resolve the boundary layer of the coolant flow since it is crucial for simulating the turbulent flow and the convective heat transfer in the channel. Taking the mesh for the core-insert with conventional cooling channel as an example, Fig. 4.5 shows the polyhedral mesh at the middle cross-sectional plane perpendicular to the inlet flow direction. As one can tell from the zoom-in view in the inset of Fig. 4.5, the cells at the interface between the solid and fluid regions are well connected. The target mesh sizes of both solid and fluid regions have also been selected in the way that the mesh in the solid region close to the cooling channel and the mesh inside the cooling channel are finer than that close to the external solid walls, since the finer mesh is required to accurately capture the higher temperature gradient in these areas and to resolve the turbulent coolant flow. Important meshing parameters are shown in Table 4.3 and are used in the mesh independence study discussed in next section to ensure the numerical results are independent on the mesh.

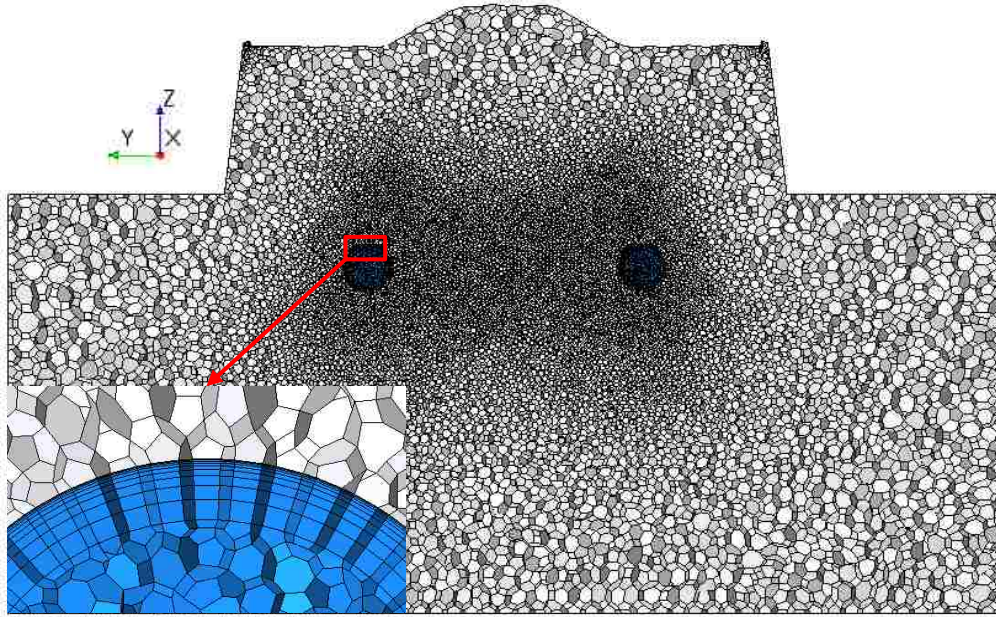


Figure 4.5: Illustration of the polyhedral mesh on the middle cross-sectional plane which is perpendicular to the inlet flow direction

Table 4.3: Important meshing parameters

Base size	1 mm
Target mesh size of solid region	400% of base size
Target mesh size of fluid region	75% of base size
Prism layer thickness	10% of channel diameter
Number of prism layers	9

#### 4.1.5.2 Mesh Independence Study

A mesh independence study has been conducted to ensure the numerical results are independent of the mesh resolution. The conventional cooling system with inlet flow rate of 0.171 kg/s is selected to conduct the mesh independence study since it has the highest Reynolds number and the numerical results are the most sensitive to the mesh resolution. The physical parameters which are important when evaluating the cooling performance, such as maximum, minimum and average temperatures on the heating

surface, coolant outlet temperature and pressure drop in the cooling channel are used to determine the influence of the meshing parameters on the numerical results.

First, considering the meshing parameters shown in Table 4.3, base cell sizes of 1.5 mm and 0.5 mm are used to determine if the base cell size of 1 mm is sufficient to ensure mesh independency. It is found that, among all the considered physical parameters, the minimum temperature on the heating surface shows the largest difference when changing the base cell size. Therefore, it is used to evaluate the mesh quality. The results are shown in Table 4.4. Changing from base cell size of 1 mm to 0.5 mm, the difference in the minimum temperature is within the tolerable range for a numerical prediction of the cooling performance. Thereafter, 1 mm is used as the base mesh size.

Table 4.4: Results of the testing with base cell size

Base cell size (mm)	1.5	1	0.5
Min. temperature (°C)	46.58	45.27	44.18
% difference	2.8		2.4

The computational domains in this study are complex; therefore, more meshing parameters are tested to check if there is any potential on saving computational time, while maintain the mesh independency. The target mesh size for the solid region, the target mesh size for the fluid region, the prism layer thickness and the number of prism layers are tested next. The results are shown in Table 4.5. It is found that the minimum temperature on the heating surface always shows the largest difference when changing the value of these meshing parameters. However, all these four meshing parameters have very little influence on the numerical results compared with base cell size. To maintain a safety margin for the mesh quality, the middle values among all tested meshing parameters are used.

Table 4.5: Results of the testing of four sub meshing parameters

<b>Target mesh size for solid region</b>			
% of base cell size	500	400	300
Min. temperature	44.86	45.37	45.05
% difference	1.2		0.7
<b>Target mesh size for fluid region</b>			
% of base cell size	100	75	50
Min. Temperature	45.37	45.20	45.10
% difference	0.4		0.2
<b>Prism layer thickness</b>			
% of channel diameter	15	10	5
Min. temperature	45.37	45.20	45.10
% difference	0.17		0.04
<b>Number of prism layer</b>			
	12	9	6
Min. Temperature	45.20	45.27	44.89
% difference	0.16		0.8

## 4.2 Results and Analyses

Figure 4.6 shows the temperature distribution on the heating surfaces for both the conventional and conformal cooling cases with total mass flow rates of 0.031, 0.078, 0.124 and 0.171 kg/s. As one can observe, for all cases shown in Fig. 4.6, the hot spots are located at the same section of the fog lamp, along the top edges. These areas are farther from the cooling channels than other areas in the both conventional and conformal cooling cases as depicted in Fig. 4.9. However, for the same total mass flow rate, the conformal cooling system results in lower temperature everywhere on the heating surface than the conventional cooling system.

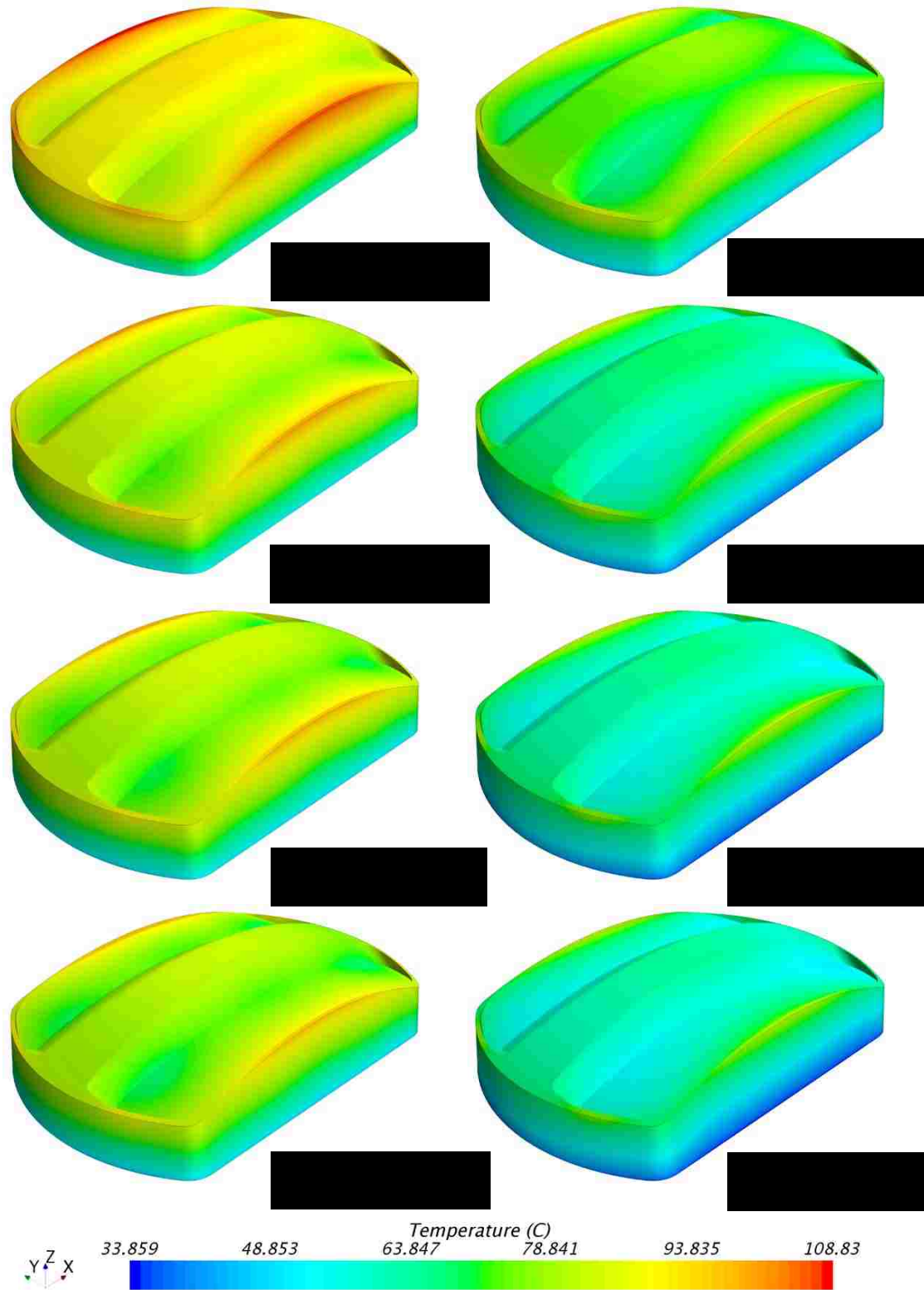


Figure 4.6: Temperature distribution on heating surfaces of core-inserts with conventional and conformal cooling channels with mass flow rates of 0.031 kg/s, 0.078 kg/s, 0.124 kg/s and 0.171 kg/s



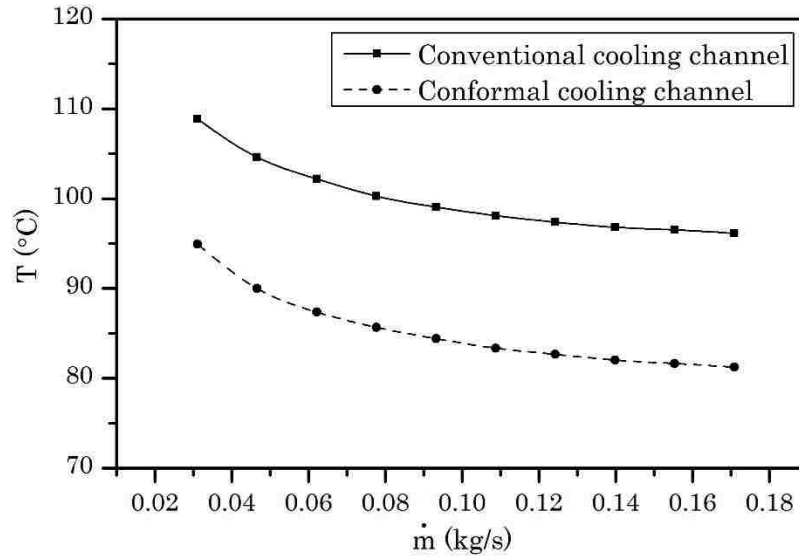


Figure 4.7: Maximum temperature on the heating surface vs total inlet mass flow rates

The most basic requirement for the ejection of the plastic part is that the temperature everywhere on the molded part has to drop below the DTUL (Deflection Temperature Under Load) of that specific plastic material. Therefore, the hot spots shown in Fig. 4.6 are the main issue that hinder the part from ejection. As shown in Fig. 4.7, the highest temperature on the working surface drops with the increase of inlet mass flow rate for both the conventional and the conformal cooling systems and they follow a similar trend. Clearly, the conformal cooling system provides a lower maximum temperature on the heating surface than the conventional cooling system for all mass flow rates. Therefore, in terms of maximum temperature on the heating surface, the conformal cooling system provides better cooling performance.

In addition to the maximum temperature on the heating surface, temperature uniformity on the heating surface is another important parameter that has significant influence on the cooling time and the quality of the molded part. During the design of the injection mold cavity, a shrinkage rate is included to consider the shrinkage of the plastic part after it is ejected. If the temperature distribution on the heating surface during and

after the cooling stage is uniform, the dimension of the molded part can be better controlled. The temperature variation on the heating surface is used to demonstrate the temperature uniformity, the smaller the temperature difference the more uniform the temperature is on the heating surface. As shown Fig. 4.8, as the inlet mass flow rate increases, the temperature uniformity drops (temperature difference increases) for both the conventional and the conformal cooling systems. Especially, it decreases more rapidly for the conformal cooling system with low inlet mass flow rate. This can be explained by Fig. 4.9 which illustrates the temperature distribution in the middle cross-section and the relative distance between the heating surface and cooling channels. For the conformal cooling system, the bottom edge of the heating surface is closer to the cooling channels than that of the conventional cooling system, but the top heating surface has similar distance to the cooling system with that of the conventional cooling system. This proximity of the bottom edge of the heating surface to the cooling system results in a shorter conductive heat transfer path in the mold body and lower temperature for conformal cooling system.

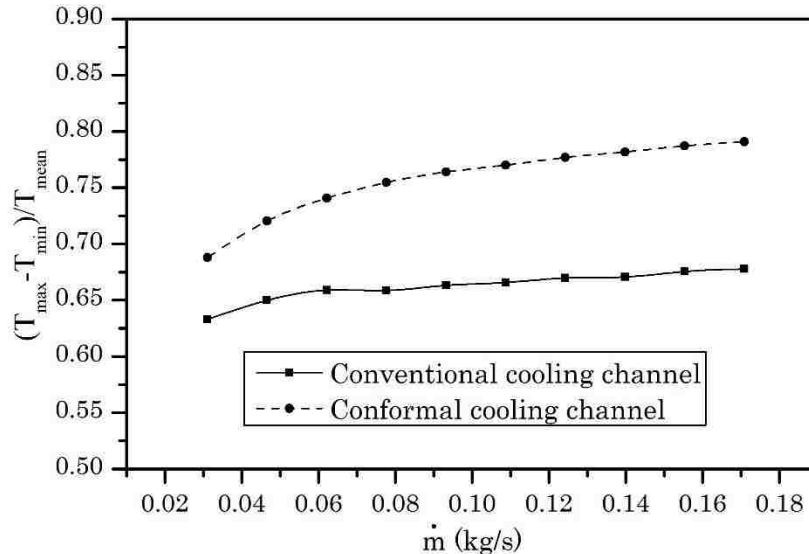


Figure 4.8: Temperature uniformity on the working surface for both conventional and conformal cooling systems

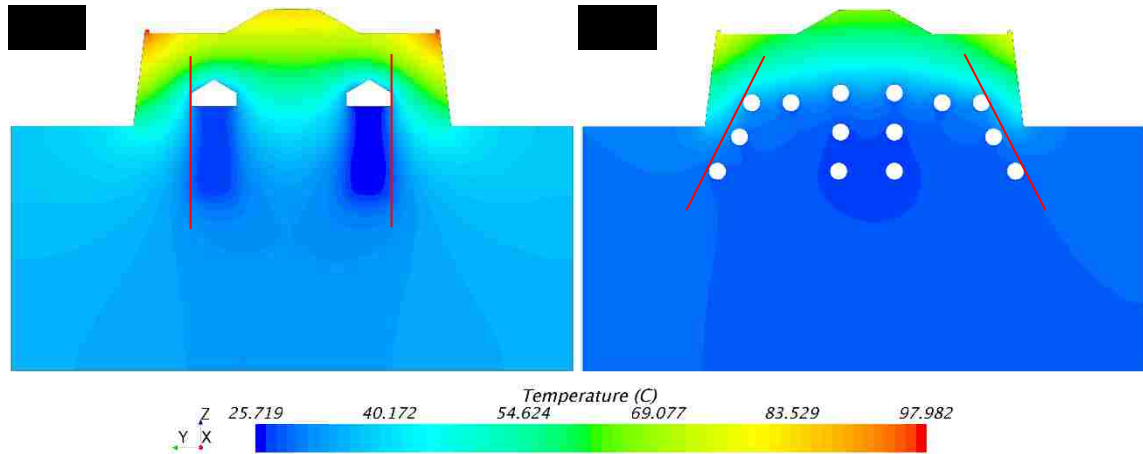


Figure 4.9: Temperature distribution in the middle cross-section of (a) conventional cooling system; (b) conformal cooling system

The required pumping power is another concern in the injection molding industry. If a molder has to purchase temperature controllers with higher pumping power instead of using the ones they already have, that is going to be an extra expense. Thus, while pursuing a better cooling performance, a lower pressure drop within the cooling system is desired. Figure 4.10 demonstrates the change of pressure drop in the cooling system for both the conventional and the conformal cooling channels at various inlet mass flow rates. At the same inlet mass flow rate, the pressure drop in the conventional cooling system is higher than that in the conformal cooling system. This difference gets larger with the increase of inlet mass flow rate. This is due to the sharp bends associated with the cooling baffles and the conjunction of the cooling baffles and main cooling line. Hence, in terms of cooling power consumption, the conformal cooling system requires lower pumping power. Also, combined with the flexibility of placing the conformal cooling channel in a restricted area, which is available by the 3D metal printing technology, configurations with more channels are more likely to be achieved. This is another reason why conformal cooling channel can be operated with much lower power consumption. In terms of pressure drop, the

inlet mass flow rate can be selected by comparing the pressure drop with the supplier information of industrial temperature controllers.

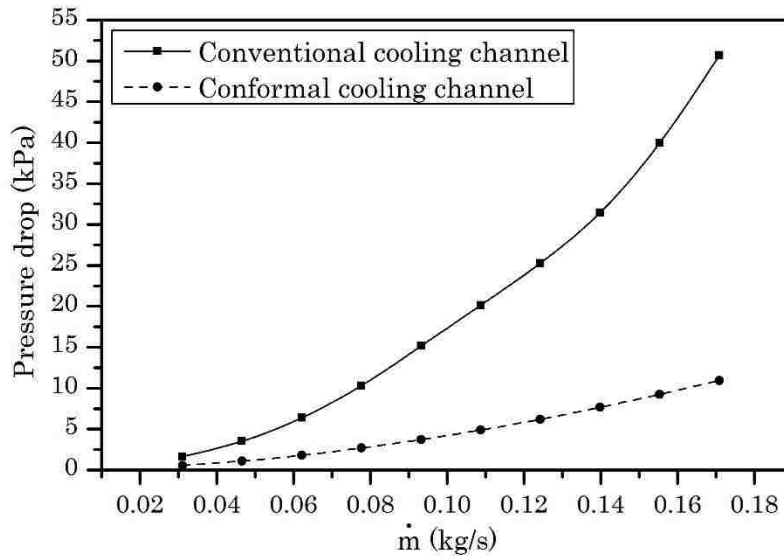


Figure 4.10: Pressure drop vs mass flow rates

Given the steady state assumption, and based on the second law of thermodynamics, the coolant temperature increase between inlet and outlet should be the same for both the conventional and the conformal cooling systems at the same total inlet mass flow rate because the same cycle averaged heat flux is applied on the heating surface. This is depicted in Fig. 4.11. According to Marques et al. [11], the coolant temperature increase from the inlet to the outlet should not be more than 3 °C, otherwise it may result in higher mold temperature and uneven cooling performance between the heating surface area close to the inlet and areas close to the outlet. Thus, for the estimate cooling time, a mass flow rate higher than 0.093 kg/s is required to maintain the coolant temperature increase within 3 degrees.

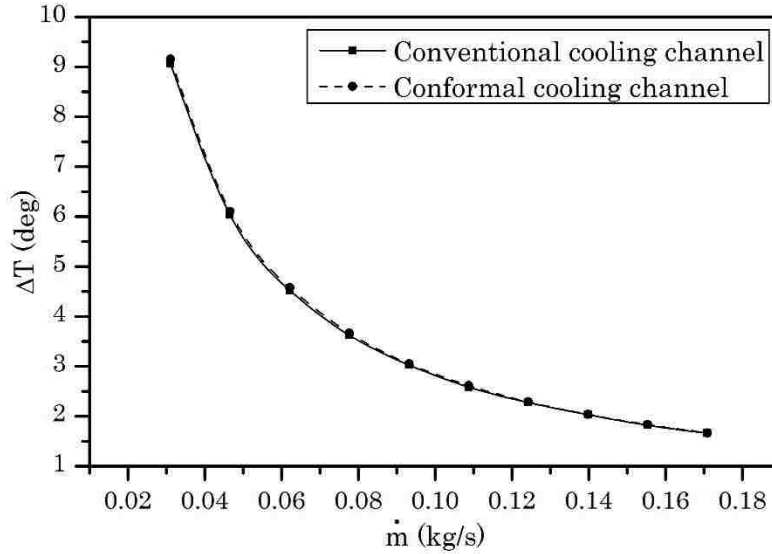


Figure 4.11: Coolant temperature increase vs mass flow rates

Figure 4.12 shows the heat transfer coefficients with ten inlet mass flow rates for both the conventional and the conformal cooling systems. The heat transfer coefficient is obtained by taking surface average over the entire surface of the conventional cooling system whereas the total of the three channel surface areas is considered in the conformal cooling system. It is found that the heat transfer coefficient rises almost linearly with the increase of inlet mass flow rate for both cooling system designs. From Fig. 4.6 and the comparison between the maximum temperature on the heating surface for both cooling system designs, it is shown that the conformal cooling system can provide better cooling performance. However, it should be noted that the total surface area of the conformal cooling system is 1.5 times that of the conventional cooling system, so the heat flux through the interface between the solid and fluid is reduced. This is a probable reason why the heat transfer coefficient associate with the conformal cooling system is lower than that of the conventional cooling system at the same mass flow rate.

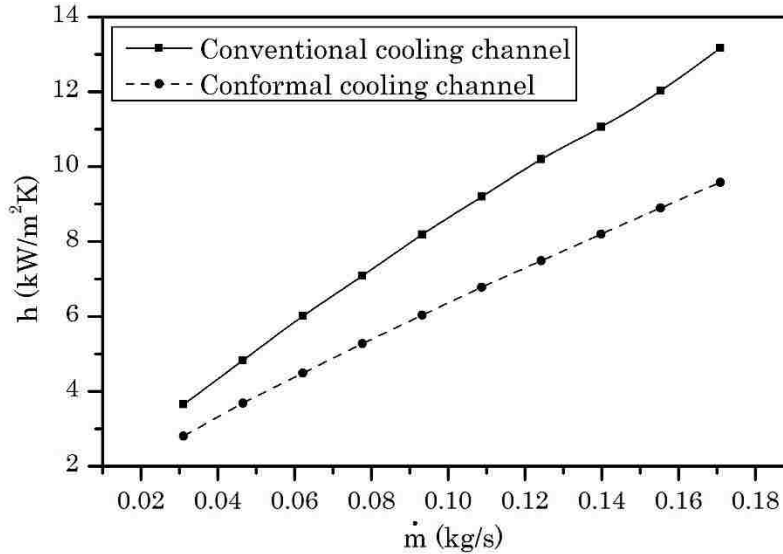


Figure 4.12: Heat transfer coefficient vs mass flow rates

### 4.3 Summary

In this chapter, the cooling performances of a conventional and a conformal cooling system are compared with ten mass flow rates. The assessment of the cooling performance is based on the maximum temperature and the temperature distribution on the heating surface and the pressure drop in the cooling system. It can be concluded that, with the same total inlet mass flow rate, the conformal cooling system provides better cooling performance while not consuming more pumping power than the conventional cooling system. It can also be noted that, considering the temperature uniformity on the heating surface, there is still room for the improvement for the design of the given conformal cooling system.

# Chapter 5

## Parametric Study

Applied to the evaluation of cooling performances of injection mold cooling systems, the significance and potential of CFD analysis reside not only in the comparison of cooling performances between different cooling system designs, but also in the ability to perform a comprehensive study to evaluate the significance of various cooling channel design parameters. CFD is a numerical tool which allows the researchers and mold designers to assess the influence of various geometrical design parameters on the cooling performance, without the need to construct test mold-inserts for experiments, thereby significantly reducing the cost of injection molds in the design stage.

By using 3D printing technologies to fabricate mold inserts, cooling systems with any shapes and configurations can be integrated into the mold insert. However, to produce general design suggestions and guidelines, cooling systems which consist of U-shape bends are of interest in this parametric study. A set of simplified CAD models, which have the characteristics of the core-inserts with deep concave geometries, is generated and geometrically characterized by utilizing CATIA v5 package. In this parametric study, three geometrical design parameters are tested; namely, the number of cooling channels, channel depth from the heating surface ( $H$ ) and the curvature ratio of the 90° bends ( $\delta$ ). The outcomes of this parametric

study will provide guidelines and recommendations to the mold designers for their future injection mold cooling system designs.

## 5.1 Design of the Parametric Study

### 5.1.1 Test Mold-insert Design

Figure 5.1 depicts an example of the structure and dimensions of the test mold-inserts used in this parametric study. The dimensions of these test mold-inserts are selected to be at the same level with the core-insert which is used to produce the fog lamp (Fig. 1.3). The upper portion of the test mold-insert represents the actual working surface with deep concave geometries and the solid mold body surrounded by it. The lower portion is used to model the surfaces of the mold-insert that are in contact with the main mold-body. Different cooling system configurations are placed inside the heating area of this test mold-insert to examine the significance of various design parameters.

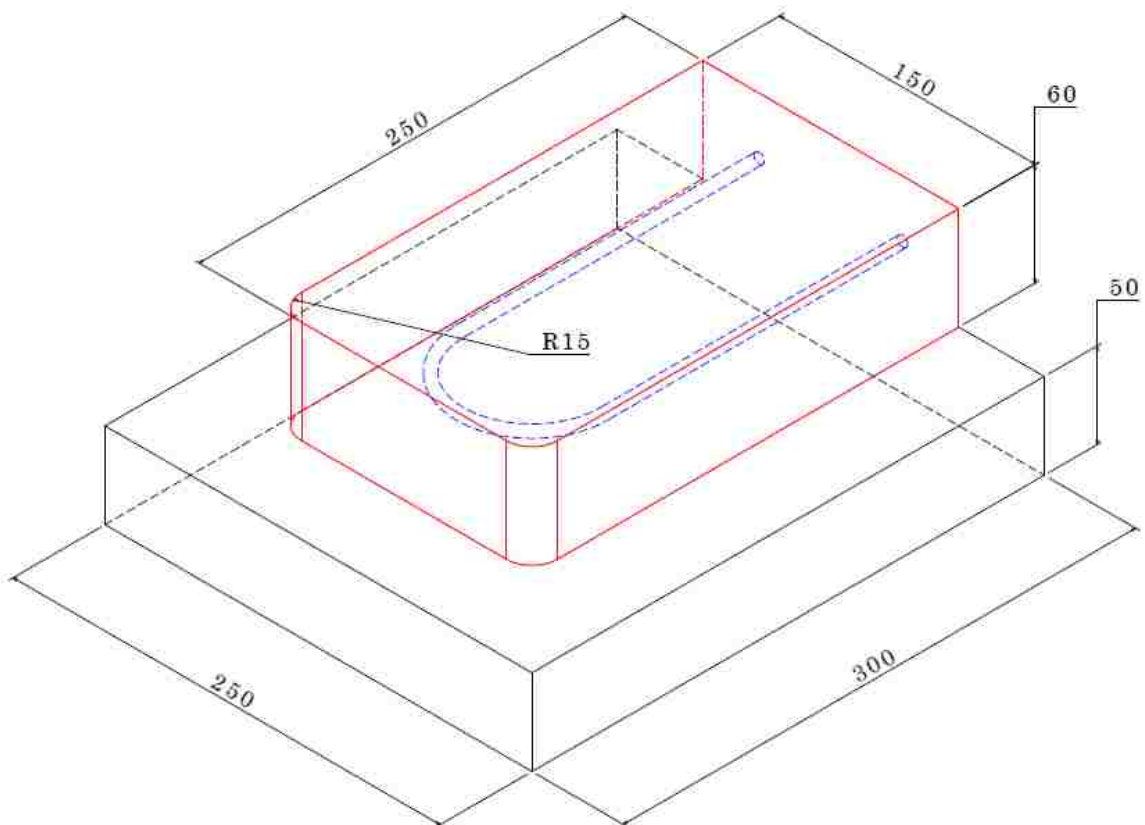


Figure 5.1: Schematic of the mold-insert for the parametric study



### 5.1.2 Cooling System Design

In the current parametric study, the influences of three geometrical design parameters are examined: the number of cooling channels, the depth of the cooling channel from the heating surfaces and the curvature ratios of the 90° turns which form the U-shape bends. The cooling system design starts with the determination of the diameter of the channel ( $D$ ) which is calculated based on the situation for which only one cooling channel is used. For cases with two and three cooling channels, the same channel diameter is used for all the channels to keep consistency within this parametric study. In these cases, the total inlet mass flow rate is equally divided by two or three and assigned to each individual channel.

The diameter of the cooling channel is determined by the following process. First, the required cooling power for the mold-insert is calculated based on Eqn. (4.2) through Eqn. (4.5). Instead of using the operational parameter values provided by Proper Group International in the comparison study (Chapter 4), representative values are chosen for the operational parameters to offer some generality in the current parametric study. The nominal wall thickness ( $s$ ) is kept at 3 mm. The injection temperature ( $T_{injection}$ ) equals 280 °C, which is the minimum melt temperature of polycarbonate (PC). The ejection temperature is taken equal to the DTUL (Deflection Temperature Under Load) of PC, which is 138 °C, and the cycle averaged mold temperature is chosen as the maximum value in the suggested range for PC, which is 95 °C [4].

For purposes of estimating the inlet diameter, it is assumed that the coolant temperature increases from the inlet to the outlet of the cooling system by 10 degrees. The volumetric inlet flow rate that is needed to satisfy both the requirement of cooling power and the coolant temperature increase can be calculated based on the following equation:

$$\dot{V}_{coolant} = \frac{\dot{Q}_{cooling,core\ insert}}{\rho_{coolant} \cdot C_{p,coolant} \cdot \Delta T} \quad (5.1)$$

For injection mold cooling applications, turbulent flow with Reynolds number more than 10000 is desired to facilitate the heat transfer process. Thus, for a specified Reynolds number of 14000, the diameter of the cooling channel, which can be calculated based on Eqn. (5.2), is 6 mm.

$$D = \frac{4 \cdot \rho_{coolant} \cdot \dot{V}_{coolant}}{\pi \cdot \mu_{coolant} \cdot Re} \quad (5.2)$$

After the cooling channel diameter is determined, the cooling channel depth from the heating surface ( $H$ ) is considered. In general, it is desirable to place the cooling channel as close to the heating surface as possible since this will reduce the heat conduction distance within the mold material between the cooling system and the heating surface. However, to ensure the structural integrity of the mold body which is operated under high stress conditions, the minimum distance must be above some critical value. An acceptable range of the distance between the cooling channel and the heating surface has been suggested by Kazmer [4]:

$$2D \leq H \leq 5D$$

Therefore, cooling channel depths of  $H = 2D$  and  $5D$  are selected to construct the test mold-inserts for the parametric study.

Lastly, the configuration of the U-shape bends is considered. All the U-shape bends studied in this research consist of two 90° turns. They are connected to each other either directly or by a section of straight cooling channel. Therefore, a curvature ratio  $\delta$  is defined to demonstrate the level of tortuosity of the 90° turns which form the U-shape bends:

$$\delta = \frac{R_c}{D} \quad (5.3)$$

where  $R_c$  represents the radius of the 90° bends.

The cases tested in this parametric study are classified into three groups by the number of cooling channels. Detailed design parameters of cooling systems with one channel are shown in Table 5.1. Figure 5.2 illustrates the schematics of four representative cases in this group. The curvature ratio of the second 90° bend is kept the same with the first 90° bend which is the closest to the inlet.

Table 5.1: Design parameters for test cases with one cooling channel

Channel depth ( $H$ )	Case number	$\delta$
$2D$	1-1	1
	1-2	2
	1-3	3
	1-4	4
	1-5	5
	1-6	6
	1-7	7
	1-8	8
	1-9	9
	1-10	10
$5D$	1-11	1
	1-12	2
	1-13	3
	1-14	4
	1-15	5
	1-16	6
	1-17	7

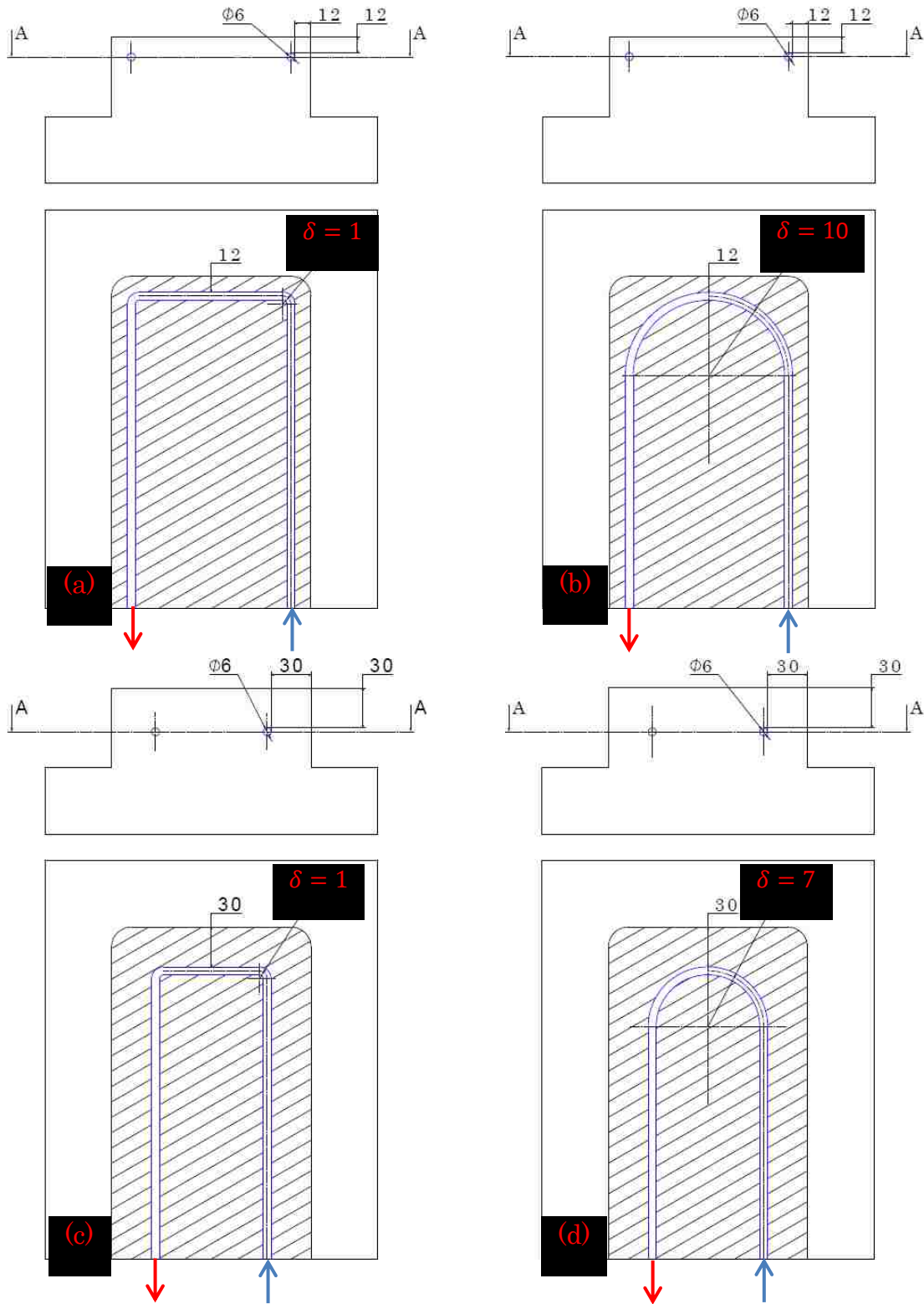


Figure 5.2: Schematics of test inserts with one cooling channel,  
 (a) Case 1-1:  $H = 2D$  and  $\delta = 1$ ; (b) Case 1-10:  $H = 2D$  and  $\delta = 10$ ;  
 (c) Case 1-11:  $H = 5D$  and  $\delta = 1$ ; (d) Case 1-17:  $H = 5D$  and  $\delta = 7$

It is known that curved channels enhance turbulence which will enhance the mixing and heat transfer process [31]. The sharper the bend, which corresponds to a lower curvature ratio, the stronger the effect. Therefore, for cases with two cooling channels, the curvature ratio of the first 90° bend after the inlet is smaller than that of the second 90° bend after inlet. Additionally, due to the limited pitch distance between the inlet and outlet of each channel, the number of configurations for the U-shape bends is fewer for cases with two and three cooling channels. The tested U-shape bend configurations for cases with two and three channels are shown in Tables 5.2 and 5.3, respectively. In these tables,  $\delta_1$  is the curvature ratio of the first 90° bend from the inlet,  $\delta_2$  is the curvature ratio of second 90° bend from the inlet and  $\delta_3$  represents the curvature ratio of the 90° bends of the centre cooling channel. Figure 5.3 and 5.4 show schematics of two representative test mold-inserts for cases with two and three cooling channels.

Table 5.2: Design parameters for test cases with two cooling channels

Channel depth ( $H$ )	Case number	$\delta_1$	$\delta_2$
2D	2-1	1	1
	2-2	1	2
	2-3	1	3
	2-4	1	4
	2-5	1	5
	2-6	2	2
	2-7	2	3
	2-8	2	4
	2-9	3	3
5D	2-10	1	1
	2-11	1	2
	2-12	1	3
	2-13	2	2

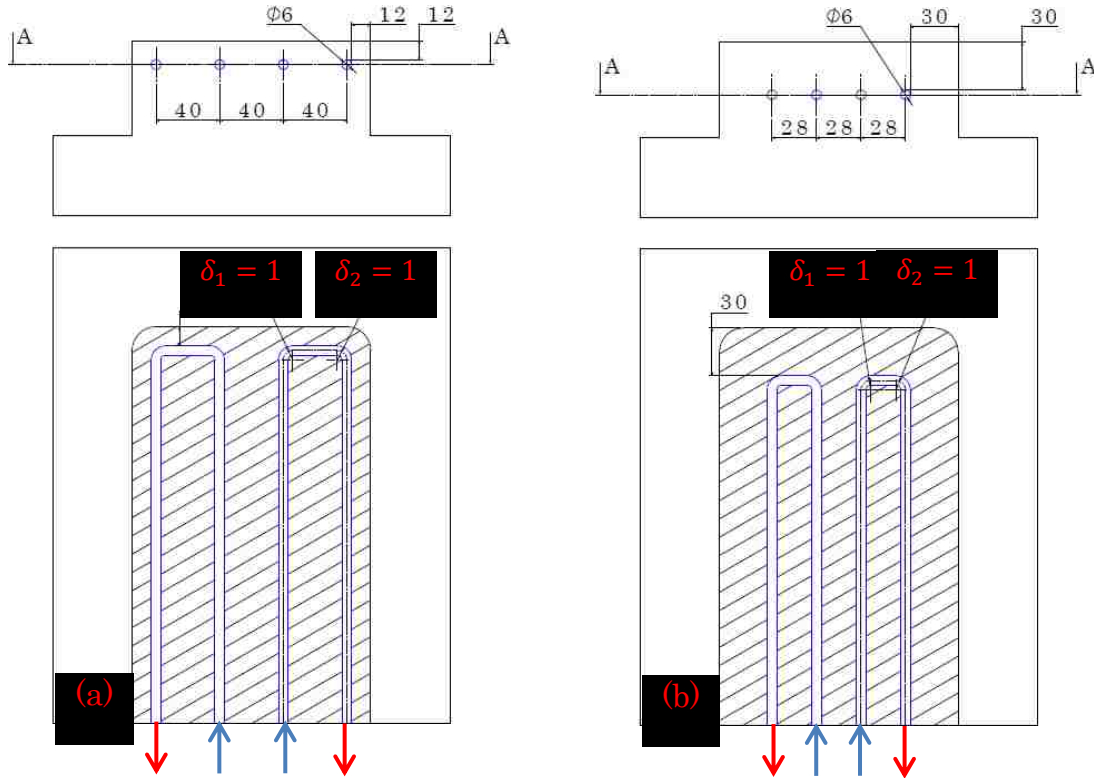


Figure 5.3: Schematic of test inserts with two cooling channels,  
 (a) Case 2-1:  $H = 2D$ ,  $\delta_1 = 1$  and  $\delta_2 = 1$ ;  
 (b) Case 2-10:  $H = 5D$ ,  $\delta_1 = 1$  and  $\delta_2 = 1$

Table 5.3: Design parameters for test cases with three cooling channels

Channel depth ( $H$ )	Case number	$\delta_1$	$\delta_2$	$\delta_3$
$2D$	3-1	1	1	1
	3-2	1	2	1
	3-3	1	3	1
	3-4	2	2	2
$5D$	3-5	1	1	1

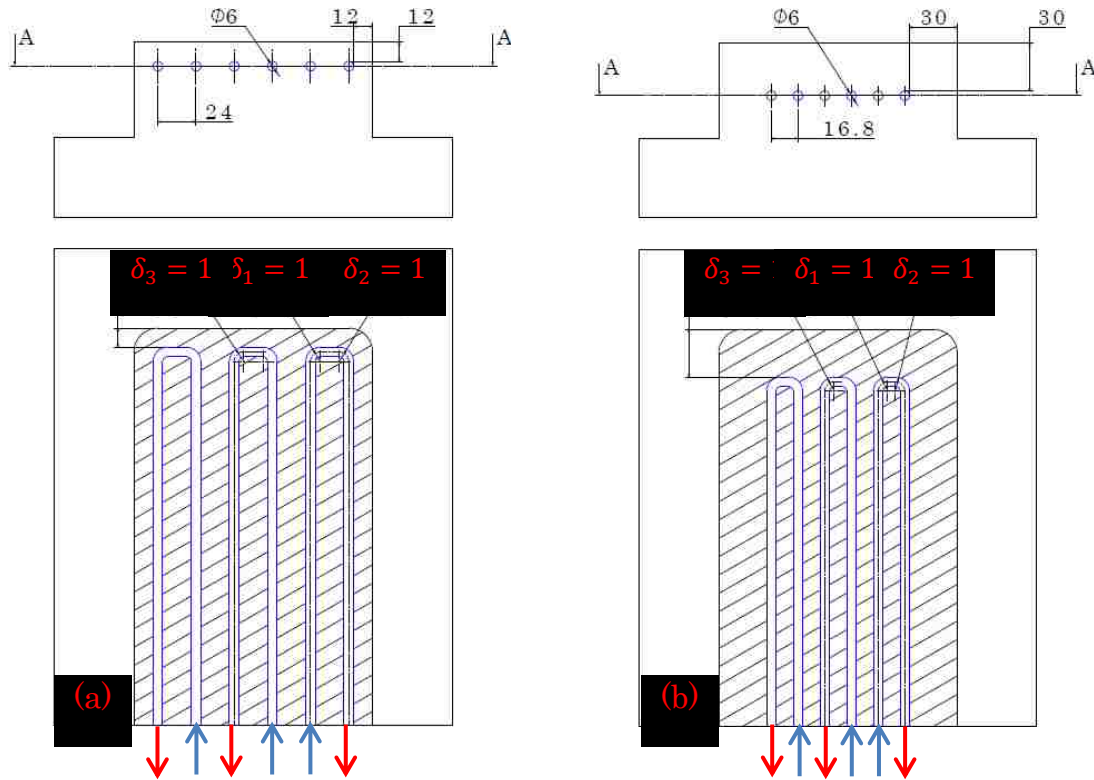


Figure 5.4: Schematic of testing models with three cooling channels,  
 (a) Case 3-1:  $H = 2D$ ,  $\delta_1 = 1$ ,  $\delta_2 = 1$  and  $\delta_3 = 1$ ;  
 (b) Case 3-5:  $H = 5D$ ,  $\delta_1 = 1$ ,  $\delta_2 = 1$  and  $\delta_3 = 1$

## 5.2 Numerical Model Setup

### 5.2.1 Computational Domain

Similar to the comparison study, the computational domains for the parametric study also consist of two types of regions, the solid region and the fluid region. The solid region is used to apply the heat source on the heating surface and to model the conductive heat transfer in the solid mold body. The fluid regions are used to model the turbulent coolant flow and the convective heat transfer along the channels. Other than the inlets and outlets, all surfaces of the fluid regions are in contact with the solid region.

### 5.2.2 Boundary Conditions

The boundary conditions of the solid region are similar with those of the comparison study. Figure 5.5 shows the CAD model of the test mold-insert, illustrating the boundary conditions of the solid region. The red surface in the figure is the heating surface and the cycle averaged heat flux is used as the boundary condition of this surface. The value of the cycle averaged heat flux is calculated by using Eqn. (4.3) to Eqn. (4.6). For simplicity, the surface with inverted T-shape, at which the inlet and outlet of coolant flow is located, is assumed to be adiabatic. The rest of the surfaces are treated as adiabatic as well.



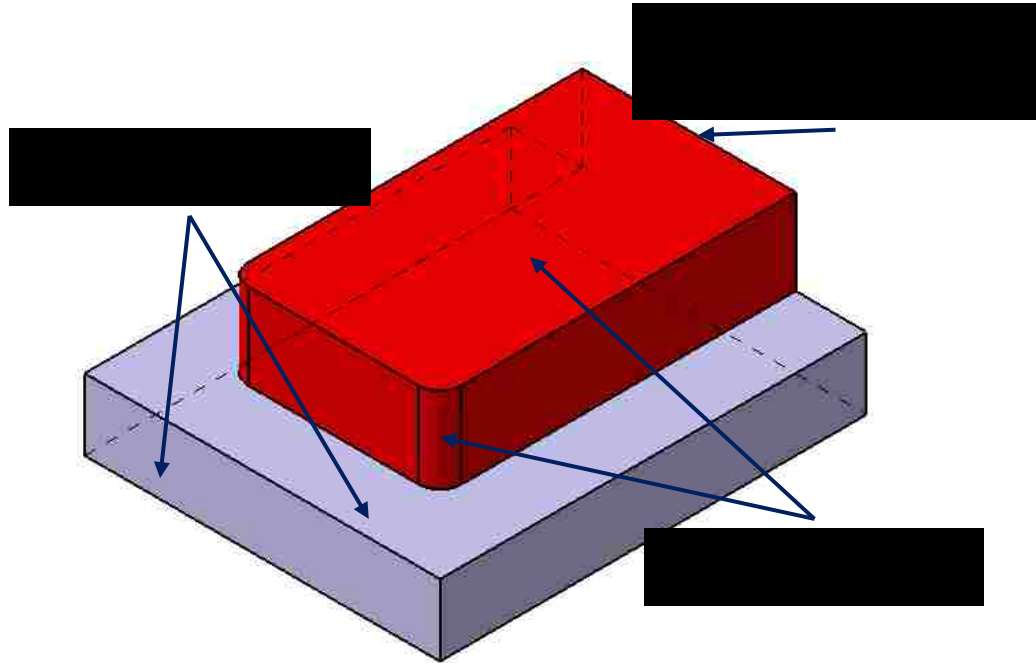


Figure 5.5: CAD model of test mold-insert and some boundary conditions

In terms of the hydraulic entrance length, the total length of each cooling channel of the parametric study is relatively short compared with those in the comparison study. Therefore, for the fluid regions of the parametric study, a fully developed inlet flow is used as the inlet boundary condition. The fully developed flow profiles are obtained from the simulations with a straight channel with the diameter ( $D$ ) of  $6\text{ mm}$  and the length of  $10D$ . A periodic boundary condition is used between the inlet and outlet of the channel to simulate an infinitely long cooling channel. The respective inlet mass flow rates of single/multiple cooling channels for the parametric study is used to drive the flow in the straight channel. After the simulations are converged, profiles of velocity, turbulence intensity and turbulence viscosity ratio data are extracted and mapped as the inlet boundary condition for the test cases of the parametric study. As in the comparison study, flow split outlet is used as the outlet boundary condition for the current study.

### **5.2.3 Physical Properties**

To keep consistency throughout this research, thermal properties of standard P20 mold steel, shown in Table 4.2, are used for the parametric study as well. Additionally, temperature dependent thermal properties of water, illustrated in Section 3.1.3, are used and programmed into the simulations.

### **5.2.4 Mesh**

Since the geometry and Reynolds number (turbulence characteristics) are kept the same as in the comparison study of Chapter 3, the meshing parameters shown in Table 4.3, are used to mesh the computational domains for the parametric study simulations.

## **5.3 Results and Analyses**

From the industrial point of view, the temperature and its distribution on the heating surface and the pressure drop within the cooling system are of vital importance when evaluating the performance of injection mold cooling systems. The former is directly related to the cooling time and quality of the molded parts while the latter determines the required pumping power. First, the influence of channel bend curvature ratio on the coolant flow patterns, temperature distribution inside the cooling channel and the heat transfer coefficient on the channel wall are analyzed using the advantage of CFD analysis to predict turbulent flows and the convective heat transfer. This can provide mold designers with a better understanding of the coolant flow patterns in channels with 90° bends or U-shape bends that are constructed with two 90° bends, providing a more scientific and data-driven basis for their future designs. Then, the individual significance of the three tested geometrical design parameters on the temperature distribution on the heating surface is analyzed along with the pressure drop in the cooling systems.

### 5.3.1 Coolant Flow Analyses

#### 5.3.1.1 Dean Vortex

Due to the centrifugal force that exists in the flow at a curved channel bend, the fluid in the centre of the channel tends to travel outwards of the bend. The fluid is then confined by the outer wall and recirculates inwards along the channel walls [33]. This phenomena introduces two large counter-rotating vortical structures in the channel, denoted as Dean vortices [34], named after the researcher who first described such vortices analytically. A schematic of Dean vortices is shown in Fig. 5.6. The U-shape channel bends tested in this parametric study are either smooth  $180^\circ$  bends or made up of two  $90^\circ$  bends which are connected by a short straight channel section. Therefore, the main flow development and the temperature distribution in the cooling channel are expected to be influenced by this secondary flow. The smooth  $180^\circ$  bends can also be considered as two  $90^\circ$  bends directly connected to each other. Between the two  $90^\circ$  bends that constitute the U-shape bends, the development of Dean vortices around the first  $90^\circ$  bend after the inlet is analyzed because the approaching flows for these  $90^\circ$  bends are almost identical and hydraulically fully developed.

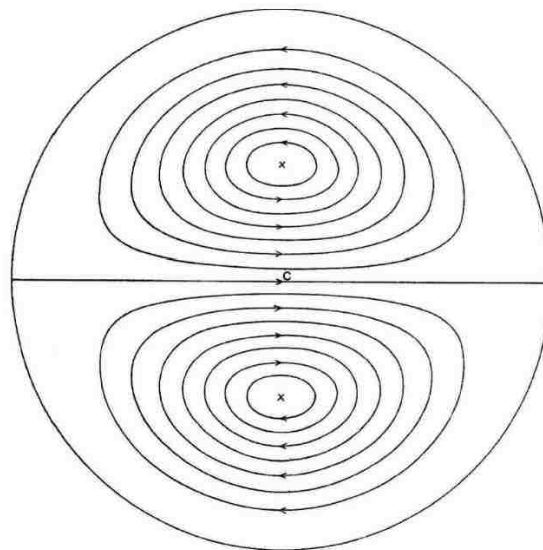


Figure 5.6: Dean vortex (reprinted from *Dean and Hurst 1927* [34])

Figure 5.7 shows the secondary flow field in the channel cross-sections at  $0^\circ$ ,  $45^\circ$  and  $90^\circ$  of the  $90^\circ$  bends of test case 1-1, 1-2, 1-5 and 1-10. Line convolution visualization method is used for its ability to capture the velocity distribution and centres of the Dean vortices. It is known that the Dean vortices oscillate around the horizontal centre plane of the channel when the flow is in the turbulent regime [35]. However, since only the mean flow and the cycle averaged cooling performance are of interest in this research, the oscillation is not considered. The stagnation points of the secondary flow are found to be located at the centre of the inner and outer side walls of the bend. It is found that with the curvature ratio increasing from  $\delta = 2$  to  $\delta = 10$ , the flow patterns in these cross-sections remain consistent but the cross-flow velocity is reduced. Also, the centres of the Dean vortices in these cases are observed at similar locations. On the other hand, the flow pattern for channels with curvature ratio of  $\delta = 1$  is quite different from the others. The maximum cross-flow velocity is found after the  $45^\circ$  cross-section of the  $90^\circ$  bend and the centres of the Dean vortices in the  $45^\circ$  cross-section of the bend shift from inner bend side to the centre of the channel.

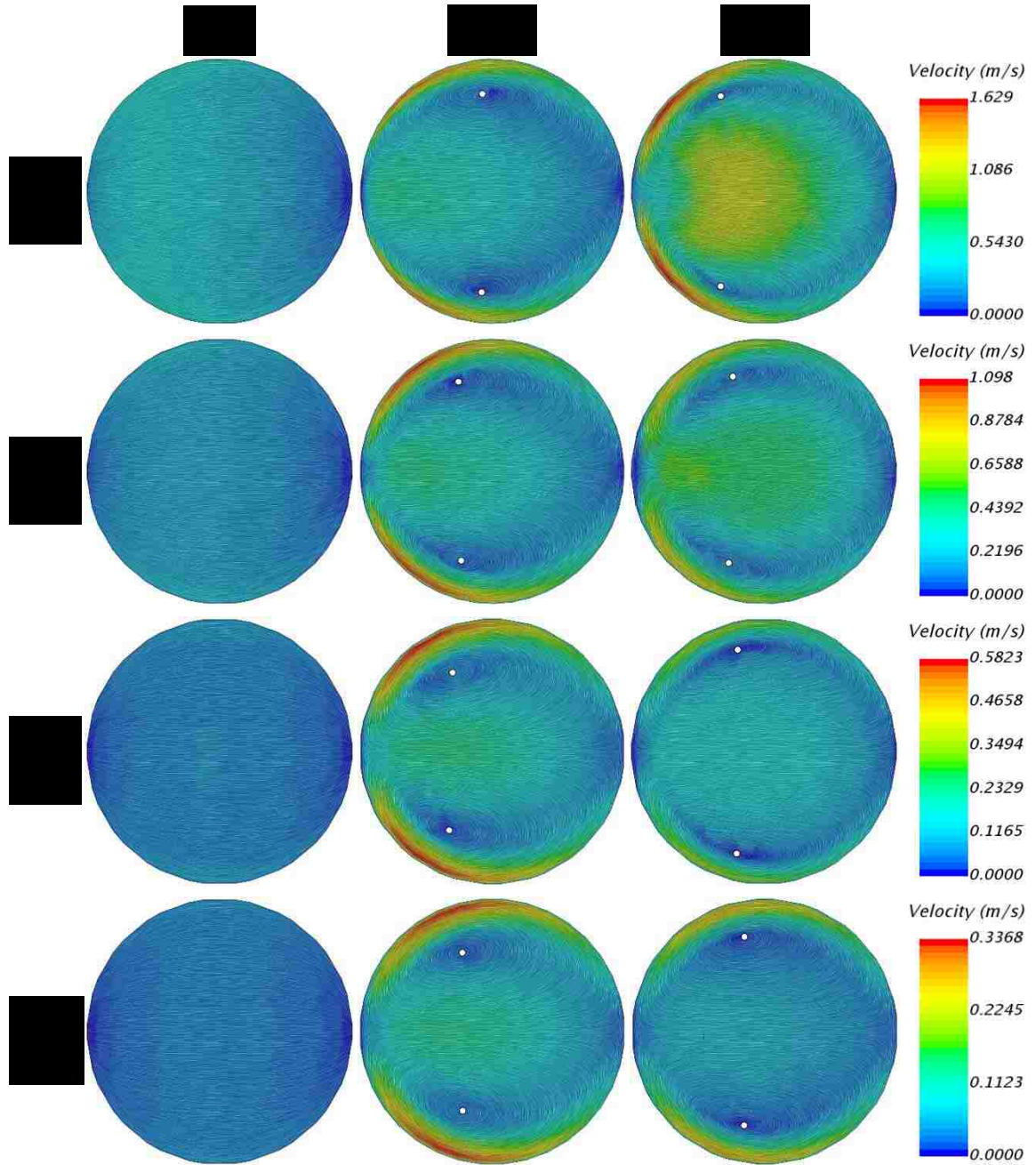


Figure 5.7: Secondary flow velocity at 0°, 45° and 90° of the 90° bend. Viewed from the streamwise direction (For all cross-sections, left-hand side is the inside of the bend. White dots in the figures represent the centre of the Dean vortices)

### 5.3.1.2 Main Flow Development

In Fig. 5.8, the first 90° bend after the inlet of test cases 1-1, 1-2, and 1-5 are presented to demonstrate the coolant velocity magnitude in the horizontal symmetry plane of the channel and the streamwise velocity in five selected channel cross-sections. These cross-sections are located at 0°, 45° and 90° through the bend and at 2D and 5D after the bend in each case. The effect of the centrifugal force on the flow is evident as the high velocity fluid gets deflected outwards of the bend. The flow will not recover from this effect even at the end of the straight channel section for all the test cases and it will further influence the flow development in the second 90° bend after the inlet. Although one might expect that this effect lasts longer after the bend with a lower curvature ratio, the data shows that the opposite is true. This can be explained by the higher turbulent kinetic energy caused by the bend with lower curvature ratio (see Fig. 5.9), which subsequently enhances the mixing of the flow after the 90° bend.

It is also observed that, only when the curvature ratio is  $\delta = 1$ , there is a strong separation zone attached to the channel wall at the inner side of the bend. This agrees with Hufnagel's report [35] which concluded that a strong curvature ( $\delta \ll 1.67$ ) leads to the flow separation in the bend which will influence the downstream flow development. Based on the above analysis of the secondary flow in the channel, the maximum cross-flow velocity occurs after the middle of the bend when the curvature ratio is  $\delta = 1$ . This produces the strong separation zone near the end of the channel bend, since the flow here is mainly influenced by the cross-flow before the end of the bend. Additionally, this phenomenon enhances the mixing after the channel bend. It could also be used to explain why the effect of the curved channel bend diminishes faster after bends with curvature ratio of  $\delta = 1$ .

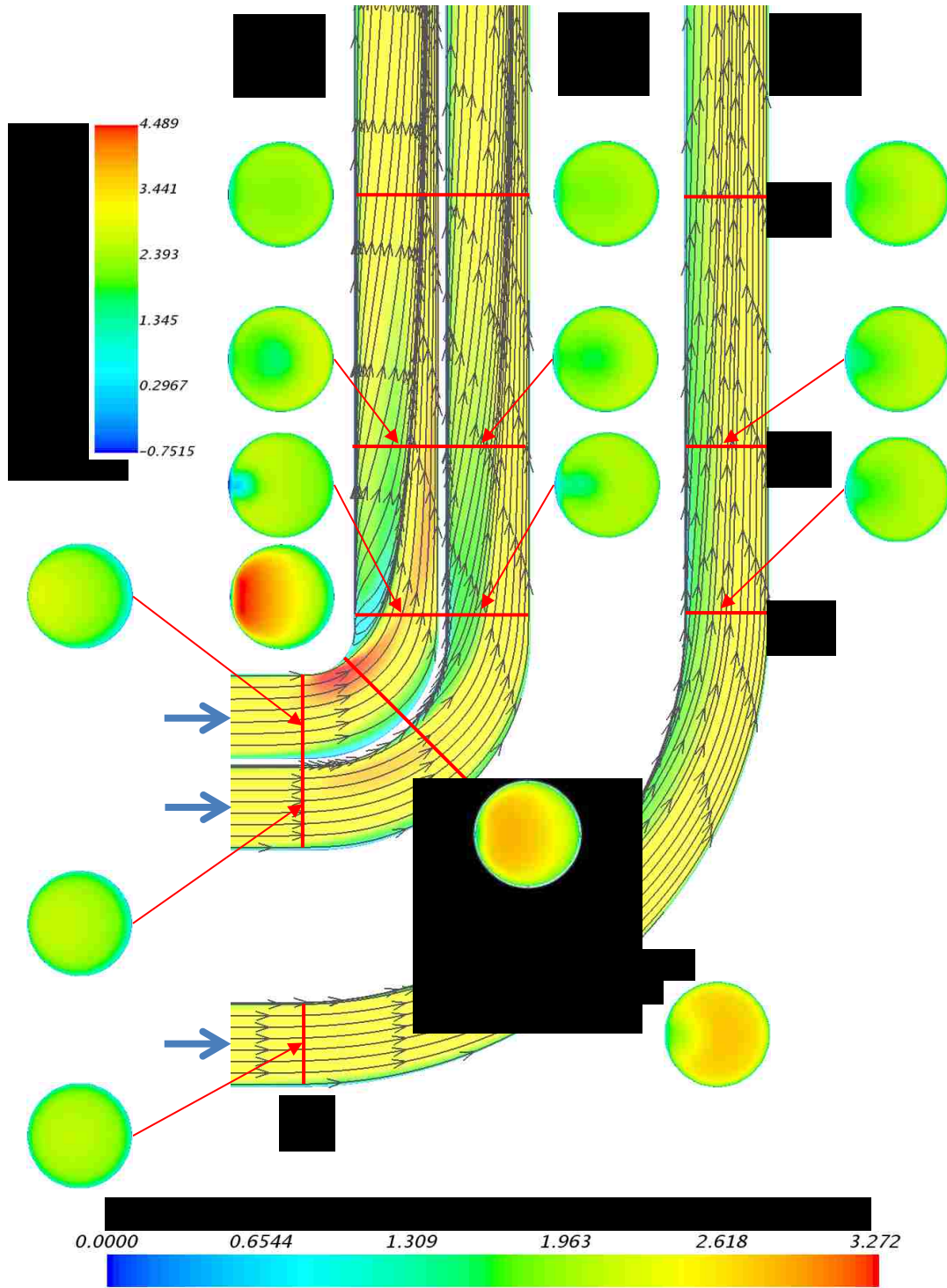


Figure 5.8: Velocity magnitude and streamlines in the symmetry planes and streamwise velocities in selected cross-sections for case 1-1, 1-2 and 1-5

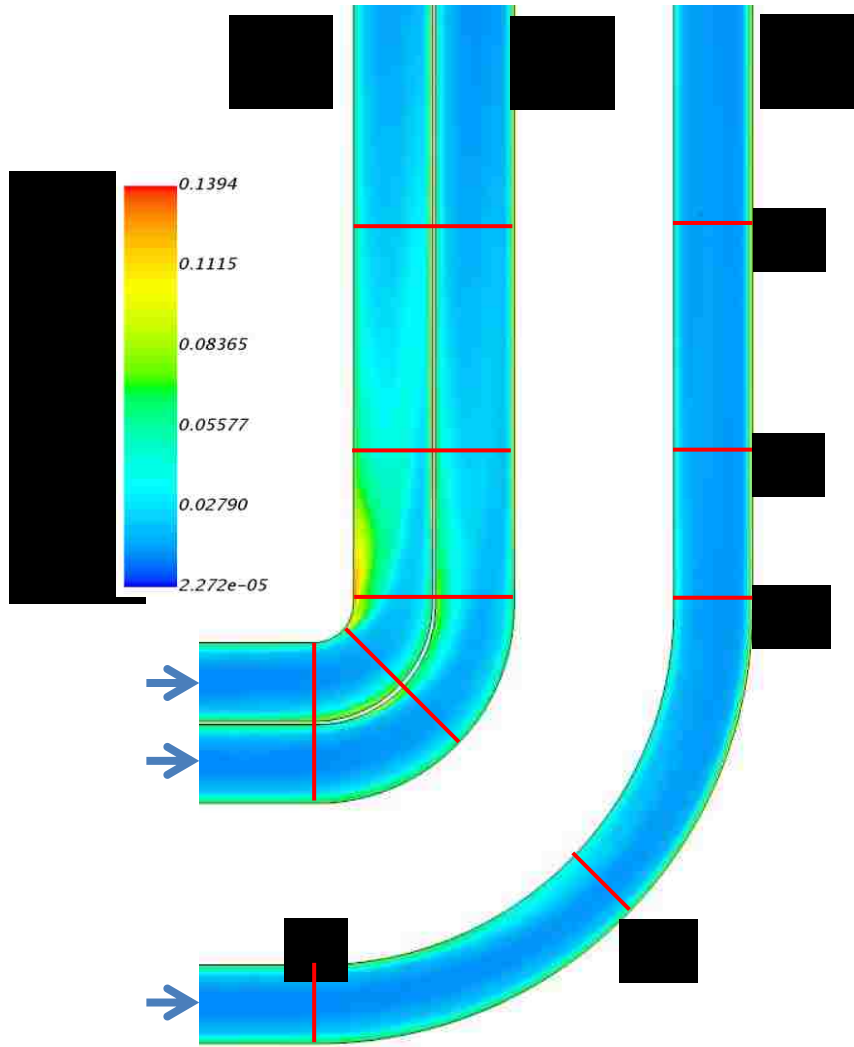


Figure 5.9: Turbulent kinetic energy in the symmetry planes for case 1-1, 1-2 and 1-5

Figure 5.10 further confirms that the strong separation zone caused by the sharp bend not only occurs with high Reynolds number flow but also exists in test cases with the lowest curvature ratio in two and three channels, where the Reynolds number is decreased proportional to the number of channels. Therefore, in the following analyses, the difference between test cases with  $90^\circ$  bends which have curvature ratio of  $\delta = 1$  and other test cases is focused to reveal the influence of the curvature ratio of  $90^\circ$  bends on the flow patterns and temperature distribution in the channel.



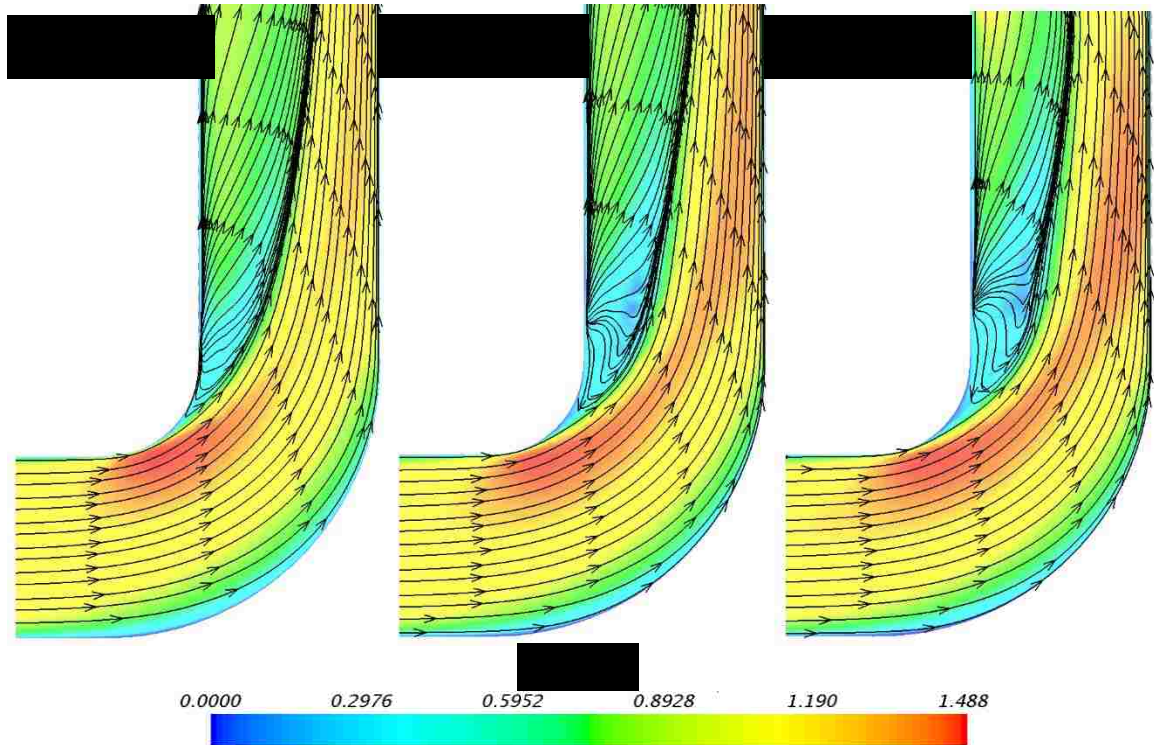


Figure 5.10: Velocity magnitude and streamlines in the symmetry planes of test case (a) 1-1, (b) 2-1 and (c) 3-1

The strong separation zone caused by the 90° bends with curvature ratio of  $\delta = 1$  results in a higher pressure drop in the cooling channel. This is depicted in Fig. 5.11. With curvature ratio of the 90° bend increasing from  $\delta = 1$  to the maximum value that is possible based on the pitch distance between inlet and outlet of the channel, the pressure drop decreases dramatically between  $\delta = 1$  and  $\delta = 2$ , then reduces slowly as the curvature ratio increases beyond  $\delta = 2$ . The high pressure drop associated with sharp ( $\delta = 1$ ) 90° bends will also accumulate in actual cooling systems when multiple 90° bends with curvature ratio of  $\delta = 1$  are used in series connection. Therefore, in terms of pumping power required by the injection mold cooling system, careful consideration should be taken when using cooling channels of 90° bend with curvature ratio of  $\delta = 1$ . It can be also noticed that, with 90° bends of the same curvature ratio, the pressure drop in the cooling systems with channel depth of  $H = 5D$  is lower than those of  $H = 2D$ . This is because

the total length of the cooling channel is shorter given the limited space when channel depth is  $H = 5D$ .

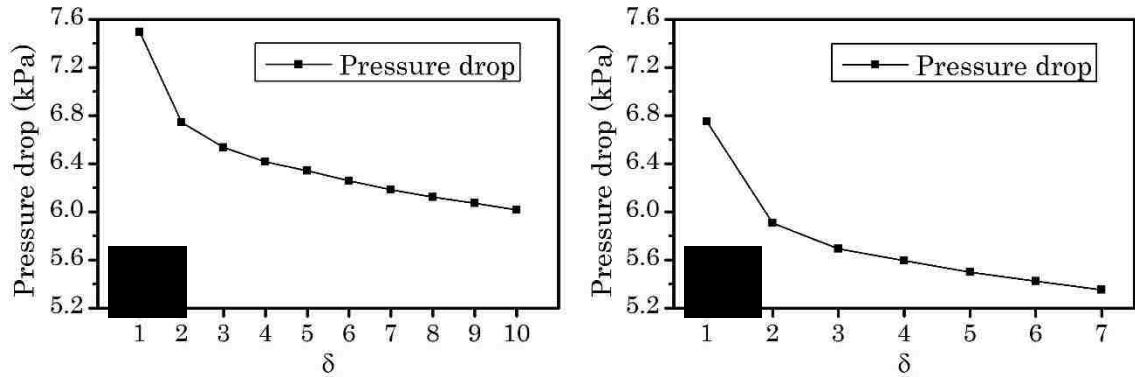


Figure 5.11: Pressure drop vs curvature ratio in the channel of test cases with one cooling channel, (a)  $H = 2D$ , (b)  $H = 5D$

### 5.3.1.3 Temperature Distribution in the Channel

Five channel cross-sections are selected to analyze the temperature distribution in the coolant flow for different curvature ratios. Their positions are illustrated in Fig. 5.12. Note that all the cross-sectional figures are viewed from the streamwise direction; hence, the adjacent heating surface is always located at the top and right-hand side of these cross-sections.

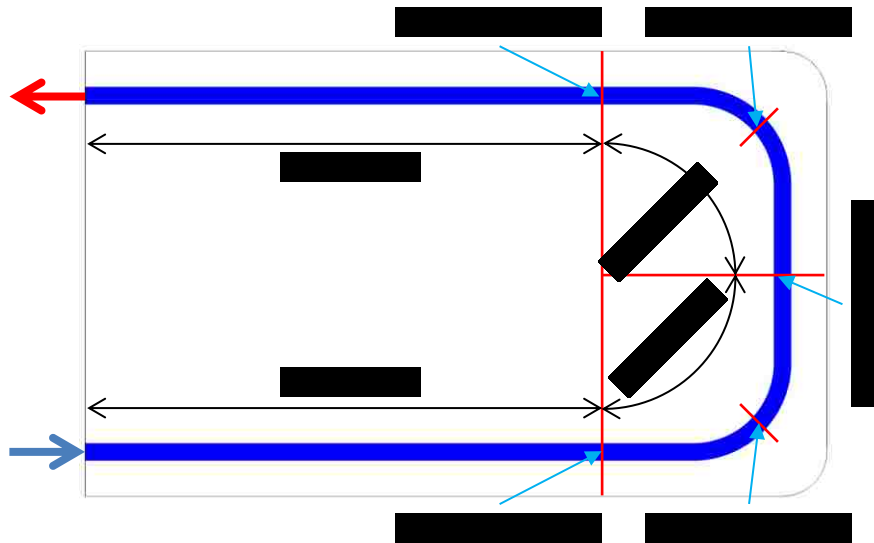


Figure 5.12: Channel cross-sections used for the study of temperature distribution in the coolant flow and channel sections used for the study of heat transfer coefficient at the cooling channel wall

Figures 5.13 and 5.14 show the temperature distribution in the five channel cross-sections which cover the entire U-shape bend. The temperature distribution at the cross-section 1 are identical for all the cases because the flow still has not entered the curved channel section and has received the same amount of heat from the heating surface. The temperature distributions in the rest of the channel cross-sections are affected by the curved channel bend. First, as discussed above, the high velocity fluid is deflected to the outer side of the bend due to the centrifugal force. This phenomenon leads to lower coolant temperature at the outer area of the bend by increasing the convective heat transfer. Due to the Dean vortices, colder fluid is pushed to the outer wall by the cross flow and extracts the heat from the side wall of the heating surface. The heated fluid is then returned to the inner side along the top and bottom walls of the channel. Because of low velocity at the inner wall where both recirculating flows meet, high temperature of the fluid is observed.

The effects of the curved channel bends on the coolant flow pattern and the temperature distribution in the channel diminish in the straight channel-section which connects the two 90° bends. This is depicted by channel cross-sections with curvature ratio of  $\delta = 1, 4$  and 7 in Fig. 5.12 and  $\delta = 1$  and 4 in Fig. 5.13. The heat concentration area at the inner side of cross-section 3 is smaller than that of cross-section 2 for these cases. In contrast, the heat concentration area continues to grow through five channel cross-sections when the two 90° bends connect to each other directly to form the U-shape bend. (Case with  $\delta = 10$  in Fig. 5.13 and case with  $\delta = 7$  in Fig. 5.14)

It can be concluded that the temperature distribution in the coolant flow is not only influenced by the curvature ratio of the 90° bends but also strongly influenced by the length of the straight channel-section which connects the two 90° bends. The shorter the straight channel-section, the more consistent is the effect of Dean vortices on the temperature distribution in the coolant flow.

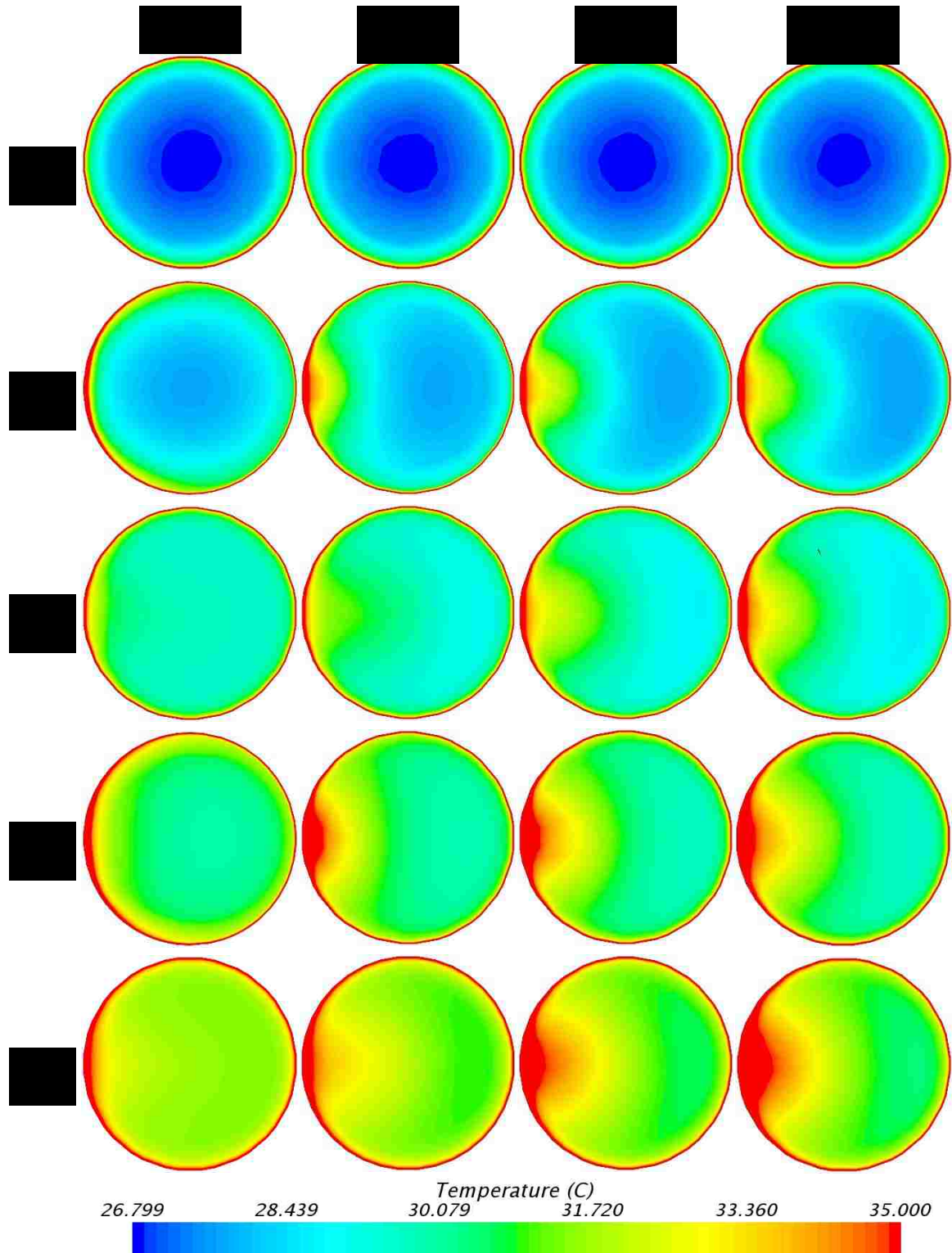


Figure 5.13: Temperature distribution in five channel cross-sections for cases with channel depth of  $2D$

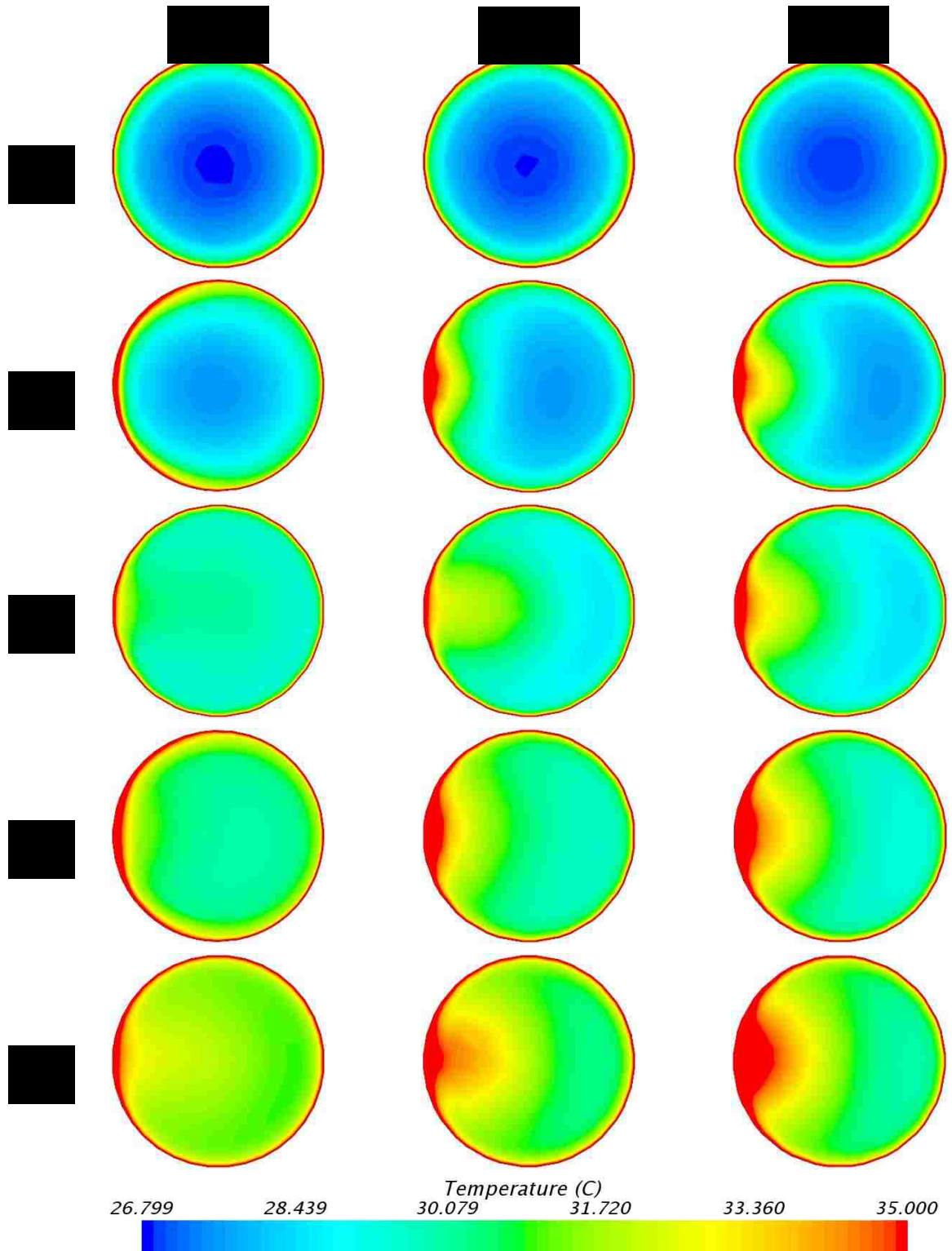


Figure 5.14: Temperature distribution in five channel cross-sections for cases with channel depth of  $5D$

#### 5.3.1.4 Heat Transfer Coefficient

Figure 5.15 shows the heat transfer coefficient at the channel wall of four consecutive channel-sections from test cases with one cooling channel. The definitions of these cooling channel sections are illustrated in Fig. 5.11. It is found that, for each test case, the heat transfer coefficients in the curved channel sections are higher than those in the straight sections and the channel-section 4 has higher heat transfer coefficient than the channel-section 1. This can be explained by the higher turbulent kinetic energy which is further enhanced by the 90° bends and the secondary flow associated with 90° bends, which also stimulate the mixing and heat transfer process. With the curvature ratio of the 90° bend increasing from  $\delta = 2$  to  $\delta = 10$ , the heat transfer coefficients of channel sections 2, 3 and 4 all increase.

For the case with 90° bends which have curvature ratio of  $\delta = 1$ , the pattern of the heat transfer coefficient change in the four channel-sections does not fit the trend of the rest of the cases because the flow pattern is different. A strong separation zone exists at the inner wall of the 90° bend. With this strong separation zone, the effect of the deflection of fluid with higher velocity to the outer wall of the bend is stronger and the turbulent kinetic energy in and after the bend is higher as well. This phenomenon results in higher heat transfer coefficient at the 90° bends with curvature ratio of  $\delta = 1$ . However, the heat transfer coefficient of the channel-section 3 is relatively lower. This is due to the fact that, in the longer straight channel that connects the two 90° bends when the curvature ratio  $\delta = 1$ , the effect of the curved bend on the flow recovers more compared to cases with curvature ratios larger than  $\delta = 1$ .

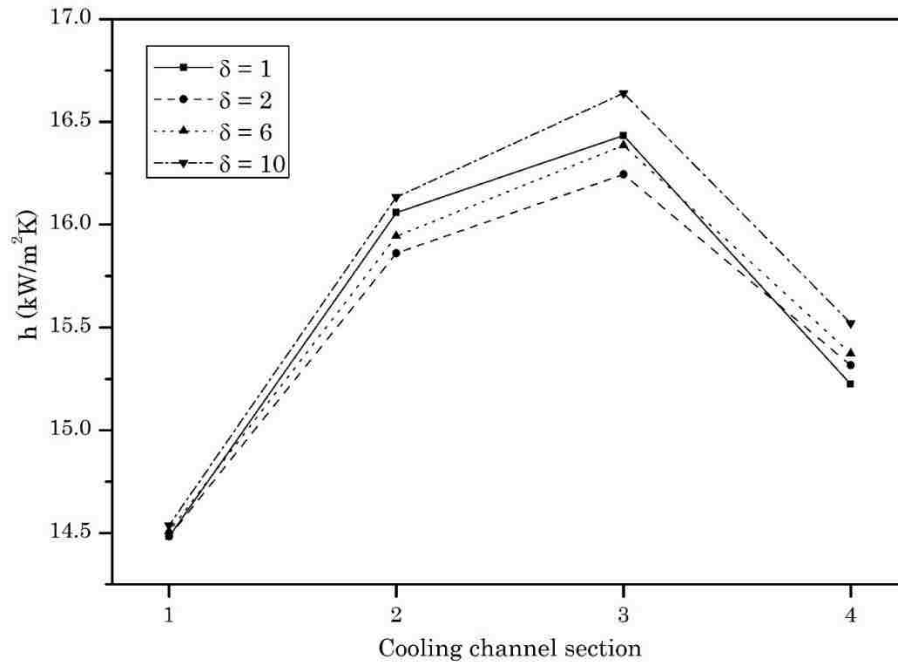


Figure 5.15: Heat transfer coefficient at channel wall of four consecutive channel-sections (defined in Fig 5.11) from test cases with one cooling channel

### 5.3.2 Cooling Performance Analyses

Thus far, the influences of the curvature ratio of 90° bends and the cooling channel depth on the coolant flow development, the temperature distribution in the cooling channel and the heat transfer coefficient on the channel wall have been investigated. Since the current study is focused on the performance of injection mold cooling systems, the temperature distribution on the heating surface and the pressure drop within the cooling system are still the main concerns when evaluating the significance of design parameters.

#### 5.3.2.1 Maximum Temperature on the Heating Surface

The most basic requirement for a part to be ejected from the mold is that the temperature on the molded part has reduced below the DTUL. Therefore, the maximum temperature on the heating surface is the main factor that influences the cooling time of an injection molding process. Figure

5.16 shows the temperatures on the heating surfaces of several representative test cases. Overall, the temperature on the heating surface in cases with channel depth of  $H = 2D$  is lower than those in cases with channel depth of  $H = 5D$ . In terms of the maximum temperature on the heating surface, smaller channel depth is desired. It can be also noticed that, when the second  $90^\circ$  bend has curvature ratio of  $\delta = 1$  and the same channel depth, the maximum temperature on the heating surfaces of cases with one, two and three channels are very close to each other. It can be concluded that the number of cooling channels has little influence on the maximum temperature on the heating surface.

The influence of the curvature ratio of  $90^\circ$  bends on the maximum temperature on the heating surface is studied by using cases with one cooling channel. By comparing (a) with (c) in Fig. 5.16, it is noticed that the hot spot changes position with different curvature ratios of  $90^\circ$  bends. This is also reflected in Fig. 5.17 (a). The maximum temperature increases very slowly with the curvature ratio when the curvature ratio is lower than  $\delta = 5$  because the hot spot located at the centre area of the top heating surface changes slowly with the increase of curvature ratio of  $90^\circ$  bends. When the channel depth is larger, such as shown in (b) and (d) in Fig. 5.16, there is no hot spot shift. The maximum temperature increases linearly with the curvature ratio of  $90^\circ$  bends, as shown in Fig. 5.17 (b). This is mainly because the distance between the curved corners of the heating surface and the channel wall of the  $90^\circ$  bend increases as the curvature ratio gets higher.



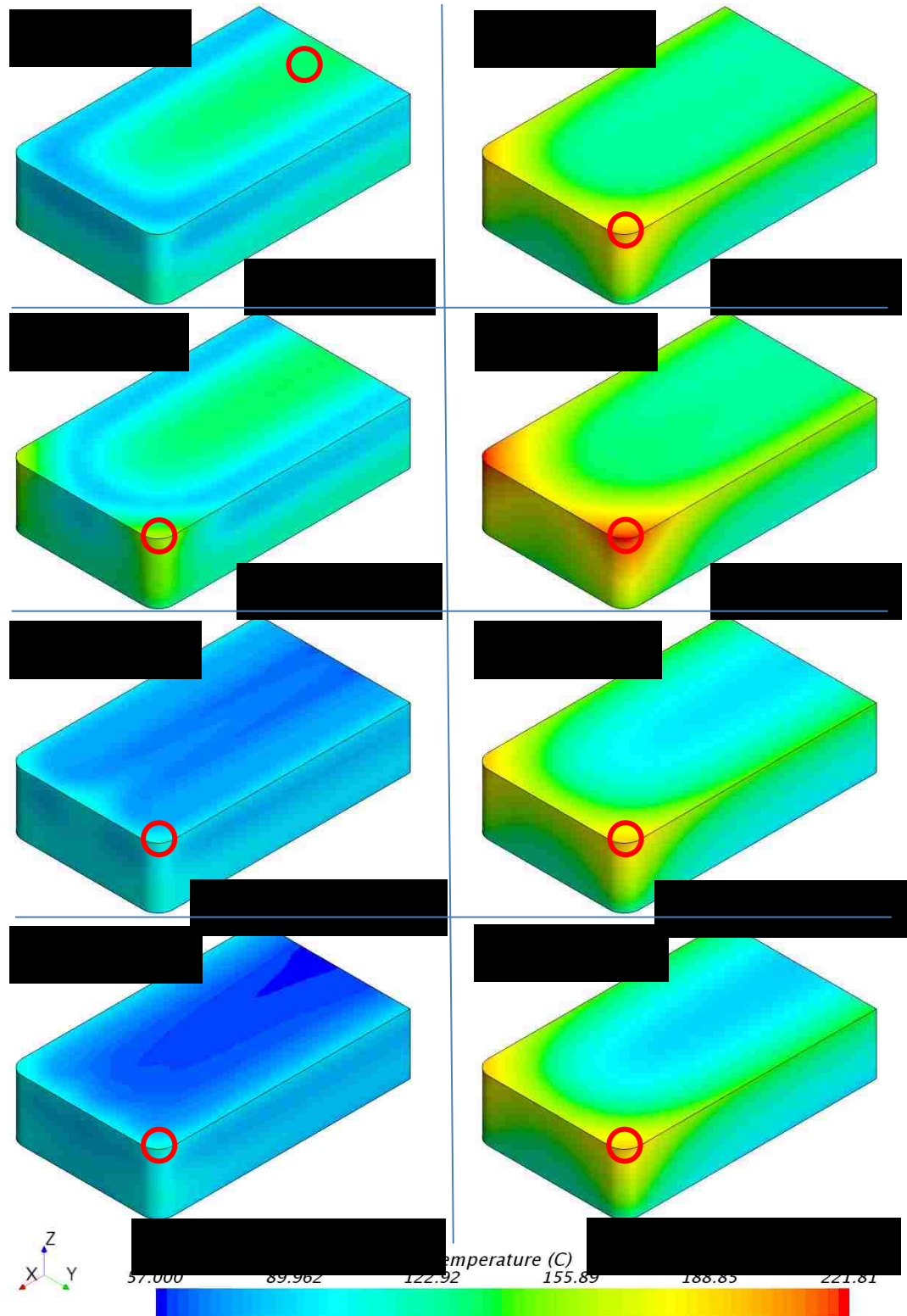


Figure 5.16: Temperature distribution on the heating surface for cooling systems with different cooling channel depths and bend configurations (red circle represents location of the hot spot)

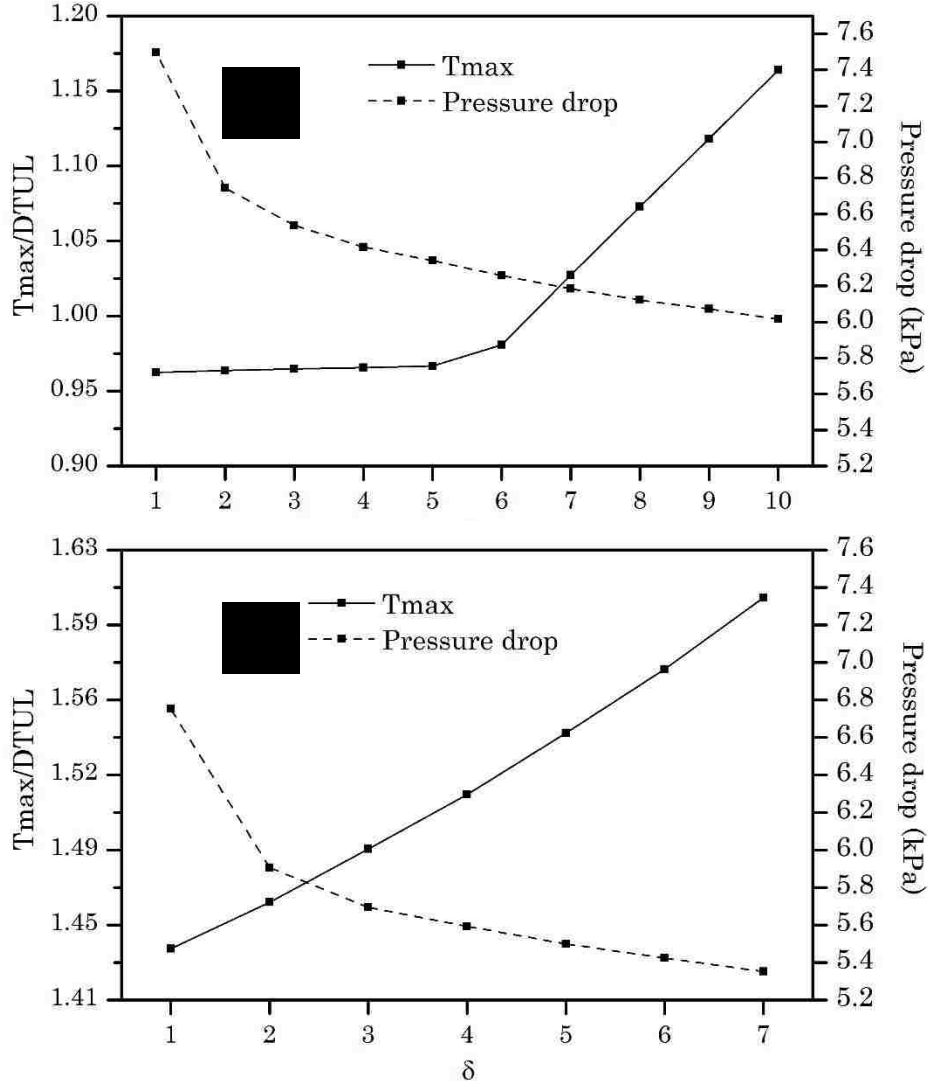


Figure 5.17: Maximum temperature and pressure drop vs. curvature ratio of the channel bend for the single channel cases, (a)  $H = 2D$ , (b)  $H = 5D$

### 5.3.2.2 Temperature Uniformity on the Heating Surface

Other than the maximum temperature on the heating surface, the uniformity of the temperature distribution on the heating surface also has influence on the cooling time of an injection molding process and the quality of the molded part. Therefore, a uniformity index provided by Star-CCM+ [29]

$$T_{uni} = 1 - \frac{\sum_f |T_f - T_{ave}| A_f}{2|T_{ave}| \sum_f A_f} \quad (5.4)$$

is used to evaluate the influence of the three design parameters, in which  $T_f$  represents temperature on each surface mesh cell,  $A_f$  is the surface area of that surface mesh cell and  $T_{ave}$  represents the average temperature on the entire heating surface.

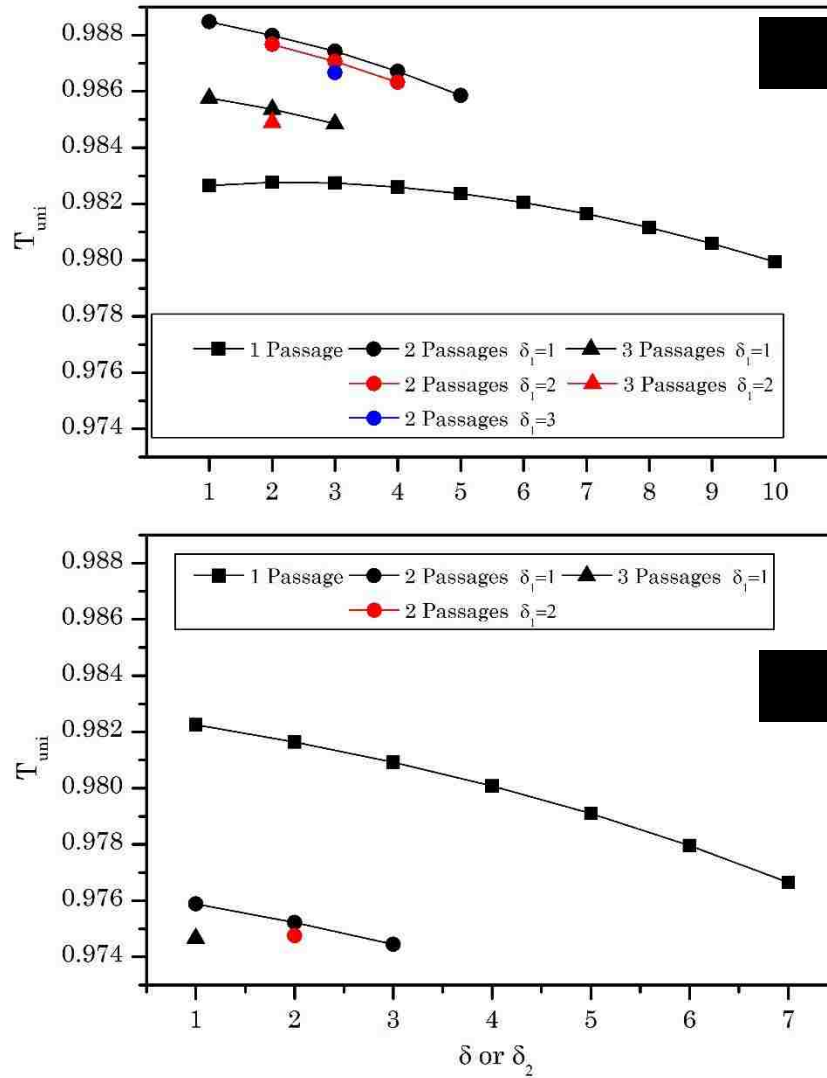


Figure 5.18: Temperature uniformity vs. curvature ratio of second 90° bend after the inlet of the cooling channel, (a)  $H = 2D$ , (b)  $H = 5D$

Figure 5.18 shows the temperature uniformity for all the test cases. It can be noted that the effect of the strong separation zone associated with 90° bends with curvature ratio of  $\delta = 1$  is insignificant on the temperature distribution on the heating surface. The temperature uniformity decreases

with the rise of the curvature ratio of the first 90° bend after the inlet but the extent of this influence is very small compare to the influence of the curvature ratio of the second 90° bend after the inlet. This can be explained by the arrangement of the coolant flow inlet and outlet shown in Figs. 5.2, 5.3 and 5.4. The curvature ratio of the second 90° bend after the inlet has more influence on the temperature distribution on the heating surface because these 90° bends are closer to the corners of the heating surface where the hot spot generally occurs. In general, cases with channel depth of  $H = 2D$  has better temperature uniformity on the heating surface than those with channel depth of  $H = 5D$ . When the channel depth is  $H = 2D$ , cases with two cooling channels provide the best temperature uniformity on the heating surface, while cases with one channel provide the best temperature when the channel depth is  $H = 5D$ .

### 5.3.2.3 Pressure Drop in the Cooling System

The pressure drop in the cooling system determines the required pumping power of the injection molding machines. It is part of the operational cost of the injection molding process. It is well known that bends in the channel generate greater pressure loss than if the channel were straight, especially if the bend is sharp [31]. Based on the previous analysis (Section 5.3.2.1), it is confirmed that there is higher pressure drop caused by the strong separation zone which only occurred in 90° bends with strong curvature (curvature ratio of  $\delta = 1$  in this study). The test cases were designed by maintaining the same channel diameter and the total inlet mass flow rate for cooling systems with one, two and three channels. Therefore, the influence of the number of cooling channels on the pressure drop in the cooling system is studied in this section.

According to the previous analyses, 90° bends with curvature ratio of  $\delta = 1$  result in much higher pressure drop in the cooling system. Therefore, the pressure drop in the cooling systems with one, two and three channels, in

which all the channel bends are with curvature ratio of  $\delta = 1$ , are used in the following study.

To validate the simulation results, the pressure drop in a cooling channel can also be calculated from Eqns. (5.5) to (5.7) [31]:

$$\Delta p = \Delta p_{major} + \Delta p_{minor} \quad (5.5)$$

$$\Delta p_{major} = f \frac{l}{D} \frac{\rho V^2}{2} \quad (5.6)$$

$$\Delta p_{minor} = K_l \frac{\rho V^2}{2} \quad (5.7)$$

in which  $f$  represents friction factor, whose value can be found based on the Moody chart [36].  $K_l$  represents the minor loss coefficient. The minor pressure loss coefficients related to 90° channel bends are reported by White [37]. Details of the analytical calculation of the pressure drop in cooling channels are demonstrated in Table 5.4.

Table 5.4: Details of the analytical calculation of the pressure drop in the cooling system

Number of channels	$Re$	$f$	$l$ (mm)	$\Delta p_{major}$ (kPa)	$K_l$	$\Delta p_{minor}$ (kPa)	$\Delta p$ (kPa)
1	14790	0.0279	566	<b>6.35</b>	0.23	<b>0.56</b>	<b>6.47</b>
2	7395	0.0335	486	<b>1.64</b>	0.23	<b>0.14</b>	<b>1.92</b>
3	4930	0.0375	470	<b>0.79</b>	0.23	<b>0.06</b>	<b>0.91</b>

In Fig. 5.19, good agreement between the pressure drop values from numerical results and analytical calculations is observed. It is found that the pressure drop reduces significantly by increasing the number of cooling channels from 1 to 2; while the reduction of pressure drop is relatively small between channel numbers of 2 and 3.

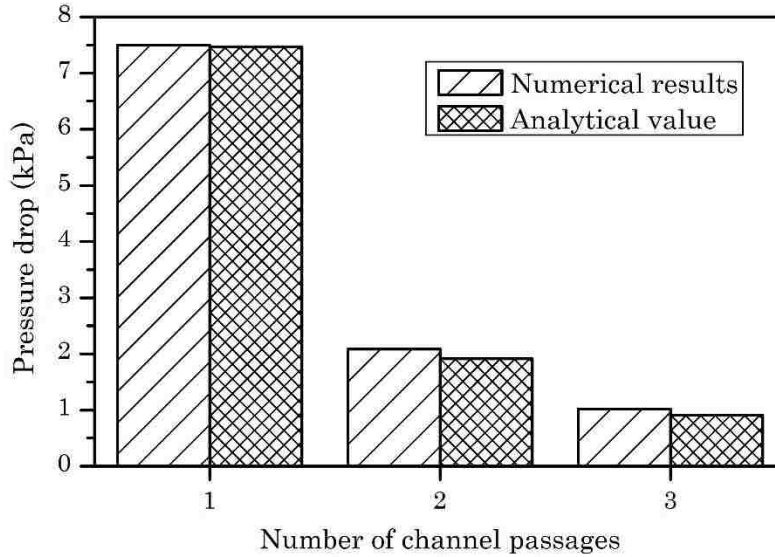


Figure 5.19: Pressure drop of cooling systems with one, two and three channels

In Fig. 5.17, among all the test cases with one cooling channel, the largest pressure drop difference between cases with different curvature ratios is  $1.5 \text{ kPa}$ , which is very small compared to the pressure drop change caused by the increase of the number of cooling channels. This can be explained based on Table 5.4, which shows that the reduction of pressure drop by increasing the number of cooling channels is largely the results of the decline of the major pressure loss due to the decline of the Reynolds number in the cooling channel as the fixed mass flow rate is equally distributed by a manifold.

## 5.4 Summary

In this chapter, a parametric study is conducted to examine the significance of three geometrical design parameters. These design parameters are associated with conformal cooling channels consisting of U-shape bends. Also, given the advantages of the CFD analysis, the influence of the secondary flow (Dean vortices) on the coolant flow development and the temperature distribution in the cooling channel are analysed.

It is concluded that the curvature ratio of the bend impacts on the coolant flow development and the temperature distribution in the channel. Curvature ratios of bends which are close to the heating surface where the hot spots are located have a significant influence on the cooling performance due to its influence on the distance between the cooling channel and the heating surface. The same observation applies for the cooling channel depth from the heating surface. The influence of the number of cooling channels on the maximum temperature on the heating surface is very small compared to the other two design parameters. However, the number of cooling channels has the strongest impact on the pressure drop in the cooling system.

# Chapter 6

## Conclusions and Future Work

In this thesis, CFD simulations are used to compare the performances of conventional and conformal injection mold cooling system designs and to evaluate the influences of three geometrical design parameters on the cooling performance. These design parameters are related to conformal cooling systems which consist of U-shape channel bends. A summary of the work conducted, the key findings of the research and some recommendations for future work are presented in this chapter.

### 6.1 Summary and Conclusions

In Chapter 3, the numerical model used in this research is validated with experimental data. As part of the validation process, two turbulence models commonly used in industry, Realizable  $k-\varepsilon$  and SST  $k-\omega$ , are adopted and compared. The influence of two different types of inlet boundary conditions, namely uniform velocity inlet and fully developed velocity inlet, on the numerical results has also been tested and discussed. It is concluded that:

- Both Realizable  $k-\varepsilon$  and SST  $k-\omega$  turbulence models have the capability to accurately simulate the conjugate heat transfer process in a straight pipe.



- Given the accuracy of the SST  $k\text{-}\omega$  turbulence model and its capability to resolve the boundary layer in flows with adverse pressure gradients and recirculation due to flow separations at channel elbows, the SST  $k\text{-}\omega$  turbulence model is more suitable for predicting the performance of injection mold cooling systems.
- When the hydraulic entrance length is relatively short compared to the length of the entire cooling channel, uniform velocity inlet and fully developed velocity inlet produce similar results. Therefore, the selection of inlet flow conditions can be made based on the interest of the specific study.

In Chapter 4, the cooling performances of two injection mold cooling system designs are compared along with ten total inlet mass flow rates. One design is the conventional cooling system which is manufactured by gun drilling and routed by cooling baffles and plugs; the other is the conformal cooling system which is fabricated by 3D printing. The advantages of using the conformal cooling system are discussed. The key conclusions are:

- With the same total inlet mass flow rate, the conformal cooling system provides lower temperature and more uniform temperature distribution on the heating surface than the conventional cooling system. Therefore, it can be concluded that the conformal cooling system has better cooling performance than the conventional cooling system.
- In terms of the maximum temperature on the heating surface, the conformal cooling system improved the cooling performance by approximately 14%.
- With the increase of total inlet mass flow rate, the pressure drop increases for both conventional and conformal cooling systems. However, the pressure drop increase is much smaller in the conformal cooling system than in the conventional cooling system. This indicates that the conformal cooling system

provides better cooling performance while not consuming more pumping power, especially when the total inlet mass flow rate is high.

Mold-inserts with a conformal cooling system need to be fabricated by 3D printing, resulting in higher cost than mold-inserts with conventional cooling systems at manufacturing stage. Thus, the desire to fully explore the potential of conformal cooling channels is the motivation behind this research. In Chapter 5, three geometrical design parameters which are related to conformal cooling systems with U-shape channel bends are evaluated by conducting a parametric study with a simplified CAD model. The following conclusions can be made from this investigation:

- The curvature ratio of 90° bends which are close to the heating surface where the hot spots are located has significant influence on both the maximum temperature and the uniformity of the temperature distribution on the heating surface due to the shorter distance between the cooling channel and the heating surface.
- The flow patterns and the temperature distribution in the cooling channel change significantly with changes in the 90° bend curvature ratio, but it does not have much effect on the heating surface.
- The cooling channel depth from the heating surface has significant influence on the overall temperature on the heating surface since it determines the distance between the cooling channel and the heating surface.
- The influence of the number of cooling channels on the maximum temperature on the heating surface is very small compared to the other two design parameters. However, the number of cooling channels has the strongest impact on the pressure drop in the cooling channel.

## 6.2 Potential Future Work

In this study, the conformal cooling system consisting of U-shape channel bends is considered. For the future work, more configurations should be examined to construct a more complete set of guidelines for future injection mold cooling system designs.

Operational parameters such as properties of various plastic materials, different inlet mass flow rates, different coolant inlet temperatures and different types of coolant can be studied. In such parametric studies, Nusselt number, which is the non-dimensional group used to demonstrate the ratio of convective to conductive heat transfer at a boundary in a fluid could be a good measure of the cooling performance.

It is known that the channel walls of injection mold cooling systems will be eroded by the coolant flow over a period of time. Therefore, surface roughness can also be integrated into the comparison and/or parametric studies to reveal how the cooling performance changes after operating the injection mold tool for some time.

# References

- [1] D. E. Dimla, M. Camilotto, F. Miani. Design and Optimisation of Conformal Cooling Channels in Injection Moulding Tools. *Journal of Materials Processing Technology*. 164-165, pp. 1294-1300, 2005.
- [2] X. P. Dang, H. S. Park. Design of U-Shape Milled Groove Conformal Cooling Channels for Plastic Injection Mold. *International Journal of Precision Engineering and Manufacturing*. 12(1), pp. 73-84, 2011.
- [3] D. M. Bryce. Plastic Injection Molding: Material Selection and Product Design Fundamentals. *Society of Manufacturing Engineers*. Dearborn, Michigan, 1997.
- [4] D. Kazmer. *Injection Mold Design Engineering*. Hanser; Hanser Gardner, Munich; Cincinnati, 2007.
- [5] E. Sachs, E. Wylonis, S. Allen, M. Cima, H. Guo. Production of Injection Molding Tooling with Conformal Cooling Channels Using the Three Dimensional Printing Process. *Polymer Engineering & Science*. 40(5), pp. 1232-1247, 2000.
- [6] T. Cedorge, J. Colton. Draft Angle and Surface Roughness Effects on Stereolithography Molds. *Polymer Engineering & Science*. 40(7), pp. 1581-1588, 2000.
- [7] C. W. Lee, C. K. Chua, C. M. Cheah, L. H. Tan, C. Feng. Rapid Investment Casting: Direct and Indirect Approaches via Fused Deposition Modelling. *International Journal of Advanced Manufacturing Technology*. 23(1), pp. 93-101, 2004.
- [8] J. P. Kruth, X. Wang, T. Laoui, L. Froyen. Lasers and Materials in Selective Laser Sintering. *Assembly Automation*. 2003.

- [9] X. Xu, E. Sachs, S. Allen. The Design of Conformal Cooling Channels in Injection Molding Tooling. *Polymer Engineering & Science*. 41(7), pp. 1265-1279, 2001.
- [10] R. X. Xu, E. Sachs. Rapid Thermal Cycling with Low Thermal Inertia Tools. *Polymer Engineering & Science*. 49(2), pp. 305-316, 2009.
- [11] S. Marques, A. F. de Souza, J. Miranda, I. Yadroitsau. Design of Conformal Cooling for Plastic Injection Moulding by Heat Transfer Simulation. *Polímeros*. 25(6), pp. 564-574, 2015.
- [12] F. H. Hsu, K. Wang, C. T. Huang, R. Y. Chang. Investigation on Conformal Cooling System Design in Injection Molding. *Advances in Production Engineering & Management*. 8(2), pp. 107-115, 2013.
- [13] F. H. Hsu, B. H. Wu, C. T. Huang, R. Y. Chang. Cooling Effects Study by Considering A Turbulence Model in Injection Molding. *AIP Conference Proceedings*. 1593(1), pp. 615-618, 2014.
- [14] A. Agazzi, V. Sobotka, R. LeGoff, Y. Jarny. Optimal Cooling Design in Injection Moulding Process – A New Approach Based on Morphological Surfaces. *Applied Thermal Engineering*. 52(1), pp. 170-178, 2013.
- [15] T. Wu, S. A. Jahan, P. Kumar, A. Tovar, H. El-Mounayri, Y. Zhang, J. Zhang, D. Acheson, K. Brand, R. Nalim. A Framework for Optimizing the Design of Injection Molds with Conformal Cooling for Additive Manufacturing. *Procedia Manufacturing*. 1, pp. 404-415, 2015.
- [16] S. A. Jahan, T. Wu, Y. Zhang, H. El-Mounayri, A. Tovar, J. Zhang, D. Acheson, R. Nalim, X. Guo, W. H. Lee. Implementation of Conformal Cooling & Topology Optimization in 3D Printed Stainless Steel Porous Structure Injection Molds. *Procedia Manufacturing*. 5, pp. 901-915, 2016.
- [17] S. A. Jahan, H. El-Mounayri. Optimal Conformal Cooling Channels in 3D Printed Dies for Plastic Injection Molding. *Procedia Manufacturing*. 5, pp. 888-900, 2016.
- [18] S. A. Jahan, T. Wu, Y. Zhang, J. Zhang, A. Tovar, H. El-Mounayri. Thermo-mechanical Design Optimization of Conformal Cooling Channels Using Design of Experiments Approach. *Procedia Manufacturing*. 10, pp. 898-911, 2017.

- [19] I. Fauzun, M. Hamdi, A. E. Tontowi, T. Ariga. Formulation of the Size and Position of Spiral Cooling Channel in Plastic Injection Mold Based on Fluent Simulation Results. *IEEE International Conference on Industrial Engineering and Engineering Management*. pp. 1728-1733, 2008.
- [20] J. C. Kurnia, A. P. Sasmito, A. S. Mujumdar. Numerical Investigation of Laminar Heat Transfer Performance of Various Cooling Channel Designs. *Applied Thermal Engineering*. 31(6), pp. 1293-1304, 2011.
- [21] P. Hu, B. He, L. Ying. Numerical Investigation on Cooling Performance of Hot Stamping Tool with Various Channel Designs. *Applied Thermal Engineering*. 96, pp. 338-351, 2016.
- [22] B. He, L. Ying, X. Li, P. Hu. Optimal Design of Longitudinal Conformal Cooling Channels in Hot Stamping Tools. *Applied Thermal Engineering*. 106, pp. 1176-1189, 2016.
- [23] L. Ying, T. Gao, M. Dai, P. Hu, L. Shen. Investigation of Convection Heat Transfer Coefficient of Circular Cross-section Short Pipes in Hot Stamping Dies. *Applied Thermal Engineering*. 138, pp. 133-153, 2018.
- [24] C. G. Cevtkovski, S. Reitsma, T. Bolisetti, D. S. K. Ting. Heat Transfer in a U-Bend Pipe: Dean Number versus Reynolds Number. *Sustainable Energy Technologies and Assessments*. 11, pp. 148-158, 2015.
- [25] K. A. Hoffmann, S. T. Chiang. *Computational Fluid Dynamics, 4<sup>th</sup> Edition*. Engineering Education System, Wichita, Kan, 2000.
- [26] H. K. Versteeg, W. Malalasekera. *An Introduction to Computational Fluid Dynamics: The Finite Volume Method*. New York: Wiley, Harlow, Essex, England: Longman Scientific & Technical, 1995.
- [27] K. Fukuda. Numerical Simulation of Fuel Sprays in Diesel Engines. *MASc. Thesis, University of Windsor*. Windsor, Canada, 2012.
- [28] B. E. Launder, D. B. Spalding. The Numerical Computation of Turbulent Flows. *Computer Methods in Applied Mechanics and Engineering*. 3(2), pp. 269-289, 1974
- [29] CD-Adapco. *STAR-CCM+ v11.06 User Guide*. 2016.

- [30] Y. A. Cengel, A. J. Ghajar. *Heat and Mass Transfer: Fundamentals and Applications, 5<sup>th</sup> Edition*. McGraw-Hill. 2015.
- [31] B. R. Munson. *Fundamentals of Fluid Mechanics, 6<sup>th</sup> Edition*. Wiley, Hoboken, NJ, 2010.
- [32] H. S. Park, X. P. Dang. Optimization of Conformal Cooling Channels with Array of Baffles for Plastic Injection Mold. *International Journal of Precision Engineering and Manufacturing*. 11(6), pp. 879-890, 2010.
- [33] A. Kalpakli, R. Örlü. Turbulent Pipe Flow Downstream a 90° Pipe Bend with and without Superimposed Swirl. *International Journal of Heat and Fluid Flow*. 44, pp. 103-111, 2013.
- [34] W. R. Dean, J. M. Hurst. Note on The Motion of Fluid in A Curved Pipe. *Mathematika*. 6(1), pp. 77-85, 1959.
- [35] L. Hufnagel. On the Swirl-switching in Developing Bent Pipe Flow with Direct Numerical Simulation. *Master in Applied and Engineering Mathematics, Royal Institute of Technology*. Stockholm, Sweden, 2016.
- [36] L. F. Moody. Friction Factors for Pipe Flow. *Transactions of the ASME*. 66, pp. 671-684, 1944.
- [37] F. M. White. *Fluid Mechanics, 6<sup>th</sup> Edition*. McGraw-Hill, New York, 2000.

# Appendix A

## Permission to Include Copyrighted Material

Figure 1.2: Simple schematics of a conventional and a conformal cooling system

JOHN WILEY AND SONS LICENSE		Dec 11, 2019
This Agreement between Mr. Shu Chen (“You”) and John Wiley and Sons (“John Wiley and Sons”) consists of your license details and the terms and conditions provided by John Wiley and Sons and Copyright Clearance Center.		
License Number	4726080861973	
License Date	Dec 11, 2019	
Licensed Content Publisher	John Wiley and Sons	
Licensed Content Publication	Polymer Engineering & Science	
Licensed Content Title	Production of Injection Molding Tooling with Conformal Cooling Channels Using the Three Dimensional Printing Process	
Licensed Content Author	Honglin Guo, Michael Cima, Samuel Allen, et al.	
Licensed Content Date	Apr 8, 2004	
Licensed Content Volume	40	
Licensed Content Issue	5	
Licensed Content Pages	16	
Type of Use	Dissertation/Thesis	
Requestor Type	University/Academic	
Format	Print and electronic	



Portion	Figure/Table
Number of Figures/Tables	2
Original Wiley Figure/Table Number(s)	Figure 7 and Figure 8
Will you be translating?	No
Title of Your Thesis/Dissertation	Numerical Investigation of Conformal Cooling Channels in Injection Molds
Expected Completion Date	Dec 2019
Expected Size (number of pages)	96
Requestor Location	Mr. Shu Chen 401 Sunset Ave. Windsor, ON N9B3P4 Canada Attn: Mr. Shu Chen
Publisher Tax ID	EU826007151
Total	0.00 CAD

## Figure 1.3: Plastic fog lamp cover

12/18/2019

University of Windsor Mail - Fog lamp picture for thesis



Shu Chen <chen1d7@uwindsor.ca>

---

### Fog lamp picture for thesis

2 messages

---

**Shu Chen** <chen1d7@uwindsor.ca>  
To: "Tabbert, Michael" <mtabbert@propergroupintl.com>  
Cc: Ronald Barron <az3@uwindsor.ca>

Wed, Dec 11, 2019 at 7:55 PM

Hi Mr. Tabbert

Hope you are doing well. I have found the attached picture of the fog lamp on which we conducted the conformal cooling channel research. It serves a good purpose of describing the motivation of my study. I was wondering if you could grant me permission to include this picture in my thesis?

Best Regards,  
Shu

Shu Chen,  
MAsc Candidate  
Mechanical, Automotive and Materials Engineering  
University of Windsor  
[chen1d7@uwindsor.ca](mailto:chen1d7@uwindsor.ca)



**Fog\_lamp\_PGI.jpg**  
369K

---

**Tabbert, Michael** <mtabbert@propergroupintl.com>  
To: Shu Chen <chen1d7@uwindsor.ca>  
Cc: Ronald Barron <az3@uwindsor.ca>

Thu, Dec 12, 2019 at 7:21 AM

Good Morning Shu,

Feel free to use any pictures you would like.

Regards,

Mike

[Quoted text hidden]

<https://mail.google.com/mail/u/0?ik=1c549b69a4&view=pt&search=all&permthid=thread-a%3Ar-8767016581733987460&simpl=msg-a%3Ar-8404030...> 1/1

Figure 5.6: Dean vortex

Copyright Clearance Center | **RightsLink** | Home | Help | Live Chat | Sign In | Create Account

**XVI. Note on the motion of fluid in a curved pipe**  
Author: W.R. Dean  
Publication: Philosophical Magazine  
Publisher: Taylor & Francis  
Date: Jul 1, 1927  
*Rights managed by Taylor & Francis*

**Taylor & Francis**  
Taylor & Francis Group

**Thesis/Dissertation Reuse Request**

Taylor & Francis is pleased to offer reuses of its content for a thesis or dissertation free of charge contingent on resubmission of permission request if work is published.

[BACK](#) [CLOSE](#)

© 2019 Copyright - All Rights Reserved | Copyright Clearance Center, Inc. | Privacy statement | Terms and Conditions  
Comments? We would like to hear from you. E-mail us at [customer@copyright.com](mailto:customer@copyright.com)

# Vita Auctoris

Name: Shu Chen

Place of Birth: Shenyang, Liaoning, China

Year of Birth: 1993

Education: M.A.Sc., Mechanical Engineering  
University of Windsor, 2016-2019

B.Eng., Mechanical Engineering  
Shenyang Aerospace University, 2011-2015